

EVALUATION OF FIELD AND FLUX DISTRIBUTION FOR  
ELECTRICAL STEELS UNDER UNIDIRECTIONAL  
MAGNETIZATION

NOOR ASHIKIN BINTI MOHD RASHID

DISSERTATION SUBMITTED IN FULFILLMENT OF THE  
REQUIREMENTS FOR THE DEGREE OF MASTER OF  
ENGINEERING SCIENCE

FACULTY OF ENGINEERING  
UNIVERSITY OF MALAYA  
KUALA LUMPUR

2012

# UNIVERSITI MALAYA

## ORIGINAL LITERARY WORK DECLARATION

---

Name of Candidate: **Noor Ashikin Mohd Rashid (I.C No:**

Registration/Matric No: **KGA060022**

Name of Degree: **Master of Engineering Science (MEngSc)**

Title of Project Paper/Research Report/Dissertation/Thesis (“this Work”):  
**Evaluation of Field and Flux Distribution for Electrical Steels under Unidirectional Magnetization**

Field of Study: **Electromagnetic (EM)**

I do solemnly and sincerely declare that:

1. I am the sole author/writer of this Work;
2. This Work is original;
3. Any use of any work in which copyright exists was done by way of fair dealing and for permitted purposes and any excerpt or extract from, or reference to or reproduction of any copyright work has been disclosed expressly and sufficiently and the title of the Work and its authorship have been acknowledged in this Work;
4. I do not have any actual knowledge nor ought I reasonably to know that the making of this work constitutes an infringement of any copyright work;
5. I hereby assign all and every rights in the copyright to this Work to the University of Malaya (“UM”), who henceforth shall be owner of the copyright in this Work and that any reproduction or use in any form or by any means whatsoever is prohibited without the written consent of UM having been first had and obtained;
6. I am fully aware that if in the course of making this Work I have infringed any copyright whether intentionally or otherwise, I may be subject to legal action or any other action as may be determined by UM.

## ABSTRACT

---

Evaluation of magnetic properties of electrical steel is vital in improving the quality of electrical machinery since it is used as magnetic cores for transformers, motors and generators. A double yoke Single Sheet Tester (SST) was modelled using two identical C-cores wound at limb side with 18 SWG copper wires in horizontal arrangement at frequency of 50 Hz. B coil and H coil sensor were used as magnetic sensor. The research was carried out using experimental analysis with the aid of Finite Element Method Magnetic (FEMM) modelling. The H-coil and B-coil sensor were positioned in the central of the sample where the uniform magnetized area can be obtained. The homogeneity of flux and field distribution of sample can be achieved at air gap length of 0.3 mm. Result indicates that yoke with dimension of (97.2x93.4x68.0) mm can generate the magnetizing field with a low reluctance flux closure path. Evaluation on specimen dimensions show that the non-uniformity of sample magnetization in overhang sample can attribute to the flux leakage between the yoke legs. The stray flux also is increased with the overhang sample. However, the so called fit in sample which is fitted nicely between the yoke end poles can be utilized to minimize the effect of stray flux. Results also indicate that the magnetic properties for both grain oriented and non-oriented silicon iron steels are influenced by the anisotropy of the material. It can be observed that the grain oriented steels have better magnetic properties than non-oriented steels. The electrical steel which has high anisotropic structures and high permeability will require less magnetic field to obtain high magnetic flux density. The differences in magnetic properties of electrical steels are due to their grain size and thickness of the sample. One-way ANOVA, T-Test and Tukey post hoc were executed at the 0.05 significance level. The statistical analysis results are in good accordance with the simulation and experimental analysis. It is statistically proven that the effectiveness of H-coil sensor is influenced by the turns of wire,  $N$  and area,  $A$ . The

data also provide sufficient evidence to conclude that length of air gap and yoke's dimension affect the magnetic measurement. It can be summarized that the evaluation of field and flux distribution for electrical steels under unidirectional magnetization are depending on anisotropy of the electrical steels and other design factors of SST such as the magnetizing method, type of sensors employed and the measuring method.

## ABSTRAK

---

Penilaian sifat magnetik keluli elektrik penting dalam meningkatkan kualiti jentera elektrik kerana ia digunakan sebagai teras magnetik untuk transformer, motor dan penjana. Penguji kepingan besi tunggal (SST) diperbuat daripada dua teras C yang sama saiznya, dililit dengan wayar tembaga 18 SWG dibahagian *limb* teras C secara mendatar pada frekuensi 50 Hz. Gulungan B and gulungan H digunakan sebagai pengesan magnet. Penyelidikan dijalankan menggunakan analisis eksperimen dengan bantuan program simulasi *Finite Element Method Magnetic (FEMM)*. Pengesan gulungan B and gulungan H diletakkan di tengah sampel di mana keseragaman pemagnetan diperoleh. Keseragaman ketumpatan fluks dan keamatan medan magnet dapat dicapai dengan menggunakan sela udara sebanyak 0.3 mm. Hasil penyelidikan mendapati penggunaan *yoke* dengan dimensi (97.2x93.4x68.0) mm berupaya menjana keamatan medan magnet yang mempunyai laluan penutupan fluks halangan. Penilaian ke atas dimensi sampel menunjukkan ketidakseragaman pemagnetan sampel dalam sampel terjuntai yang mengakibatkan kebocoran fluks di kaki yoke. Fluks yang terkeluar juga bertambah dengan penggunaan sampel terjuntai. Hasil penyelidikan mendapati bahawa pengagihan ketumpatan fluks dan keamatan medan magnet untuk kepingan besi silikon dipengaruhi oleh anisotropi bahan. Bijian berorientasikan anisotropi mempunyai kebolehtelapan yang tinggi berbanding bijian bukan berorientasikan isotropi. Keluli elektrik yang mempunyai struktur anisotropi dan resapan yang tinggi akan memerlukan keamatan medan magnet yang sedikit untuk mendapatkan ketumpatan fluks yang tinggi. Perbezaan ke atas ciri magnetik keluli elektrik adalah disebabkan oleh saiz bijian dan ketebalan sampel. Kaedah statistik iaitu ANOVA satu hala, ujian T dan ujian Tukey diaplikasikan pada tahap signifikansi 0.05. Hasil statistik bertepatan dengan hasil analisis simulasi dan eksperimen. Statistik

membuktikan keberkesanan gulungan H dipengaruhi oleh bilangan gulungan wayar, N dan luas, A. Data juga menunjukkan bukti mencukupi untuk menyimpulkan panjang sela udara dan dimensi yoke mempengaruhi pengukuran magnet. Kesimpulannya, sifat pemagnetan keluli elektrik di bawah satu pengukuran dimensi pemagnetan bergantung kepada anisotropi keluli elektrik dan faktor reka bentuk SST seperti kaedah pemagnetan, jenis sensor yang digunakan dan kaedah pengukuran yang dilaksanakan.

## ACKNOWLEDGEMENT

---

Alhamdulillah, all praise belongs to Allah. Thank you Allah for your blessing and provided me with the strength to finally complete this research.

My profound gratitude is due to my supervisor, Dr. Wan Nor Liza Mahadi who originated and supervised this study, and for guidance throughout the research.

My deepest appreciation to my lovely husband, Muhammad R. Aszeman, my son, Muhammad Haikal Haziq, my parents, Hj. Mohd Rashid Hassan and Hjh Aishah Saleh, my siblings and my family in law for their unlimited encouragements, time and financial support throughout the period of my studies. Thanks you so much for always believing in my potential, never give up and always stand by my side no matter whether it is good times or bad times throughout the years.

I would also like to thank Pn Aisyah Hartini and Mr. Zailani for their help and consultation.

I am also grateful to National Science Fellowship (NSF) for their financial support towards these studies.

## TABLE OF CONTENTS

---

<b>ORIGINAL LITERARY WORK DECLARATION</b> .....	ii
<b>ABSTRACT</b> .....	iii
<b>ABSTRAK</b> .....	v
<b>ACKNOWLEDGEMENT</b> .....	vii
<b>LIST OF FIGURES</b> .....	xii
<b>LIST OF TABLES</b> .....	xvii
<b>LIST OF SYMBOLS AND ABBREVIATIONS</b> .....	xviii
<b>CHAPTER 1 INTRODUCTION</b>	
1.0 Introduction.....	1
1.1 Objectives of the Research .....	2
1.2 Organization of the Thesis.....	3
<b>CHAPTER 2 BACKGROUND THEORY</b>	
2.0 Introduction.....	4
2.1 Magnetic Field Strength, H.....	4
2.2 Magnetic Flux Density, B.....	6
2.3 Magnetic Circuit .....	7
2.4 Magnetic Measurement .....	9
2.4.1 Measuring Magnetic Field Strength, H .....	9
2.4.2 Measuring Flux Density, B .....	11
2.5 Soft Magnetic Material .....	12

2.5.1	Grain Oriented Silicon Steel.....	13
2.5.2	Non-Oriented Silicon Steel .....	15
2.5.3	Magnetic Domain and Magnetization Process.....	15
2.6	Finite Element Method Magnetic (FEMM).....	18
2.7	Statistical Analysis.....	20
<b>CHAPTER 3 LITERATURE REVIEW</b>		
3.0	Introduction.....	22
3.1	Reviews on Magnetic Behaviour of Electrical Steels.....	22
<b>CHAPTER 4 DESIGN AND SIMULATION OF SINGLE SHEET TESTER USING FINITE ELEMENT METHOD MAGNETICS SOFTWARE</b>		
4.0	Introduction.....	28
4.1	One Dimensional Single Sheet Tester (SST).....	28
4.2	FEMM Modelling.....	29
<b>CHAPTER 5 DESIGN AND DEVELOPMENT A HARDWARE MODEL OF SINGLE SHEET TESTER</b>		
5.0	Introduction.....	31
5.1	Single Sheet Tester .....	31
5.2	Yoke Construction .....	35
5.3	Samples under Test.....	38
5.4	Detection of Magnetic Flux Density and Magnetic Field Intensity .....	39
5.4.1	B-Coil Sensor .....	39
5.4.2	H-coil Sensor .....	40
5.6	Development of Electronic Circuitry.....	44

5.6.1	Negative Feedback Circuit .....	44
5.6.2	B-Channel Circuit.....	44
5.6.3	H-channel Circuit .....	45

## **CHAPTER 6 EXPERIMENTAL CALIBRATION**

6.0	Introduction.....	49
6.1	Calibration of H-Coil Sensor .....	49
6.2	Calibration of Electronic Circuitry .....	51

## **CHAPTER 7 RESULT AND DISCUSSION**

7.0	Introduction.....	54
7.1	Finite Element Method Magnetic (FEMM) Simulation .....	54
7.1.1	Optimization of Magnetic Sensor's positioning.....	54
7.1.2	Optimization of Single Sheet Tester (SST) Set Up.....	58
7.1.3	Optimization of Sample's Dimension .....	72
7.1.4	Evaluation of Sample under Test .....	76
7.2	Magnetic Hardware Set up .....	85
7.2.1	Evaluation of Sample under Test .....	87
7.2.2	Evaluation on Stray Flux.....	94
7.3	Statistical Analysis.....	99
7.3.1	Normality of Data.....	99
7.3.2	The Effect on H-Coil Dimension .....	101
7.3.3	The Effect of Air Gap.....	104
7.3.4	The Effect of Yokes Dimension.....	106

7.3.5	The Effect of Sample Dimension .....	107
7.3.6	The Effect of Anisotropy.....	108
7.4	Validation on FEMM Simulation Analysis and Experiment Analysis.....	110
<b>CHAPTER 8 CONCLUSION AND RECOMENDATION</b>		
8.0	Conclusion .....	114
8.1	Recommendation .....	117
<b>REFERENCES .....</b>		<b>118</b>
<b>LIST OF PUBLICATIONS.....</b>		<b>126</b>
<b>APPENDICES .....</b>		<b>127</b>

## LIST OF FIGURES

---

Figure 2.1 Magnetic lines of force, $H$ of a conductor with current, $I$ (reproduced from Jiles, 1991) .....	5
Figure 2.2 A simple magnetic circuit with an air gap (reproduced from Sydney, 2011)...	7
Figure 2.3 Air gaps (a) with fringing and (b) ideal (reproduced from Sydney, 2011).....	8
Figure 2.4 H-coil Sensor (reproduced from S. Tumanski, 2007).....	10
Figure 2.5 B-coil Sensor (reproduced from S. Tumanski, 2007).....	12
Figure 2.6 Atomic structure aligned in grain oriented steel to the rolling direction (reproduced from Thompson, 1968) .....	14
Figure 2.7 Qualitative description of magnetization processes (reproduced from Brailsford, 1968) .....	17
Figure 3.1 Single sheet tester measuring strategy (reproduced from Antonelli, et al., 2005) .....	24
Figure 3.2 Distributions of eddy current density vectors on the surfaces of the specimen (reproduced from Nakata, et al., 1990) .....	25
Figure 3.3 Side view of the Single Sheet Tester setup (reproduced from Stupakov, et al., 2009).....	27
Figure 4.1 A complete assembly of SST in FEMM interface.....	29
Figure 4.2 Meshed geometry of single sheet tester.....	30
Figure 5.1 Block diagram for Single Sheet Tester of one dimensional magnetization system.....	32
Figure 5.2 A complete measuring system of Single Sheet tester (SST) .....	33
Figure 5.3 Side view of the Single Sheet Tester .....	34
Figure 5.4 Top view of the SST .....	35
Figure 5.5 A complete assembly of SST.....	36
Figure 5.6 Complete assembly of unidirectional magnetization system of SST .....	37

Figure 5.7 Test specimen of electrical steel sheet.....	38
Figure 5.8 Arrangement of B-coil in the central region of the specimen .....	39
Figure 5.9 B-coil sensor .....	40
Figure 5.10 H-coil sensor.....	42
Figure 5.11 Cross-section view and arrangement of H-coil sensor in the central region of the sample .....	43
Figure 5.12 Schematic circuit diagram of negative feedback and B-channel.....	46
Figure 5.13 Schematic circuit diagram of H-channel circuitry.....	47
Figure 5. 14 Electronic Circuitry .....	48
Figure 6.1 Calibration of H-coil sensor using Helmholtz coil.....	50
Figure 6.2 Calibration of electronic circuitry.....	52
Figure 6.3 Input and output signal waveforms for the electronic circuitry calibration...	53
Figure 7.1 Positioning of magnetic sensors along the sample .....	55
Figure 7.2 Flux distributions along grain-oriented electrical steel, grade M4.....	56
Figure 7.3 Field distributions along grain-oriented electrical steel, grade M4 .....	57
Figure 7.4 Side view plot of SST set up with air gap insertion (0 mm).....	58
Figure 7.5 Mesh plot of SST set up with air gap insertion (0.3 mm).....	59
Figure 7.6 Flux plot of air gap length at (a) effective air gap and (b) 0.3 mm for grain- oriented sample, M4 (zoomed-in-view).....	61
Figure 7.7 Flux density waveforms for different air gap length .....	62
Figure 7.8 Field strength waveforms for various air gap lengths .....	62
Figure 7.9 Stray flux distributions of various air gap lengths insertion.....	64
Figure 7.10 Yoke A with dimension of (97.2 x 93.4 x 68.0) mm.....	65
Figure 7. 11 Yoke B with dimension of (145.8 x 140.1 x 68.0) mm.....	66
Figure 7.12 A mesh view of Yoke B .....	66
Figure 7.13 Comparison of flux density distribution for Yoke A and Yoke B.....	67

Figure 7.14 Comparison of magnetic field strength distribution for Yoke A and Yoke B .....	67
Figure 7.15 Zoom-in-view of flux plots for (a) Yoke A with N=180 and (b) Yoke B with N=180 .....	69
Figure 7.16 Flux distribution pattern for Yoke A and Yoke B .....	70
Figure 7. 17 Field distribution pattern for Yoke A and Yoke B .....	71
Figure 7.18 Flux plot for Yoke B with magnetizing winding, N of 720 turns.....	71
Figure 7.19 A mesh view of horizontal double yokes SST with overhang sample .....	72
Figure 7.20 Comparison of flux density distribution for different sample's dimension at the centre of sample .....	73
Figure 7.21 Comparison of field distribution for different sample's dimension at the centre of sample .....	73
Figure 7.22 Comparison of flux distribution for different sample's dimension measured at the upper and lower end of the samples .....	75
Figure 7.23 Comparison of field distribution for different sample's dimension measured at the upper end and lower end of the samples .....	75
Figure 7.24 Side view of the assembly for grain-oriented silicon steel or non-oriented silicon steel.....	76
Figure 7.25 Magnetic flux distributions on different grade for non-oriented silicon steels, M27 and M19 .....	77
Figure 7.26 Magnetic field strength distributions for non-oriented silicon steels, grade M19 and M27.....	77
Figure 7.27 Magnetization curves for non-oriented steels, grade M19 and M27 .....	78
Figure 7.28 Flux distributions for grain-oriented steels, grade M3 and M4.....	79
Figure 7.29 Field distributions for grain-oriented steels, grade M3 and M4 .....	80

Figure 7.30 Comparison of magnetization curves for grain oriented electrical steels, grade M3 and M4 .....	81
Figure 7.31 Comparison of magnetic flux density distribution for electrical steels, grade M4 and M19 .....	82
Figure 7.32 Comparison of magnetic field strength distribution for electrical steels, grade M4 and M19 .....	82
Figure 7.33 Magnetization curves of electrical steels, grade M4 and M19 .....	84
Figure 7.34 Induced voltage waveform from H-coil sensor .....	85
Figure 7.35 Induced voltage waveform from B-coil sensor .....	86
Figure 7.36 Flux density distribution for non-oriented steels, grade H18 and H60.....	87
Figure 7.37 Field strength distributions for non-oriented steels, grade H18 and H60....	88
Figure 7.38 Flux density distribution of grain oriented steels, grade M5 and Z6H.....	89
Figure 7.39 Field strength distributions of grain oriented steels, grade Z6H and M5 ....	89
Figure 7.40 Comparison of flux density distribution for GO and NO steels, grade M5 and H60 .....	90
Figure 7.41 Comparison of magnetic field distribution for grain oriented and non-oriented steels, grade M5 and H6O.....	91
Figure 7. 42 Comparison of magnetization curves for GO and NO steels, grade M5 and H60.....	93
Figure 7.43 Arrangement of search coil placed on the surface of overhang sample .....	94
Figure 7.44 Flux density distributions of normal flux with variation of angle, $\Theta$ of search coil axis to the sample's surface .....	95
Figure 7.45 Flux distributions of normal flux measured at the centre of non-oriented sample, grade H6.....	96
Figure 7.46 Location of B-coil sensor on the sample surface.....	97

Figure 7.47 Flux density distributions measured at the centre, lower end and upper end of overhang and fit in sample.....98

Figure 7.48 Flux distributions for different types of silicon steel using FEMM software ..... 111

Figure 7.49 Flux distributions for different types of silicon steel using hardware ..... 112

Figure 7.50 Field distributions for different types of silicon steel using FEMM software ..... 112

Figure 7.51 Field distributions for different types of silicon steel using hardware ..... 113

## LIST OF TABLES

---

Table 2.1 Assumptions for T-test, (Weiss, 2005) .....	20
Table 5.1 The geometric parameters of the H-coil sensors.....	41
Table 6.1 The parameters of the H-coil sensors.....	51
Table 7.1 Correlation test for normality for H-coil analysis .....	100
Table 7.2 Correlation test for normality for air gap length analysis .....	100
Table 7.3 Correlation test for normality for yokes dimension analysis .....	100
Table 7.4 Correlation test for normality for sample dimension analysis .....	101
Table 7.5 Correlation test for normality for anisotropy analysis .....	101
Table 7.6 Summary of T-Test with $\alpha=0.05$ for the different specification of H-coil ...	102
Table 7.7 One-way ANOVA summary test for the H-coil dimension analysis.....	103
Table 7.8 Homogenous subsets H-coil dimension analysis for Tukey post hoc tests...	103
Table 7.9 One-way ANOVA summary test for the lengths of air gap analysis.....	104
Table 7.10 Homogenous subsets lengths of air gap for Tukey post hoc test .....	105
Table 7.11 Summary of T-Test with $\alpha =0.05$ for the different yoke dimension .....	106
Table 7.12 One-way ANOVA summary test for the different sample dimensions .....	107
Table 7. 13 T-Test summary test for the different types of samples.....	108

## LIST OF SYMBOLS AND ABBREVIATIONS

---

B	Magnetic flux density	ANOVA	Analysis of variance
H	Magnetic field strength	CRO	Cathode ray oscilloscope
I	Current	DVM	Digital voltmeter
A	Ampere	ASTM	American National Standard
T	Tesla	S	Sensitivity
$\phi$	Magnetic flux	$\mu_0$	Permeability of free space
N	Number of turns	AC	Alternating current
A	Cross sectional area		
F	Frequency		
Hz	Hertz		
$V_{rms}$	Voltage induced in the loop		
e.m.f	Electromagnetic force		
$\partial B/\partial t$	Derivative value of flux density		
$\partial H/\partial t$	Derivative value of field strength		
m	Meter		
NO	Non oriented		
GO	Grain oriented		
SST	Single sheet tester		
FEM	Finite element method		
FEMM	Finite element method magnetic		
SWG	Standard wire gauge		

# CHAPTER 1

## INTRODUCTION

---

### 1.0 Introduction

Electrical steel sheets are widely used in many AC applications as a result of their ability to enhance the flux produced by an electrical current. The electrical steels are indispensable in satisfying the basic requirement in society such as in electrical power generation and transmission, the storage and retrieval information, telecommunications (F. Fiorillo, 2010),(Pluta, 2010). Therefore, an approach to characterizing and modelling magnetic properties in electrical steels are needed as demands increase for efficient electrical power generation and distribution equipment, (A.J. Moses, 2012).

The magnetic characteristics of electrical steels are determined by considering the magnetic flux density,  $B$  and the magnetic field strength,  $H$  of the material in the direction of an applied magnetic field. Magnetic properties of electrical steels in the rolling direction can be measured using a unidirectional Single Sheet Tester (SST) with horizontal double yokes at a magnetizing frequency of 50 Hz. The H-coil and B-coil sensor were used to determine the magnetic properties of electrical steel sheets.

Finite Element Method Magnetic (FEMM) software is used to design and optimise of a SST under unidirectional magnetization. However, the experimental analysis is needed to determine the homogenous area of field and flux in electrical steels since numerical simulations based on finite element software which need many assumptions are not sufficient to precisely analyse the field and flux homogeneity in the sample (Nencib et al., 1996). In general, the characterisation of magnetic behaviour under unidirectional SST magnetizing set up are not only depend on anisotropy of the electrical steels but also on other design factors of SST such as the magnetising method, type of sensors employed and the measuring method.

## **1.1 Objectives of the Research**

The aim of this research is to design and develop the magnetizing system and to evaluate magnetic properties under one dimensional magnetization. The aim can be summarized as follows:

- i. To design and simulate one-dimensional Single Sheet Tester (SST) that can uniformly magnetize electrical steel samples using Finite Element Method Magnetic (FEMM) software.
- ii. To investigate and optimize the effect of design factors of one-dimensional SST on the magnetic properties of electrical steels using FEMM software.
- iii. To design and develop a hardware model of SST, magnetic sensors and interface circuitry.
- iv. To evaluate and analyse the magnetic properties of different types of electrical steels when subjected to one dimensional magnetisation.
- v. To validate results of hardware and software simulation.
- vi. To perform statistical analysis to interpret statistical significance on effect factor of Single Sheet Tester to the magnetic properties of electrical steels

## 1.2 Organization of the Thesis

This thesis covers the design and analysis of a magnetizing system for the measurement of properties in electrical steel sheet. Following is a brief chapter-by-chapter summary:

- i. **Chapter 1** presents an introduction on the soft magnetic materials, objectives of the thesis and overview of organization of the thesis contents.
- ii. **Chapter 2** presents the fundamentals of magnetic properties of magnetic materials, magnetic circuits, magnetic sensors, Finite Element Method Magnetic (FEMM) concepts and statistical analysis methods.
- iii. **Chapter 3** covers a comprehensive review on Single Sheet Tester, following some current research on these fields.
- iv. **Chapter 4 and Chapter 5** describe a design concept and construction on hardware model of Single Sheet Tester (SST) together with the simulation of the measuring system using Finite Element Method Magnetics (FEMM) software.
- v. **Chapter 6** presents experimental calibration of H-coil and electronic circuitry.
- vi. **Chapter 7** provides the results of optimization on magnetising system, magnetic sensor's positioning and evaluation on magnetic materials from the simulation and experiment. Results were evaluated in terms of their magnetic properties characteristics, field and flux distribution plots and through statistical analysis approaches.
- vii. **Chapter 8** presents the conclusion of the research findings and recommendations for the future research.

## CHAPTER 2

### BACKGROUND THEORY

---

#### 2.0 Introduction

A magnetic field can be conceptualized as lines of forces. When such flux lines encounter any sort of matter, an interaction takes place in which the number of flux lines is either increased or decreased. The original magnetic field therefore becomes amplified or diminished in the body of matter. This is true whether the matter is a magnetic material or nonmagnetic material since different substances possess varying degrees of magnetization.

#### 2.1 Magnetic Field Strength, $H$

In 1820, Oersted discovered the deviation of a compass needle near a current-carrying conductor. Ampere assumed from those results that a magnetic field,  $H$  is originated from moving electrical charges. According to Ampere, the magnetic field generated by an electrical charge depended on the shape of the circuit and the current carried. The basic law of magneto-motive force given as

$$NI = \oint_s H \cdot dl \quad (2.1)$$

where  $N$  is the number of current-carrying conductors with current,  $I$ ,  $H$  is the source of the magnetic field and  $l$  is a line vector. However, this equation is restricted for steady currents only.

Ampere's law and the Bio-Savart law can be shown to be equivalent. Consider the field due to a steady current flowing in a long current-carrying conductor as illustrated in Figure 2.1.

By the Bio-Savart law, the field at a radial distance,  $r$  from the conductor is

$$H = \frac{NI}{2\pi r} \quad (2.2)$$

While the Ampere's circuital law state

$$\int \mathbf{H} \cdot d\mathbf{l} = NI \quad (2.3)$$

By integrating along a closed path around the conductor at a distance,  $r$  with number of turns,  $N=1$  leads to

$$H = \frac{I}{2\pi r} \quad (2.4)$$

where the magnetic field strength,  $H$  is measured in Ampere per meter, A/m.

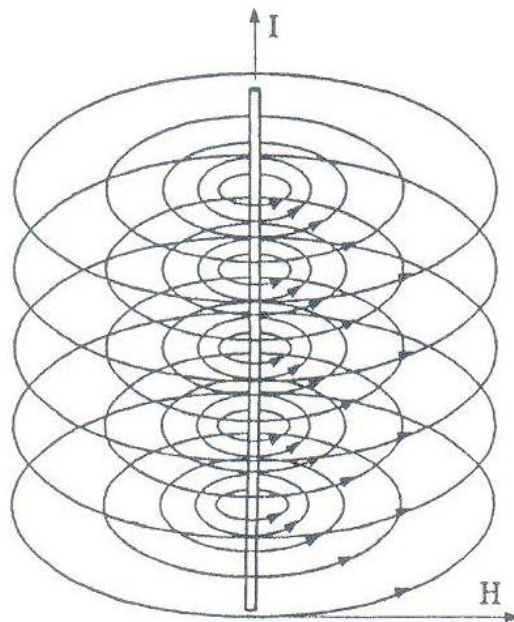


Figure 2.1 Magnetic lines of force,  $H$  of a conductor with current,  $I$  (reproduced from Jiles, 1991)

## 2.2 Magnetic Flux Density, $B$

The flux density can be defined as a response of the medium to a magnetic field. It is usually described in terms of the force on a moving electric charge or electric current. It is measured in units of Weber/metre<sup>2</sup> (Wb/m<sup>2</sup>) which is identical to a magnetic induction of one Tesla, T. In many media,  $B$  is a linear of  $H$ . In particular in free space, it can be written

$$B = \mu_0 H \quad (2.5)$$

where permeability of the free space, is  $\mu_0 = 4\pi \cdot 10^{-7}$  which in unit of Henry per meter (H/m). However in magnetic materials, the magnetic flux density,  $B$  is no longer a linear function of  $H$  since it is depends on the permeability of the medium,  $\mu$  and Equation 2.6 yields to

$$B = \mu_0 \mu_r H \quad (2.6)$$

Now, the permeability is defined as

$$\mu = \frac{B}{H} \quad (2.7)$$

and the relative permeability of a medium, denoted  $\mu_r$  is given by

$$\mu_r = \frac{\mu}{\mu_0} \quad (2.8)$$

The different types of magnetic materials are classified on the basis of their permeability.

## 2.3 Magnetic Circuit

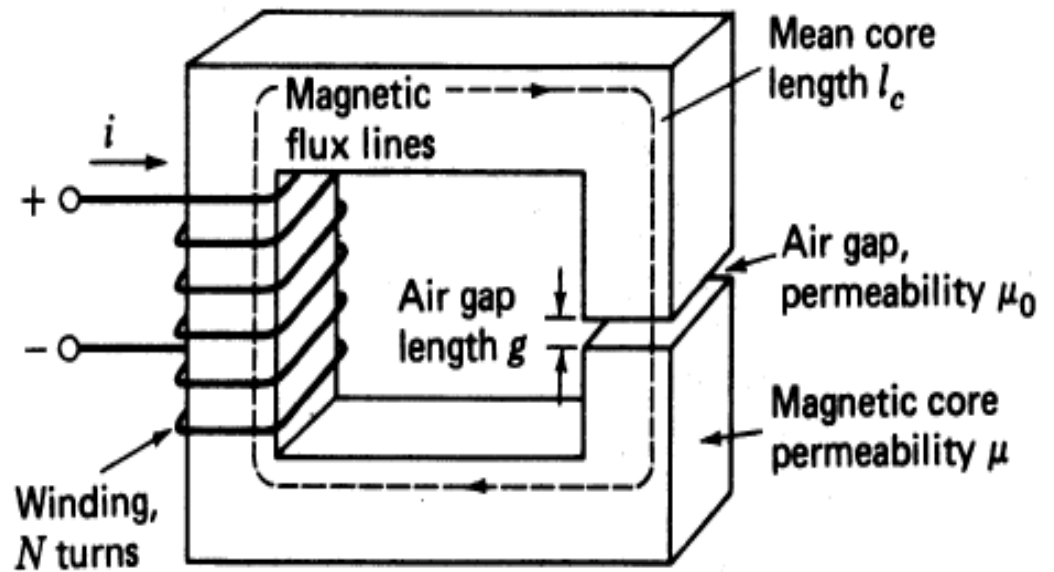


Figure 2.2 A simple magnetic circuit with an air gap (reproduced from Sydney, 2011)

Figure 2.2 shows a simple magnetic circuit with an air gap of length,  $l_g$  cut in the middle of a leg. The winding provides  $NI$ , *Ampere-turn*. The magneto-motive force is the total current linked with the magnetic circuit. The field is given by,

$$H = \frac{NI}{l} \quad (2.9)$$

The spreading of the magnetic flux lines outside the common area of the core for the air gap is known as fringing field which is illustrated in Figure 2.3 (a). For simplicity, this effect is negligible and the flux distribution is assumed to be as in Figure 2.3 (b). It can be seen that the magnetic flux generated in the air gap is equal to the magneto-motive force,  $NI$  divided by the sum of the reluctances of the core and the air gap. By applying the Ampere's circuital law, the Equation 2.20 can be written as

$$NI = H_c l_c + H_g l_g \quad (2.10)$$

where the subscript of  $c$  and  $g$  refer to the core and air gap respectively. The path  $l_c$  in the core is the length measured along the centre of the cross section of the core.

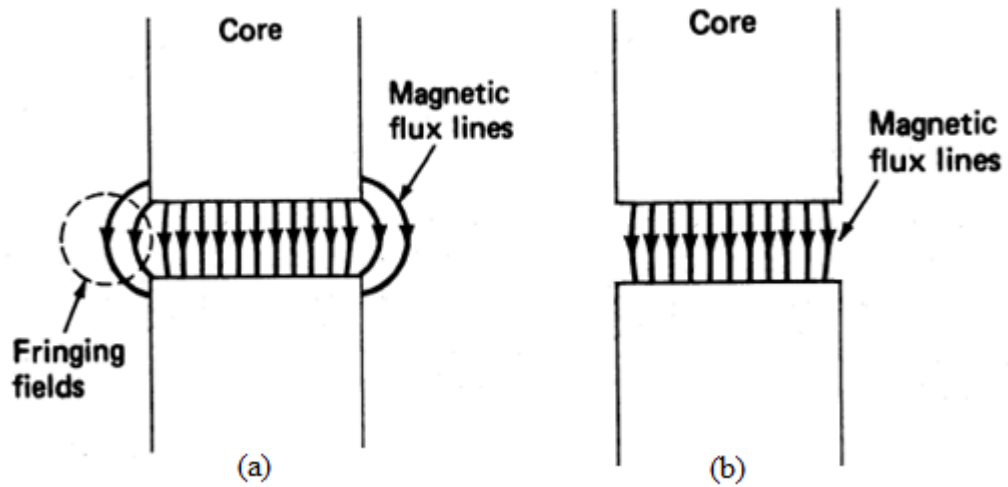


Figure 2.3 Air gaps (a) with fringing and (b) ideal (reproduced from Sydney, 2011)

According to Gauss's law of magnetism, the net outward flux of  $B$  through any closed surface must be equal to zero.

$$\oint B \cdot ds = 0 \quad (2.11)$$

The total flux must be the same over any cross section,  $A$  of the magnetic circuit, thus

$$\Phi = BA \quad (2.12)$$

Combining Equation 2.11 and Equation 2.12 gives

$$B_g A_g \left[ \frac{l_c}{\mu_c A_c} + \frac{l_g}{\mu_0 A_g} \right] = NI \quad (2.13)$$

And the magnetic flux is

$$\Phi = B_g A_g = \frac{NI}{\frac{l_c}{\mu_c A_c} + \frac{l_g}{\mu_0 A_g}} \quad (2.14)$$

The denominator of Equation 2.15 gives the reluctances of the core and air gap in series.

Hence, the total reluctance in a magnetic circuit given as

$$R_{total} = \frac{l_c}{\mu_c A_c} + \frac{l_g}{\mu_0 A_g} \quad (2.15)$$

## 2.4 Magnetic Measurement

The behaviour of magnetic material can be described by its magnetic properties which are magnetic field strength, H and flux density, B. Several methods can be used to determine their magnetic characteristic as will be discussed in the following subsections.

### 2.4.1 Measuring Magnetic Field Strength, H

The magnetic field strength in electrical steel sheet can be determine using indirect and direct method. In the indirect method, the magnetizing current is only can be used if the length of the magnetic path is well defined whereas in the direct method, it rely on concept where the tangential components of magnetic field at the surface of a magnetic material to be equal to magnetic field inside the material. Various sensors are used to detect the tangential magnetic field, which are H-coil, Rogowski coil and Hall Effect sensor. However for this research, the H coil sensor is selected because it is relatively easy to prepare and gain the averaging effect due to large area of the sensor. Besides

that, it is also offers unlimited range of the measured field with outstanding linearity and yet immune to the orthogonal field components.

#### 2.4.1.1 H-Coil Sensor

The induction coil, which is one of the simplest magnetic field sensing devices, is based on Faraday's Law. Figure 2.4 shows the example of H-coil sensor.

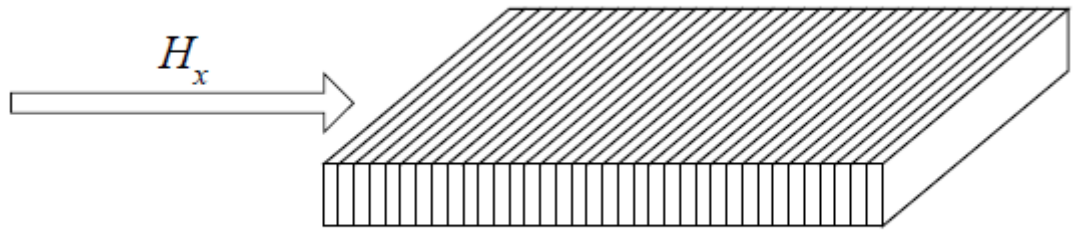


Figure 2.4 H-coil Sensor (reproduced from S. Tumanski, 2007)

This law states that if a loop of wire known as coil is subjected to a changing magnetic flux,  $\phi$ , through the area enclosed by the loop, then a voltage will be induced in the loop that is proportional to the rate of change of the flux with a number of turn,  $N$  of wire.

$$e(t) = -N \cdot \frac{d\phi}{dt} \quad (2.17)$$

The magnetic flux,  $\phi$  in the coil is given as

$$\phi = B \cdot A \quad (2.18)$$

where  $A$  is the core cross-sectional area of the coil.

Using (2.18) and (2.19), the voltage induced in a coil can be simplified as

$$e(t) = -\mu \cdot N \cdot A \cdot \frac{dH}{dt} \quad (2.19)$$

Measurements of the magnetic field strength in magnetic materials based on the fact that the tangential components of magnetic field in the air,  $H_a$ , is the same as magnetic field in the material,  $H_m$ .

## 2.4.2 Measuring Flux Density, B

Localised flux density measurement in magnetic material is measured by means of two methods which are search coil and needle probe techniques. The detected flux densities are averaged values over the cross-sectional area of sample limited by the positions of the holes or needles, (Krismanic, 2004). In this study, the search coil will be adopted as a localised flux density sensor due to versatility of this sensor in detecting the flux density averaged over a cross-section of bulk or laminated magnetic material, (Zurek, 2006).

### 2.4.2.1 B-Coil Sensor

The search coil is the most common sensor in magnetic measurements. This technique rely on Faraday's law, which states that the voltage induced in the coil,  $V$  is proportionally change with the rate of change of flux density,  $B$ , in the area enclosed by the area-turns product,  $NA$ , of the B-sensing coil where  $A$  is a cross-sectional area of the sample enclosed by the search coil.

$$V = -NA \frac{dB}{dt} \quad (2.20)$$

Figure 2.5 illustrates the example of B-coil sensor which have one turn coil wound through two micro holes with diameter of about 2.0mm. The symbol  $t$  is indicates as the thickness of the steel sheet and  $d$  is the distance between the holes.

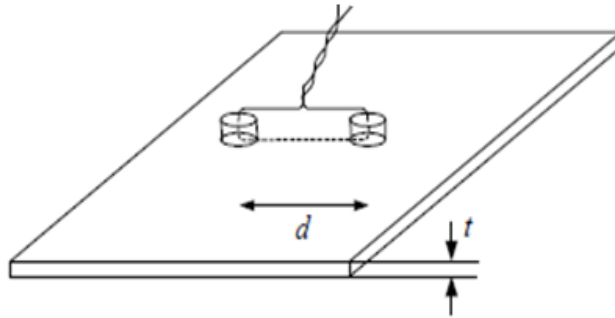


Figure 2.5 B-coil Sensor (reproduced from S. Tumanski, 2007)

The sinusoidal flux density,  $B_{peak}$  can be calculated using the well-known equation derived from Faraday's law which is

$$B_{peak} = \frac{V_{rms}}{4.44 f N A} \quad (2.21)$$

where  $V_{rms}$  is the voltage induced in the loop ,  $f$  is frequency,  $N$  is number of turn and  $A$  is the cross-sectional area of the coil.

## 2.5 Soft Magnetic Material

Materials that easily to magnetize and demagnetize are called soft magnetic material. Soft magnetic materials are mainly utilized in alternating-current machinery in which the soft has to amplify the flux generated by the electrical current or by a permanent magnet. The principal characteristics of soft magnetic materials are

remanence, coercivity, permeability, saturation value of magnetic field, H and flux density, B. Silicon steels are the most important soft magnetic material since they are used as core of the construction of electrical machines such as transformers, generators and motor.

The earlier soft magnetic material was iron, which contained many impurities. The improvement in magnetic properties obtainable by alloying iron with silicon was revealed by Barret, Brown and Hadfield. It was found that by adding silicon to the iron can be raised the maximum permeability reduced the area of the hysteresis loop, eliminated ageing troubles and substantially raised the electrical resistivity. Soft magnetic material can be classified into three types which are the conventional steels; grain oriented, non-oriented and new material; amorphous steel. However, only conventional steels will be discussed since the amorphous steel has poor mechanical properties and expensive cost as twice compared as conventional steel making it cost effectively only for some large distribution-type transformers.

### **2.5.1 Grain Oriented Silicon Steel**

Grain oriented silicon irons are used in large quantities in the electrical engineering industry. They are produced in so-called conventional form, a high permeability material with improved texture and coating or after special surface treatment, a high performance domain refined grade. The silicon level ranges from 2.9% to 3.2% in the grain oriented steels. These magnetic materials exhibit their superior magnetic properties in the rolling direction. This directionality occurs because the steels are specially processed to create a very high proportion of grains within the steel which have similarly oriented atomic crystalline structures relative to the rolling direction.

This yields anisotropic properties and is useful for stationary applications where the magnetic flux has a static and non-changing direction.

In iron-silicon alloys, this atomic structure is cubic and the crystals are most easily magnetized in a direction parallel to the cube edges as illustrated in Figure 2.6. By a combination of precise steel composition and strictly controlled cold rolling and annealing procedure the crystals of these oriented electrical steels are aligned with their cube edges nearly parallel to the direction in which the steel is rolled. Consequently, they provide superior permeability and lower core loss when magnetized in this direction. They are use most effectively used in transformer cores, generators when the design allows the directional magnetic characteristics to be used efficiently.

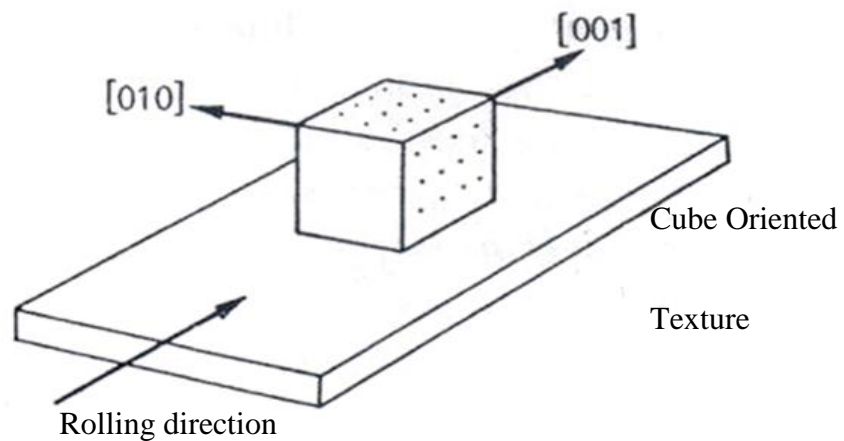


Figure 2.6 Atomic structure aligned in grain oriented steel to the rolling direction

(reproduced from Thompson, 1968)

### **2.5.2 Non-Oriented Silicon Steel**

The demand for a cheap product with good mechanical strength, has led to today's highly developed production route for non-oriented steels. Non-oriented electrical steel contain between 0.5 % to 3.25% silicon and 0.5% aluminium which can increase the resistivity and lower the temperature of primary recrystallization. Grain growth is very desirable in the non-oriented grades but is much smaller than for the oriented grades. The sheet is normally supplied with a thin organic or inorganic surface coating to provide inter-laminar insulation in use. Non oriented steels are not sensitive to strain as the oriented product. Therefore shearing strains comprise the only strain effects, which should decrease the magnetic quality. Laminations of these steels are commonly large thus shearing strains can be tolerated.

The non-oriented steels have similar magnetic properties in all direction of magnetization in the plane of material, which makes it isotropic. They are implemented where efficiency is less important and towards high magnetic efficiency for use in applications where increased material cost was offset by higher efficiency. They are commonly used in large rotating machine, including electric motors, Alternating Current (AC) alternators and power generators where the direction of magnetic flux is random.

### **2.5.3 Magnetic Domain and Magnetization Process**

The concept of magnetic domain is one of the most important features of modern magnetic theory. Theoretical contributions by Neel and subsequent confirmatory experimental work reported by Bozorth, William and others have greatly advanced the subject of domain structure in ferromagnetic. A magnetic domain describes a region within a magnetic material which has uniform magnetization. Neel

showed that a condition of equilibrium, when the sum of these energy components. Neel showed that a condition of equilibrium, when the sum of these energy components was a minimum, would be attained in simple cases when the domains had certain particular sizes and geometrical configurations. The boundary between two domains is spread over a region many atoms wide. Bloch pointed out that the exchange energy of crystal anisotropy is a minimum when the spins are parallel to a direction of easy magnetization. The magnitude of the anisotropic behaviour is given quantitative expression by the values of the anisotropy constant.

A qualitative elaboration of the magnetization processes in taking a sample from the demagnetized condition to saturation is illustrated in Figure 2.7. The squares symbolize a small portion of the surface of a single crystal of iron where the sides of the squares being parallel to cube-edge directions of the crystal. At the origin of the magnetization curve when  $H=0$ , the magnetization will be made zero in the figure by the four equal domains forming a closed magnetic circuit. The application of a small field causes an increase of the resultant magnetization in the field direction by a small and ideally reversible movement of the domain boundaries.

When the field is still further increased the boundaries may give comparatively large Barkhausen jumps causing a steeper rise in the magnetization curve as indicated at point **B**. This process of irreversible jumps will be about complete for relatively low field strength at point **C** which is the knee of the curve where most of the domain vectors are turned into the nearest cube-edge direction to the field direction. Over the region **D** of the curve, the resultant magnetization in the direction of **H** increases by a smooth rotational process in which the magnetization of the domains is pulled gradually into line as **H** increases. This process is reached saturation at point **E** where the resultant magnetization in the individual domains has the same direction of **H**.

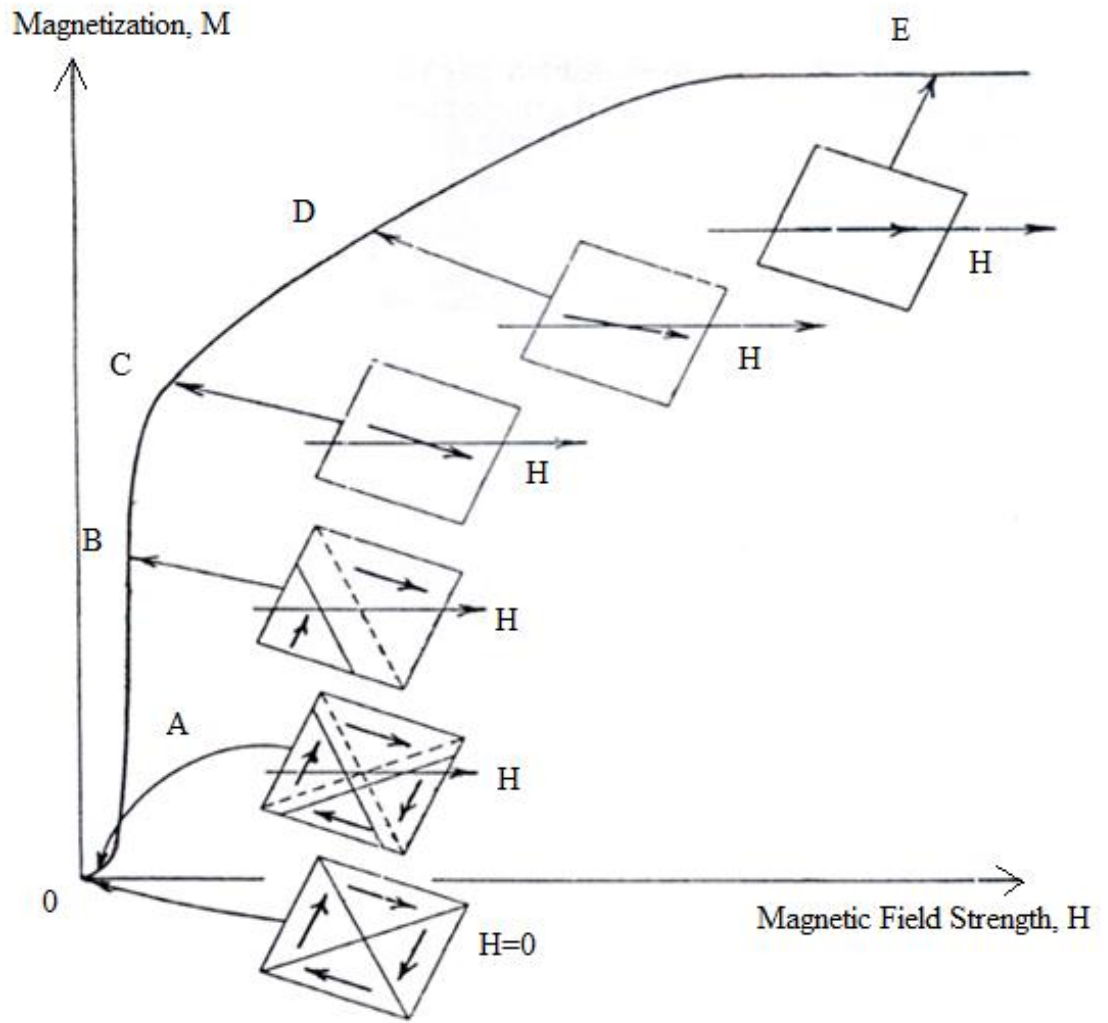


Figure 2.7 Qualitative description of magnetization processes (reproduced from Brailsford, 1968)

## 2.6 Finite Element Method Magnetic (FEMM)

The finite element method (FEM) is a computational method that can be applied to obtain solutions to the partial differential equations that occur in engineering and scientific applications. FEMM is a finite element software package for solving low frequency electromagnetic problems using FEM. The program addresses 2D planar and 3D axisymmetric linear and nonlinear harmonics low frequency magnetic, magnetostatic problems and linear electrostatics problems. In the finite element method, it combines geometrical adaptability and material generality for modelling arbitrary geometries and materials of any composition without alter the formulation of the computer code that executes it.

The basic concept of the method is to break up the problem domain into a large number of sub domains where each finite elements. Algorithms exist that permit the resulting problem to be solved in a short amount of time. In electromagnetic, a discretization method, which implicitly includes most of theoretical features of the problem under analysis, is one of best solution to get accurate results in a variety of problems. FEMM software package has been developed in addressing some limiting cases of Maxwell equations. In case of magnetostatic problems, the fields are time-invariant. For such cases, the field intensity,  $\vec{H}$  and flux density, B must obey

$$\vec{\nabla} \times \vec{H} = \vec{J} \quad (2.22)$$

Where,  $\vec{J}$  denotes current density,

$$\vec{\nabla} \cdot \vec{B} = 0 \quad (2.23)$$

The constitutive relationship between  $\vec{B}$  and  $\vec{H}$  for each material is given as

$$\mu = \frac{\vec{B}}{\vec{H}} \quad (2.24)$$

The flux density can be written in terms of vector potential,  $\vec{A}$  as:

$$\vec{B} = \vec{\nabla} \times \vec{A} \quad (2.25)$$

As the definition of  $\vec{B}$  always satisfies Eq. (5.2) can be written as:

$$\vec{\nabla} \times \left( \frac{1}{\mu(\vec{B})} \vec{\nabla} \times \vec{A} \right) = \vec{J} \quad (2.26)$$

For linear isotropic material and also assuming the Coulomb gauge,  $\vec{\nabla} \cdot \vec{A} = 0$ , Equation 5.6 reduces to

$$-\frac{1}{\mu} \vec{\nabla}^2 \vec{A} = \vec{J} \quad (2.27)$$

FEMM retains the Equation 2.26, so that magneto static problems with a non-linear  $B-H$  relationship can be resolved.

Over each sub region, the solution of the partial differential equation is approximated by a polynomial function where these polynomials have to be pieced together so that the edges of adjoining elements overlap the field to maintain continuity of the field. Then the variation integral is evaluated as a total of contributions from each finite element resulting in an algebraic system with a finite size than the original infinite dimensional partial differential equation. The advantage of breaking the domain down into a sub elements is the problem transformation from a small but too complex into a big but relatively easy to solve. Unlike other computational methods, in the finite element method the approximate solution is known throughout the domain as a piecewise function.

## 2.7 Statistical Analysis

Statistical analysis is performed in order to draw conclusions about group differences on several interests of sample results, (SPSS, 2002). Statistics are available for variables at all measurement levels and it is important to match the proper statistic to a given level of measurement. In this research, three logic and procedure of testing for mean differences are chosen to draw conclusions about population differences based on sample measurement as listed below.

### i. T-Test

The T-Test is commonly used to obtain a probability statement about differences in means between populations whether the population differs from the specified value. The four assumptions are required for performing a pooled T-test as listed in Table 2.1.

Table 2.1 Assumptions for T-test, (Weiss, 2005)

Assumption	Description
i. Simple random samples	The samples taken from the population under consideration are simple random samples.
ii. Independent samples	The samples taken from the population under consideration are independent of one another.
iii. Normal populations	For each population, the variable under consideration is normally distributed.
iv. Equal standard deviations	The standard deviations of the variable under consideration are the same for all the populations.

### ii. One-Way ANOVA

Analysis of variance provides methods for comparing the means of a variable for populations that result from a classification by a factor. One-way ANOVA is the generalization to more than two populations of the pooled t-procedure. As in T-test, the four assumptions listed in Table 2.1 are required for performing a One-way ANOVA test.

iii. Tukey multiple-comparison method

Tukey post hoc test is used to determine the relationship among all the population means. This test is distinguished between the individual confidence level and the family confidence level. The individual confidence level is the confidence that have any particular confidence interval contains the difference between the corresponding population means. The family confidence level is the confidence that have all the confidence intervals contain the differences between the corresponding population means. The assumptions used in the Tukey test are similar to the pooled T-Test as stated in Table 2.1.

## CHAPTER 3

### LITERATURE REVIEW

---

#### **3.0 Introduction**

Electrical steels are the most important soft magnetic materials since they are used as magnetic materials in electrical machinery and appliances, mainly as a core of transformer. They are intensively studied to improve the performance of the transformer within a prescribed range for the purpose of effectively reflecting the material characteristics on the performance of the practical devices, (Michiro et al., 2002). In order to fully relate the basic properties of core steel to the performance in devices it is essential to be able to accurately and conveniently measure the magnetic properties.

#### **3.1 Reviews on Magnetic Behaviour of Electrical Steels**

Normann et al., (1982) studied the influence of grain orientation on the magnetic behaviour of a Fe-Si material. Generally, the magnetic behaviour of the specimen was determined by two different methods which are observation of the domain structure and measurement of the stray field near the surface. They found out that the grain orientation strongly influences the magnetic behaviour even at the external field. This is revealed by measurements of the normal component of the stray field at the surface of the specimen. The observed stray fields showed the reduction of the magnetic flux in the sample under test due to disoriented grains.

J. Liu and Shirkoohi, (1993) investigated the anisotropy behaviour of magnetic material using finite element method. One single B-H curve was used to describe the characteristic of isotropic materials with the assumption that B was in the same direction with magnetic field, H. Meanwhile, for anisotropic materials, the B-H

relationship varies according to the direction of the applied magnetic field, H and the behaviour of material in each direction is different.

The Single Sheet Tester (SST) is increasingly replacing the Epstein machines as reference frames for soft magnetic material either for laboratory measurements and the industrial measurements. Apart from easier sample preparation and substantial saving of material, SST is capable to reproduce with more accuracy in determination of real magnetic materials as SST's measure the average value of magnetic flux density, B and the maximum value of the magnetic field, H in the sample. Moreover, the SST's measurement is made in real condition of unidirectional scalar field where anisotropy and corner effects can be neglected without practical loss of accuracy (Antonelli et al., 2005), (Sievert, 2000).

Antonelli, et al., (2005) used the magnetising apparatus which constitutes by one or two U-shaped laminated magnetic cores enclosing the sample under test. The apparatus is shown in Figure 3.1. The excitation magnetic field is given by the exciting coil. The mean magnetic induction is derived by the voltage induced in the measuring coil while the exciting magnetic field, H is deduced by the relation

$$H(t) = \frac{NI(t)}{l_{Fe}} \quad (3.1)$$

where N is the number of the load coil turns, I is the exciting current, and  $l_{Fe}$  is the length of the part of the sample out of the U-shaped laminated magnetic cores. The magnetic flux density is determined using relation

$$B(t) = \frac{1}{NA_{Fe}} \int v(t) dt \quad (3.2)$$

where  $A_{Fe}$  is the cross-section of the sample under test and  $v(t)$  is the induced voltage of the measuring coil.

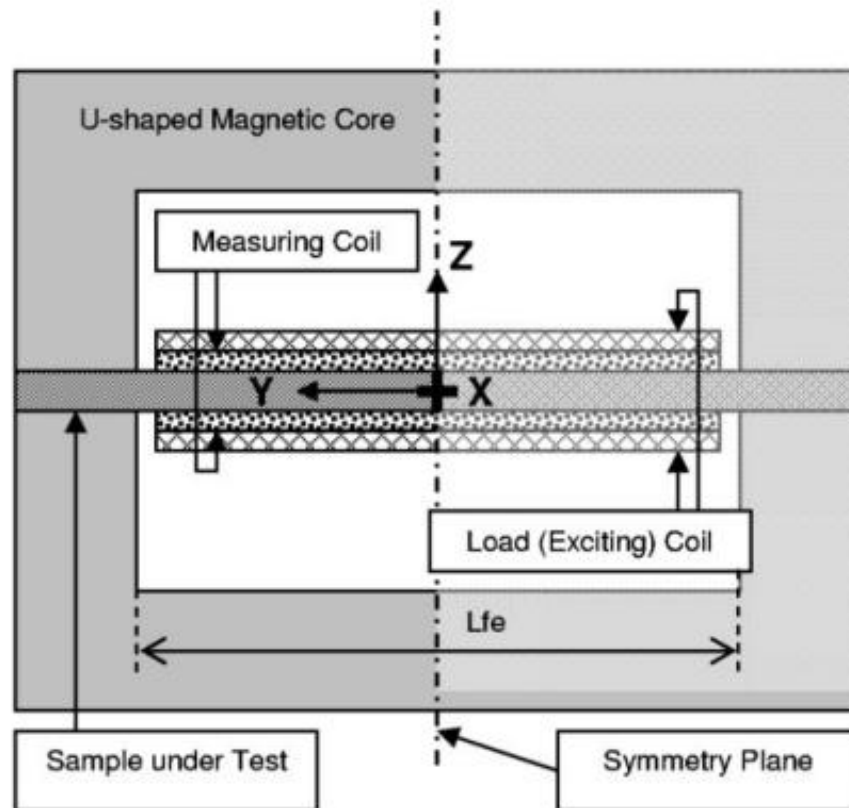


Figure 3.1 Single sheet tester measuring strategy (reproduced from Antonelli, et al., 2005)

Nakata et al., (1990) have considered the effects of eddy currents in the grain oriented steels of M-4 grade using two types of yoke arrangement of SST. They constructed the vertical single yoke type SST called the *S-type* and vertical double yoke type tester which is denoted as the *D-type*, which having an addition of the upper yoke. The eddy current flows from one surface to opposite surface. Results showed that for case of *D-type*, the  $x$ -component of eddy current density in the sample was negligible small and the eddy current path of the *D-type* is not influenced by  $L_o$ , Figure 3.2 (a). In contrast, for case of the *S-type*, the eddy current density in  $x$ -components appeared and the eddy current path of the *S-type* is affected by the overhang sample,  $L_o$ , Figure

3.2(b). (Beckley, 2002), also stated that the eddy current pools can be cancelled by using double yoke type tester.

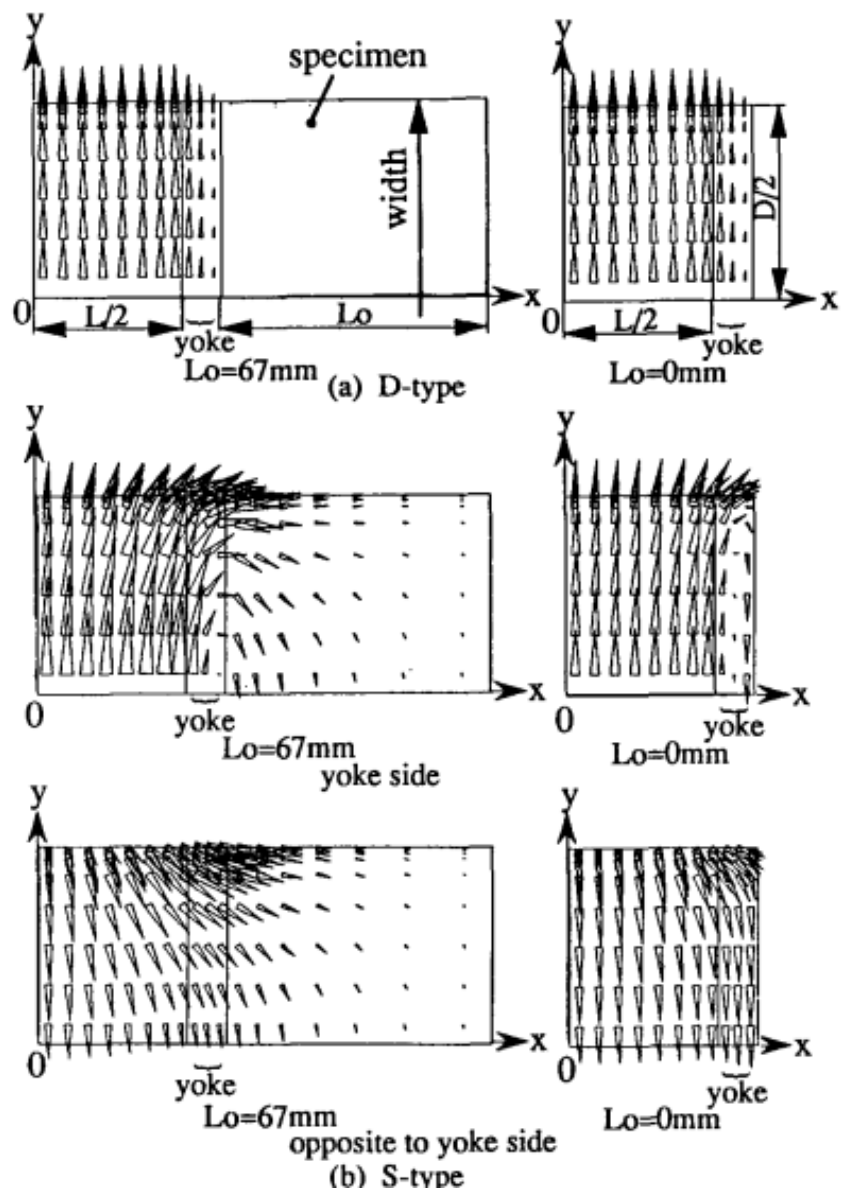


Figure 3.2 Distributions of eddy current density vectors on the surfaces of the specimen (reproduced from Nakata, et al., 1990)

Jahidin and Mahadi, (2007) compared the magnetic properties of electrical steel obtained using the horizontal and vertical yoke system. They observed that the horizontal SST set up gave higher value of magnetic field and flux density of the electrical steel. This is due to stress that produced to the sample when the top C-core impressed the sample. (Miyagi et al., 2009) have reported that the measurement of magnetic field and flux density should be carried out in the region of uniform magnetic field strength for the accuracy of measurement.

Stupakov et al., (2009) studied the applicability of local magnetic measurements using single yoke measuring set up. The apparatus of the single yoke system is shown in Figure 3.3. The magnetic characteristics of closed ring-shaped were obtained based on the surface field measurements and their extrapolation to the sample surfaces. They found that the usage of single yoke leads to instability of the magnetization process with respect to the frequently occurred fluctuations of yoke sample contact. In the case of infinite sample overhang, the extrapolation field techniques are able to provide repeatability of the measurements with respect to the yoke lift-off within the quasi-static magnetization limit. However, the current and the surface field methods were only stable for the coercivity testing. The measurement repeatability was improved using integrated yoke based sensor equipped with the field and the sensing elements between the yoke poles.

Stupakov et al., (2012) stated that the stabilization of the magnetization conditions makes the measurement results independent of the experimental configuration of the magnetizing sensing unit which are repeatable even in the magnetically open configuration.

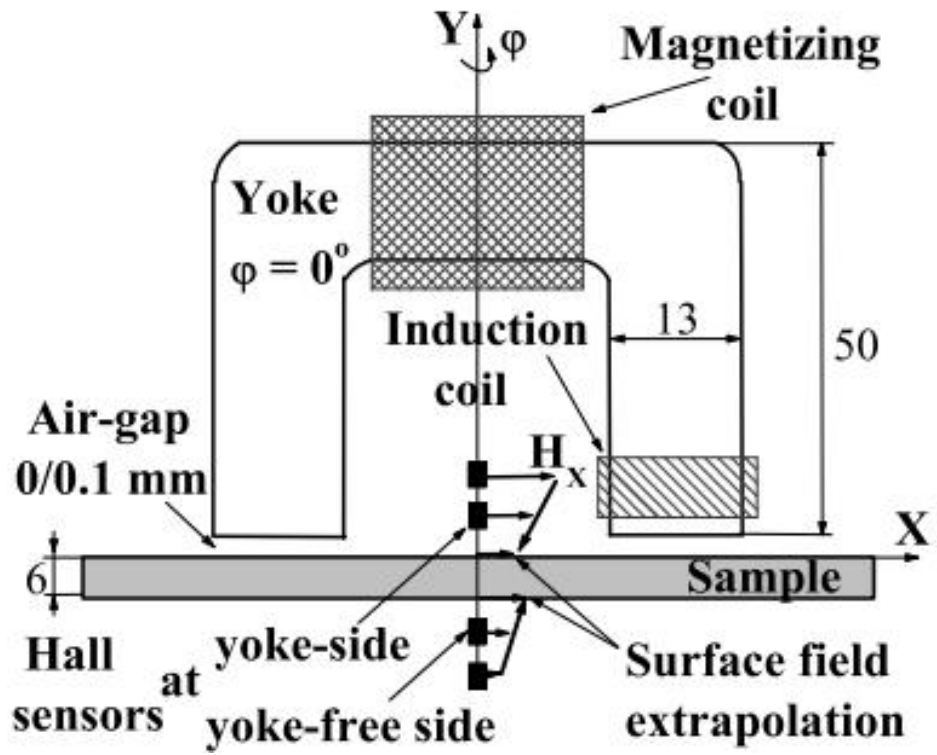


Figure 3.3 Side view of the Single Sheet Tester setup (reproduced from Stupakov, et al., 2009)

**CHAPTER 4**

**DESIGN AND SIMULATION OF SINGLE SHEET TESTER USING FINITE  
ELEMENT METHOD MAGNETICS SOFTWARE**

---

**4.0 Introduction**

Finite Element Method Magnetics (FEMM) software is used to analyse the magnetic properties of silicon iron steel sheet under one dimensional magnetizing system. It implies a finite element method, which uses Maxwell's equation as the basis of the electromagnetic field analysis. The simulation tool is useful in optimizing the best fit design of Single Sheet Tester (SST) set up within a short time. The effect of air gaps between the sample and the yoke pole faces, sample dimensions, yoke dimensions, and the positioning of magnetic sensors on samples are examined. Later, the optimized model will be adapted in a hardware model.

**4.1 One Dimensional Single Sheet Tester (SST)**

A two dimensional cross-section of SST geometry was constructed inside FEMM interface, which included the double yoke of C-core, coil windings and sample under test. The laminated C-cores with thickness of 68mm were positioned horizontally with the sample placed between them. Each limb side of yokes were wound with 180 turns of enamelled 18 SWG copper wires. The double yokes form a magnetic circuit that is driven by magnetizing coils at frequency of 50 Hz ,with currents in the range of 0.2 A to 2.4A. The air gap was inserted between the end pole faces and sample to achieve homogenous magnetization conditions. The complete assembly of SST is illustrated in Figure 4.1.

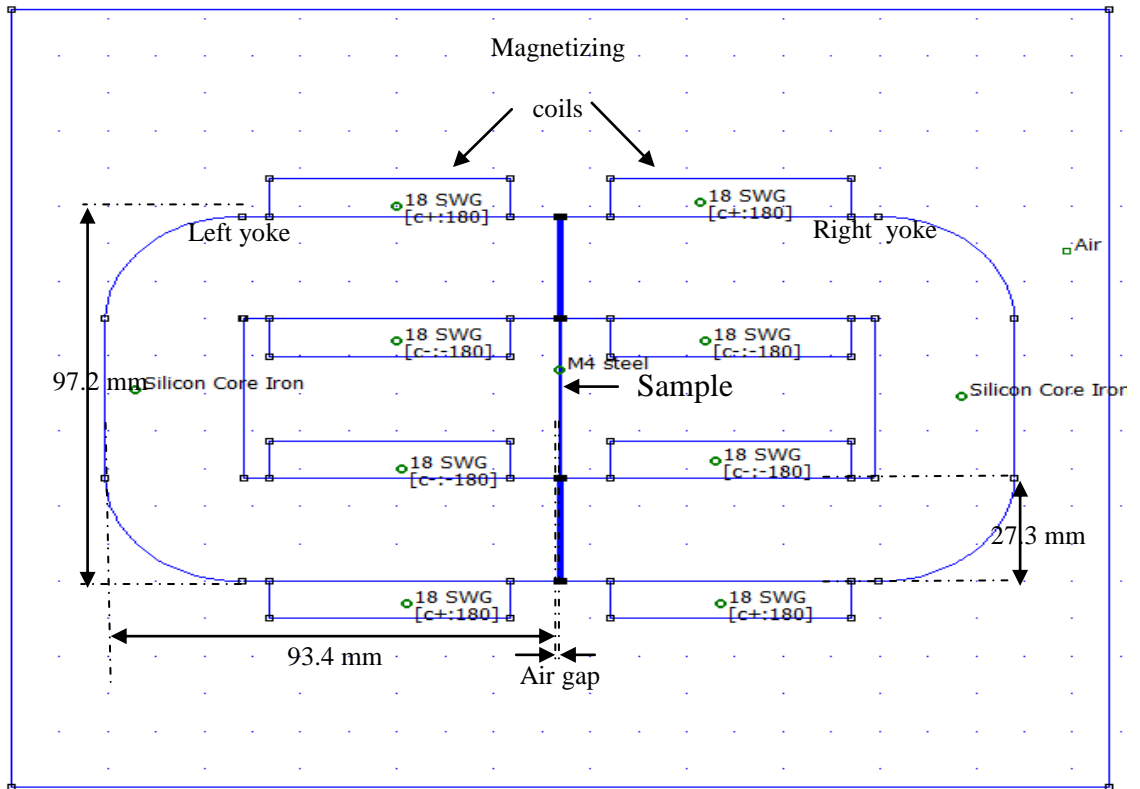


Figure 4.1 A complete assembly of SST in FEMM interface

## 4.2 FEMM Modelling

The FEMM contains a CAD interface for laying out the geometry of two dimensional SST. The geometric construction steps can be described into three parts:

### i. Pre-processor

The SST model is designed accordingly to the actual size of the C-cores, (97.2 x 93.4 x 68.0) mm and sample under test, (97.2 x 68.0) mm. The material properties are defined for the each block as coil, yoke and sample. FEMM has a built in library that allows a variety of material.

ii. Linear Solver

The calculation domain must be assigned with a boundary condition. Prescribed A boundary condition is depicted as boundaries of solution domain where the flux passing normal to the specified boundary. The triangular mesh is adopted into SST model as shown in Figure 4.2. The mesh segmented the magnetic problem domain into a large number of sub elements. Different mesh size values can be set in each area to increase the accuracy of the solver solution.

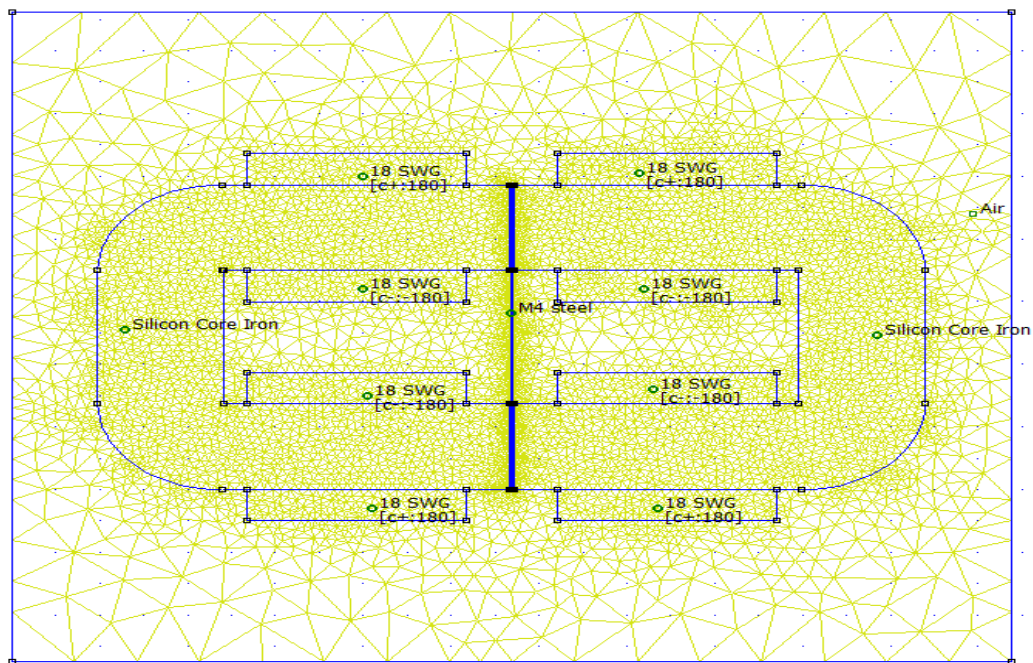


Figure 4.2 Meshed geometry of single sheet tester

iii. Post-processor

The field solutions can be viewed in density and contour plot form. The density plot can be measured at one specific coordinate. The field strength is shown in a graduation of colour; each colour represents its magnitude of field strength.

**CHAPTER 5**  
**DESIGN AND DEVELOPMENT A HARDWARE MODEL OF SINGLE**  
**SHEET TESTER**

---

**5.0 Introduction**

In this chapter, the design and development of the one-dimensional magnetizing and measuring system used to produce an alternating field and flux density in electrical steels are described. The magnetic properties of electrical steels which are grain oriented steel sheet and non-oriented steel sheet so as the effect of stray flux on the tested sample were evaluated under 50 Hz magnetizing frequency.

**5.1 Single Sheet Tester**

The single sheet tester of one-dimensional magnetization and measuring system is illustrated and pictured in Figure 5.1 and Figure 5.2. It consists of magnetizing circuit, magnetic sensors, and interface circuitry with additional feedback circuitry. A variable transformer is used to energize the magnetic circuit. The generated magnetization signal,  $dB(t)$  and  $dH(t)$  measured using H-coil and B-coil sensors are passed through an interface circuitry where the magnetizing signals are being amplified, filtered, integrated and buffered. Output signal from interface circuitry,  $B(t)$  is fed back to the magnetizing circuit in order to control the sinusoidal flux waveforms. The resultant output of magnetizing output,  $B(t)$  and  $H(t)$  can be measured using Cathode Ray Oscilloscope (CRO) and Digital Voltmeter (DVM).

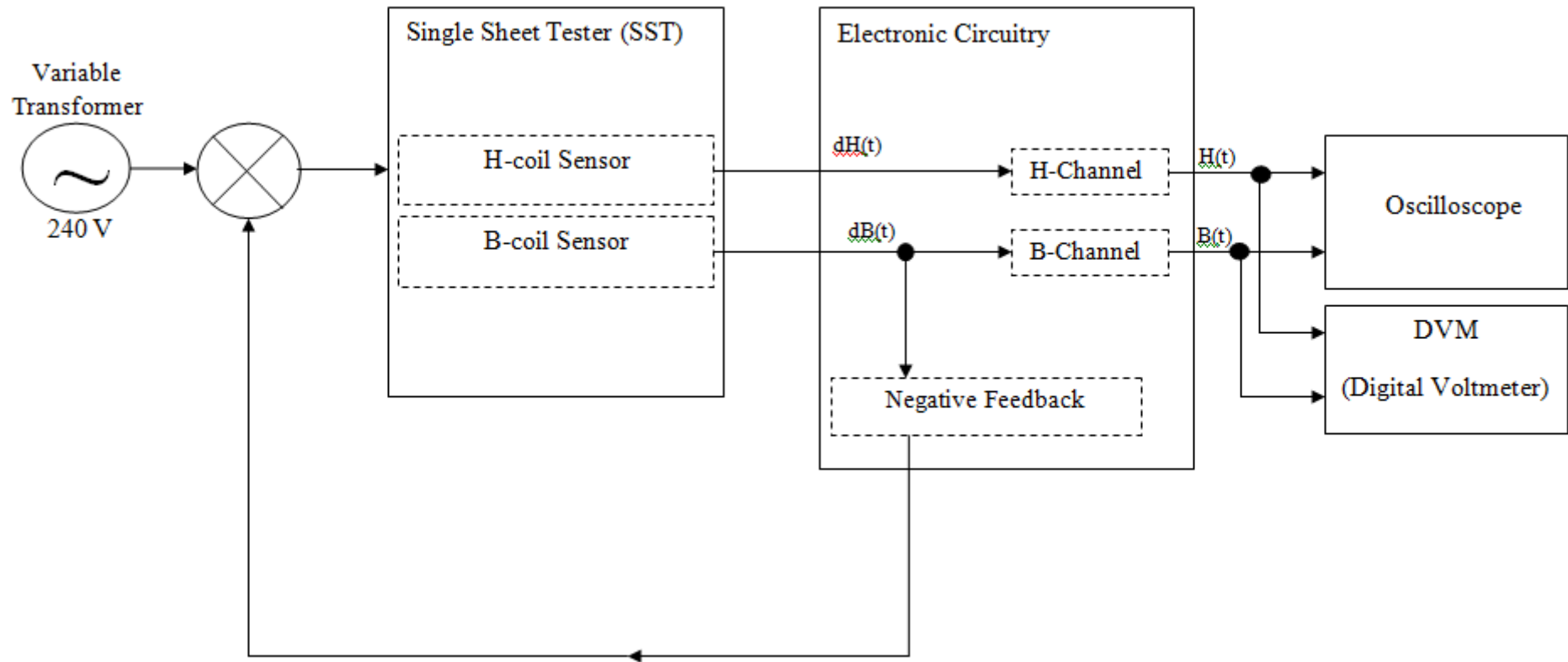


Figure 5.1 Block diagram for Single Sheet Tester of one dimensional magnetization system

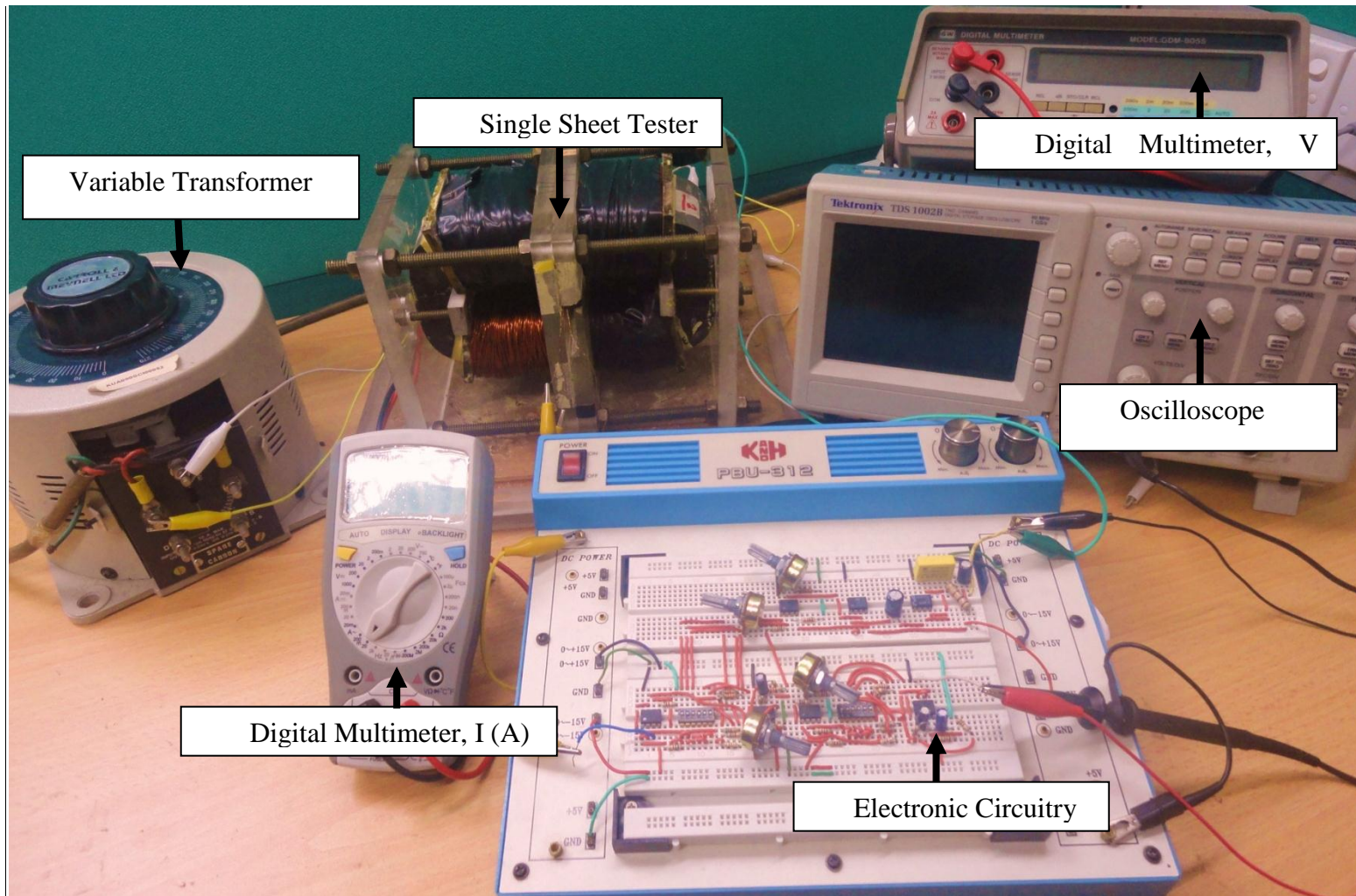


Figure 5. 2 A complete measuring system of Single Sheet tester (SST)

A double yoke single sheet tester (SST) set up was modelled and developed using two symmetrical C-cores, made from laminated grain oriented 3% silicon steel and placed horizontally on each side of sample. The hardware model is adopted from optimized simulation model which is designed according to an American National Standard: A 804/A804M-9 (ASTM, 2000). Side view of the principle sketch and Figure dimension of utilized SST set up is presented in Figure 5.3.

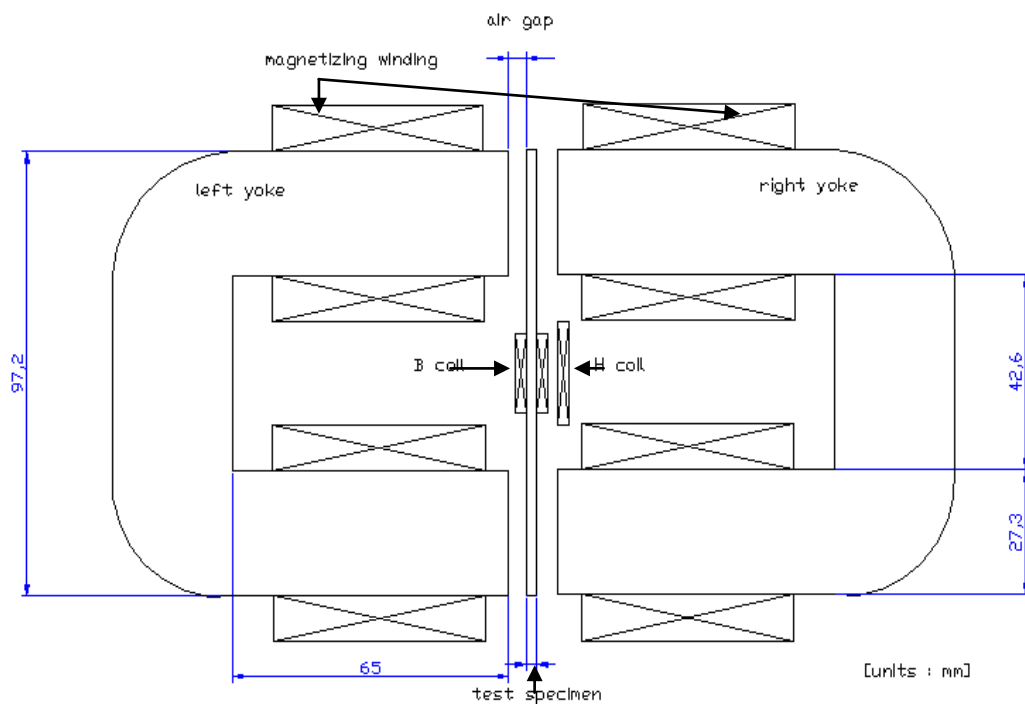


Figure 5. 3 Side view of the Single Sheet Tester

The sample was placed in between two C-type yokes, which carrying the magnetizing coils as shown in Figure 5.4. 180 turns of 18 SWG magnetizing copper wire wound on the yoke limb side to provide constant field gradient at the yoke side sample surface. Measurements were performed on single sheets of grain oriented, GO and non-oriented, NO electrical steel at frequency of 50 Hz. The sinusoidal waveform of current with the range of 0.2 A to 2.4 A is applied. An air gap was inserted between the sample and the C-core pole faces to achieve a homogenous field distribution.

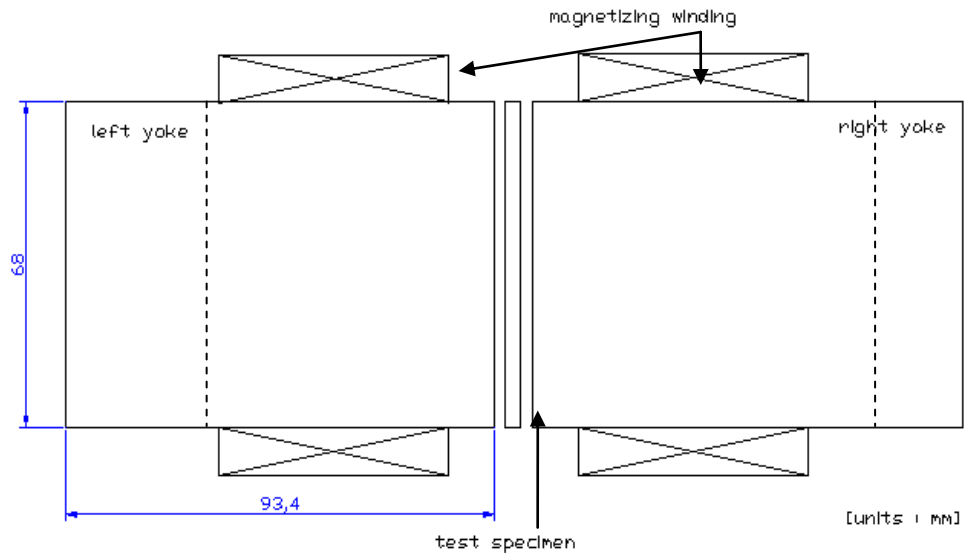


Figure 5. 4 Top view of the SST

## 5.2 Yoke Construction

The fixtures of SST were built using thick perspex. The complete assembly of SST is shown in Figure 5.5 and Figure 5.6. The square perspex plates on each side of magnetic circuit firmly supported the left and right yoke. The square plates can be shifted along the rods to alter the air gap between the sample and yoke pole faces. Thick perspex base bearded the assembly of SST from any vibrations. The middle perspex plates accommodated the sample and magnetic sensors; B-coil and H-coil. The clamps attached to perspex holder were holding the double yokes maintain in position. A set up treatment must be taken into consideration when modelling the magnetizing system. The C-core must be insulated with adhesive tape and coated with varnish. At each edge of C-core poles was covered with nonconductive material. These steps can prevent current leakage and electrical stress between conductive parts, C-core and wires. An enamelled magnetizing copper wire of C-core was coated with varnish so that it can hold tight the winding into its position within leg yokes.

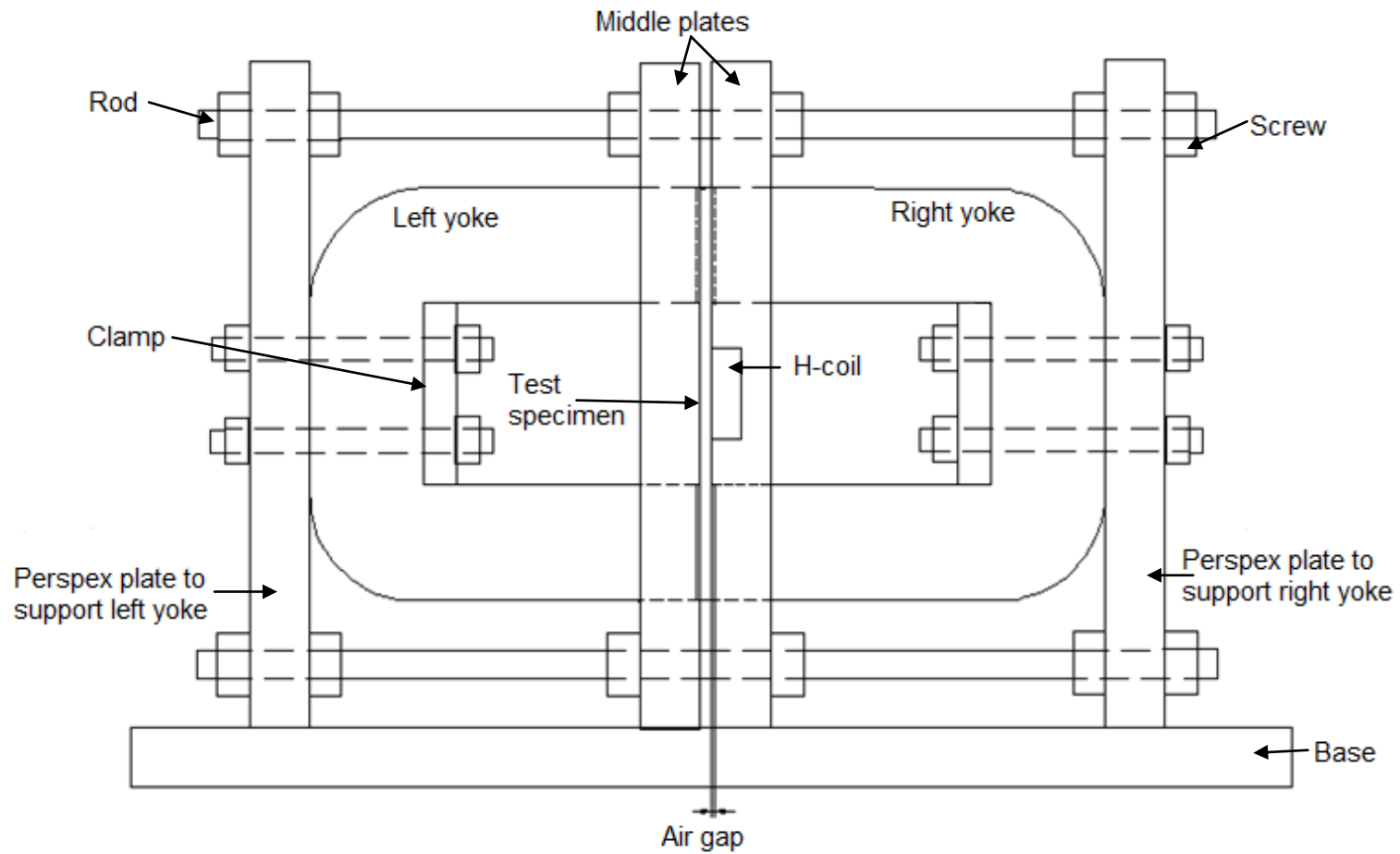


Figure 5.5 A complete assembly of SST

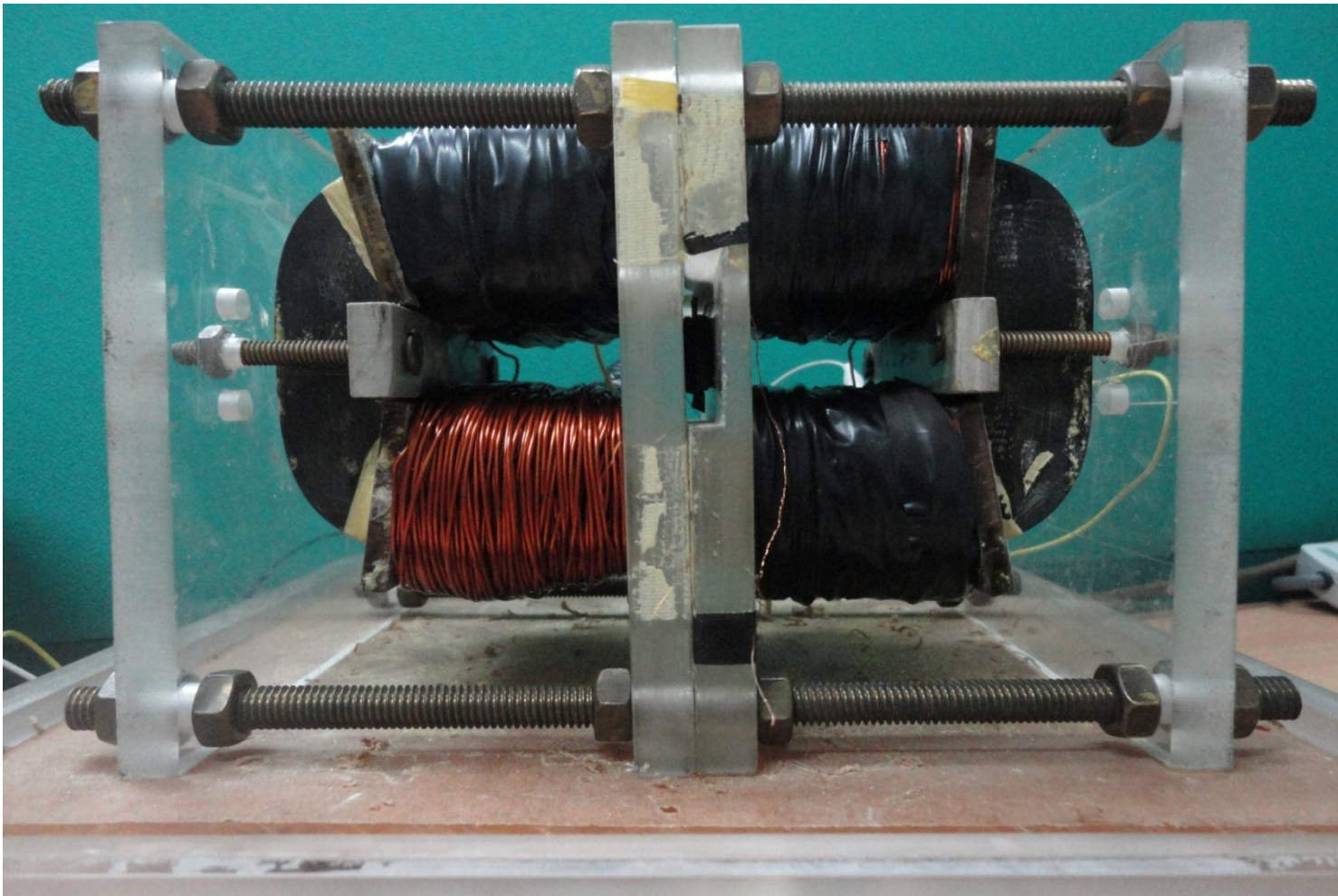


Figure 5.6 Complete assembly of unidirectional magnetization system of SST

### 5.3 Samples under Test

The samples under test were magnetized between the yoke poles by a laminated 3% silicon iron C-core carrying the magnetizing coils. Two types of electrical steels were tested:

- i. Grain Oriented 3% silicon iron steels (GO) : Grade: M5, Z6H
- ii. Non-Oriented 3% silicon iron steels (NO) : Grade: H18, H60

The dimension of the sample was chosen so that it can be placed within the yoke pole faces as illustrated in Figure 5.7. The thickness of the grain oriented silicon steel, grade M5 and Z6H is 0.3 mm while thickness for non-oriented silicon steels, grade H18 and H60 is 0.5 mm. The test specimens used for the determination of properties of magnetic materials will vary in form depending upon the test equipment and the dimensions of the material to be tested.

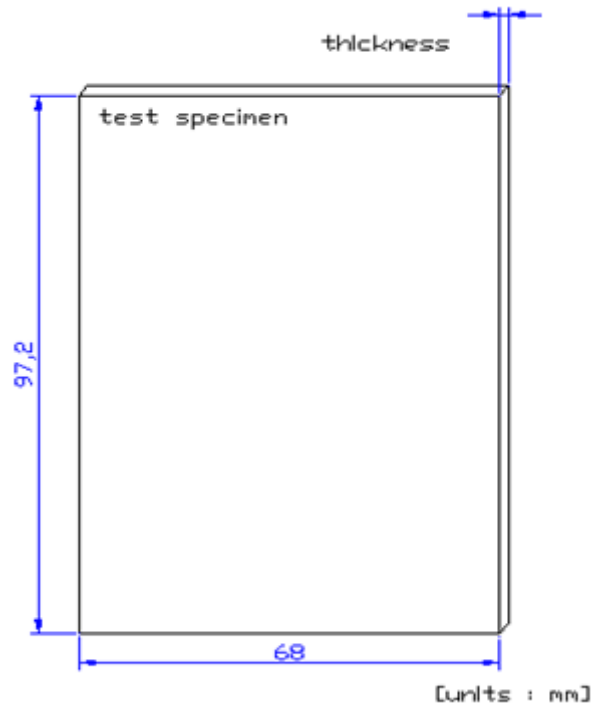


Figure 5.7 Test specimen of electrical steel sheet

## 5.4 Detection of Magnetic Flux Density and Magnetic Field Intensity

### 5.4.1 B-Coil Sensor

Local flux density was determined by means of two turn search coil. Insulated copper wire with 0.2mm diameter, directly wound enclosed the sample under test. Two holes with diameter of 0.2mm were cautiously drilled through the sample in an approach to lessen a mechanical stress within 20 mm distance from each hole. The drilled holes of B-coil also coated with varnish to prevent short circuit between wires and magnetic material. The winding length should be less than a third of the sample length and must be centred on the sample. The leads shall be twisted tightly to reduce errors caused by stray magnetic fields. Figure 5.8 and Figure 5.9 illustrate the basic feature of B-coil. The sinusoidal magnetic flux density,  $B_{peak}$  can be calculated using Equation 2.21.

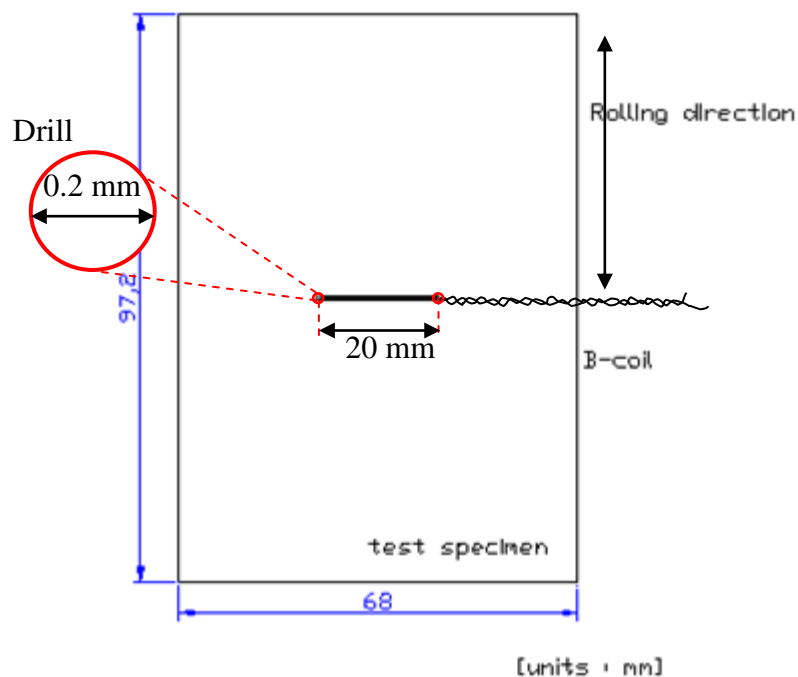


Figure 5.8 Arrangement of B-coil in the central region of the specimen

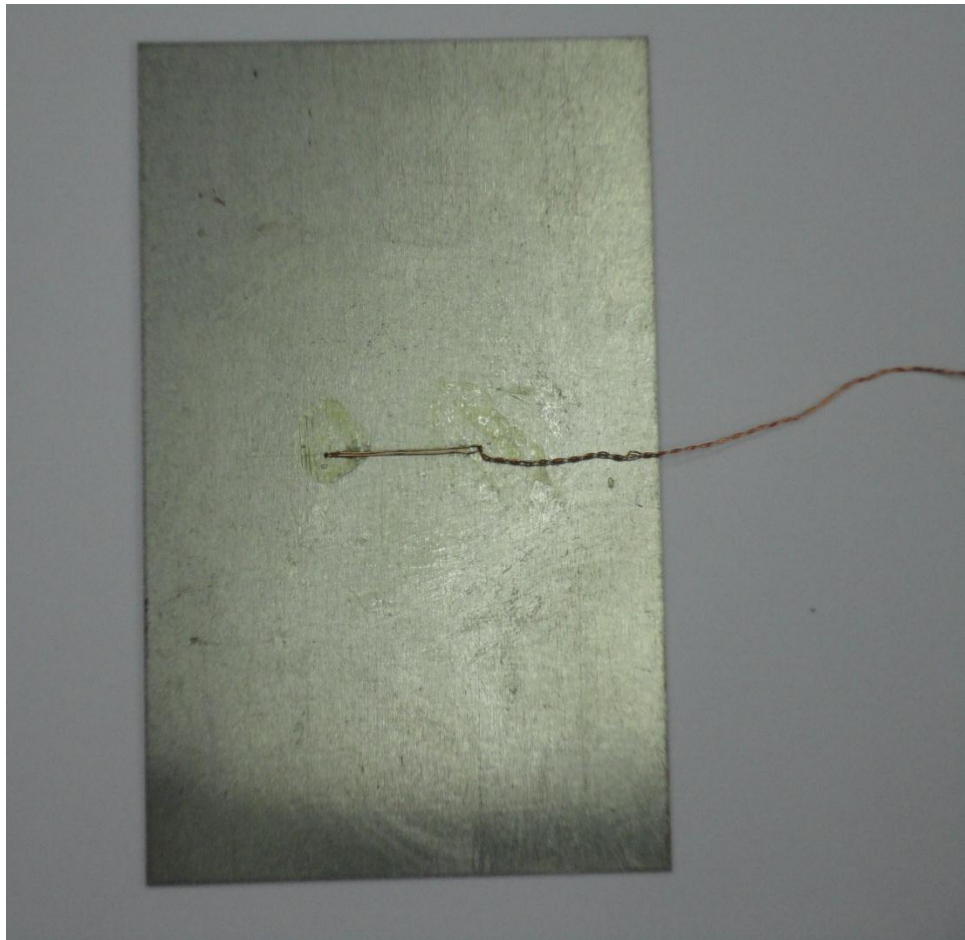


Figure 5.9 B-coil sensor

#### 5.4.2 H-coil Sensor

The magnetic field strength,  $H$  inside the specimen is detected by the single H coil placed on the surface of the specimen. Three H-coils were designed and constructed. Table 5.1 summarized the geometric designed parameters for different H-coil sensors. The (20 x 20) mm is chosen as dimension of H-coil because the uniform magnetized area can be achieved in the range of 20mm as per shown in Figure 7.2. Each H-coil densely wound around a non-magnetic former, tufnol using enamelled copper wires. The coils were fixed by solid adhesive on a tufnol to ensure high stability of sensor. The conducting leads from H sensing coil should be twisted together to minimise the influence of the magnetic field on the sensing and measuring equipment.

Table 5.1 The geometric parameters of the H-coil sensors

	H <sub>A</sub>	H <sub>B</sub>	H <sub>C</sub>
Diameter of wire, d (mm)	0.20	0.13	0.20
Former thickness, t (mm)	0.6	0.6	0.6
Width of inner dimensions of the coil, w (mm)	25	20	20
Length of inner dimensions of the coil, l (mm)	20	20	20
Number of windings, N	500	500	1000
Thickness of wire, t <sub>w</sub> (mm)	0.2	0.2	0.2

Figure 5.10 shows the features of H-coil sensor. Figure 5.11 illustrates the cross-sectional view and the location of the H coil sensor on the sample surface. The H-coil sensor must be placed very close to the sample surface so that reliable results of measurement of the sensor can be obtained. It is recommended that the H-coil should be placed about 1 mm to 3 mm from the sample as placing H-coil extremely close to the sample surface will cause deterioration of magnetic field due to the stray field from domain and grain boundaries, (S. Tumanski, 2002). Each sensor was positioned at the central part of the sheet sample where the magnetic field is more uniform and constant.

The output signal of the H-coil sensor,  $V$  at fixed frequency can be defined as

$$V = 2\pi\mu_0 Nf(w + t_w)(t + t_w)H \quad (5.1)$$

where  $\mu_0$  is permeability of free space,  $N$  is turns of winding,  $f$  is magnetization frequency, 50 Hz and  $(w+t_w)(t+t_w)$  is cross-sectional area of H-coil sensor.

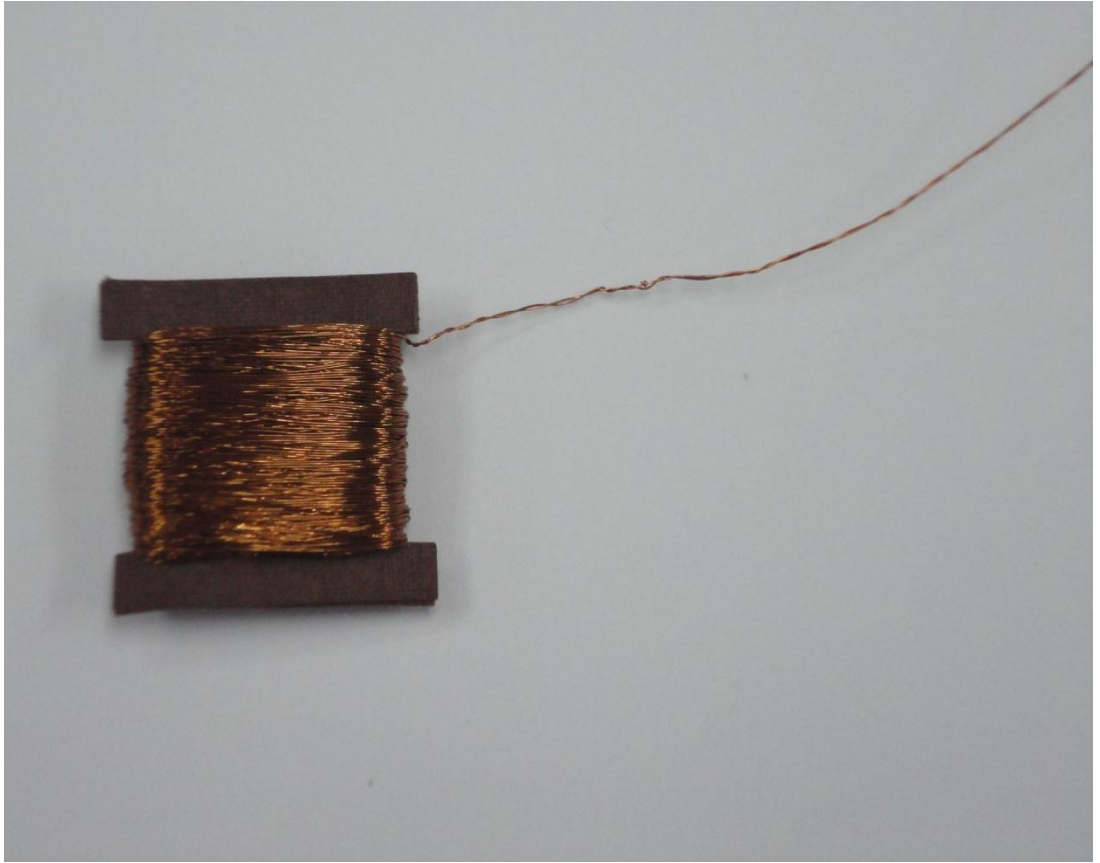


Figure 5.10 H-coil sensor

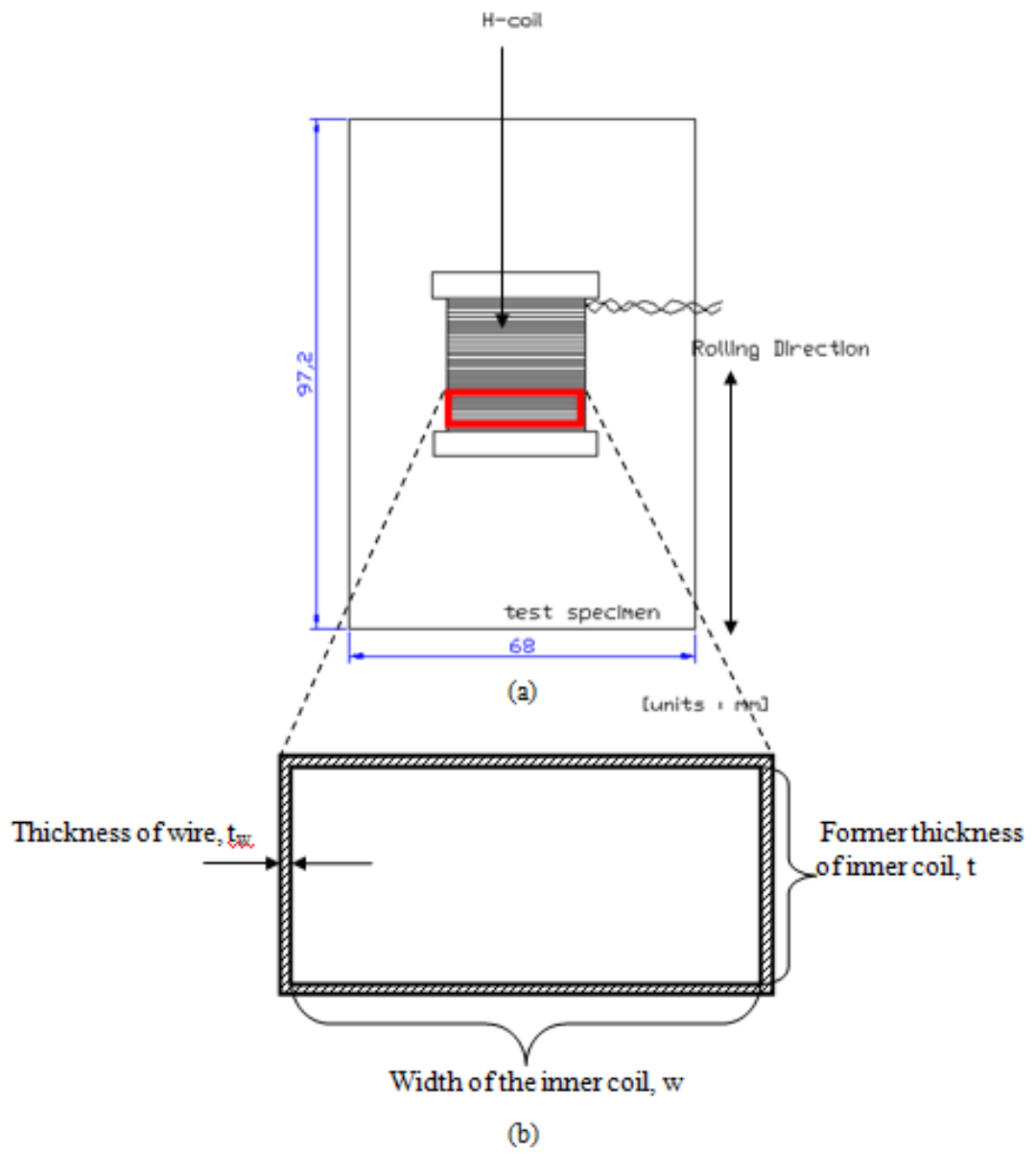


Figure 5.11 Cross-section view and arrangement of H-coil sensor in the central region of the sample

## 5.6 Development of Electronic Circuitry

The output signal of a B-coil and H-coil sensor is dependent on the small derivative of the magnetic field,  $\frac{\partial H}{\partial t}$  and flux density,  $\frac{\partial B}{\partial t}$ . Therefore, electronic circuitry which comprises of negative feedback circuit, B-channel circuit and H-channel circuit is adopted to recover the original signal.

### 5.6.1 Negative Feedback Circuit

An efficient negative feedback control is needed in order to maintain a sinusoidal shape of the magnetic induction by suitable combination of exciting waveform and the sensor output signal, (Lancarotte and Jr., 2004). The negative feedback circuit is illustrated in Figure 5.12. Each amplifier circuit was developed using TL082 operational amplifier which exhibit low noise and offset voltage drift. In every stage of feedback circuit, the gain signals were amplified and added to the sinusoidal exciting signal from the other variable transformer. The gain signal of the feedback circuit was adjusted using variable resistor. The resultant buffered signal was passed through power amplifier type, LM308 and fed to the magnetising coil.

### 5.6.2 B-Channel Circuit

The output signal of B-coil sensor is dependent on the small derivative values of field density,  $\frac{\partial B}{\partial t}$  which are in the milliVolt (mV) ranges. For that reason, the small derivative signals need to be buffered, amplified and filtered by using B-channel circuit. The circuit built using low noise and offset voltage drift operational amplifier, type TL082. The gain of  $\frac{\partial B}{\partial t}$  of each amplification stage can be selected and adjusted via

the switches and potentiometer. The potentiometer is used for offset correction and resistor is used for the limitation of the low frequency bandwidth, (S. Tumanski, 2007). The B-channel circuitry diagram is shown in Figure 5.12.

### 5.6.3 H-channel Circuit

H-channel circuit was developed to amplify and integrate the derivative output signal of H-coil sensor,  $\frac{\partial H}{\partial t}$ . This signal was fed to buffer, inverting amplifier, inverting integrator and filter circuit. The circuit diagram of H-channel is shown in Figure 5.13. An operational amplifier, type TL082 was used to construct the circuit. A buffer amplifier was used to restore stability of the signal while non-inverting amplifier provided a positive gain of input signal. The drift and offset voltage signal can be reduced by using an inverting integrator. The resultant amplified signal was passed through a low pass Bessel filter, which has a linear phase shift. Lastly, the output from the filter is buffered and measured using Oscilloscope.

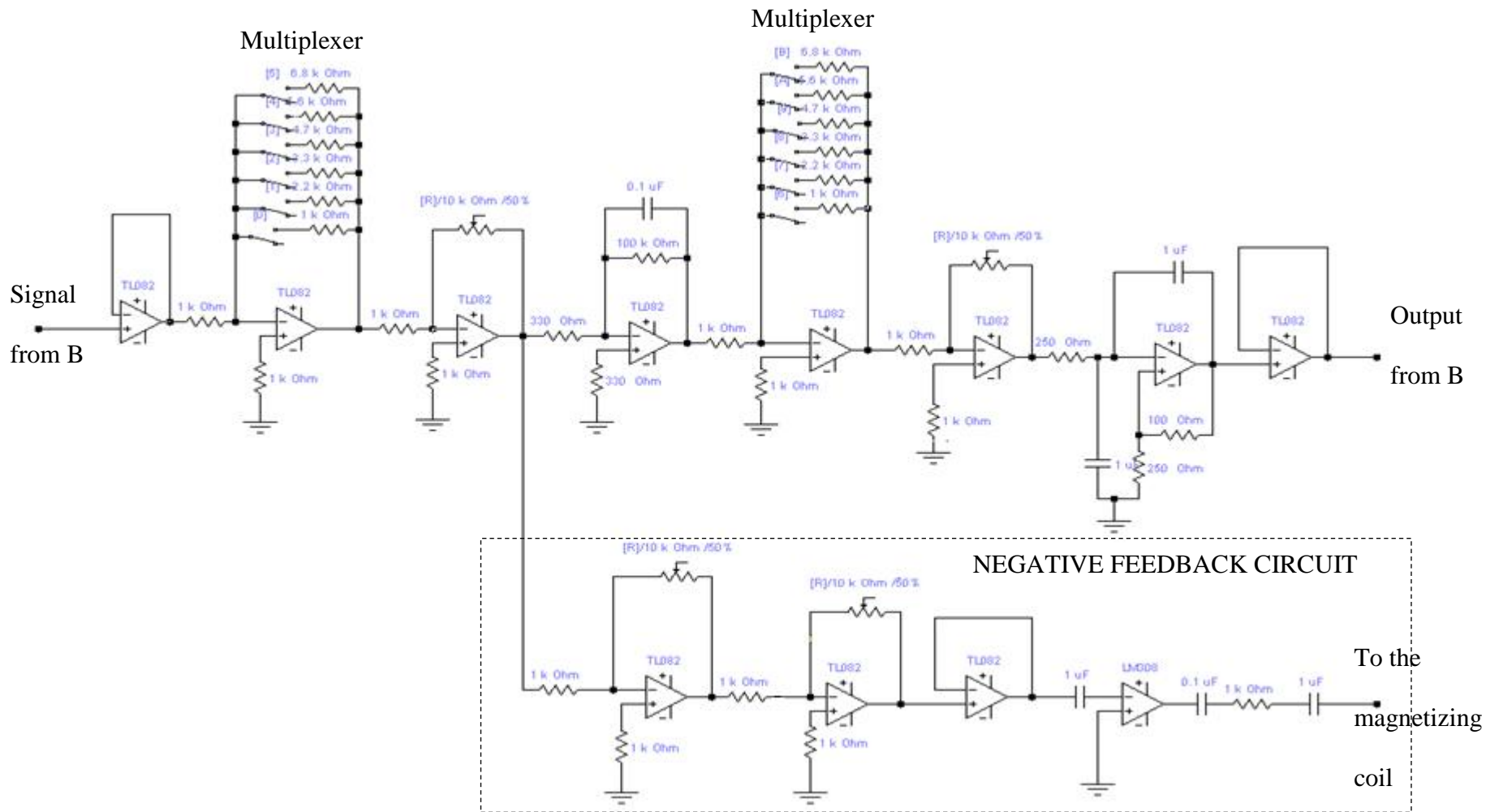


Figure 5.12 Schematic circuit diagram of negative feedback and B-channel

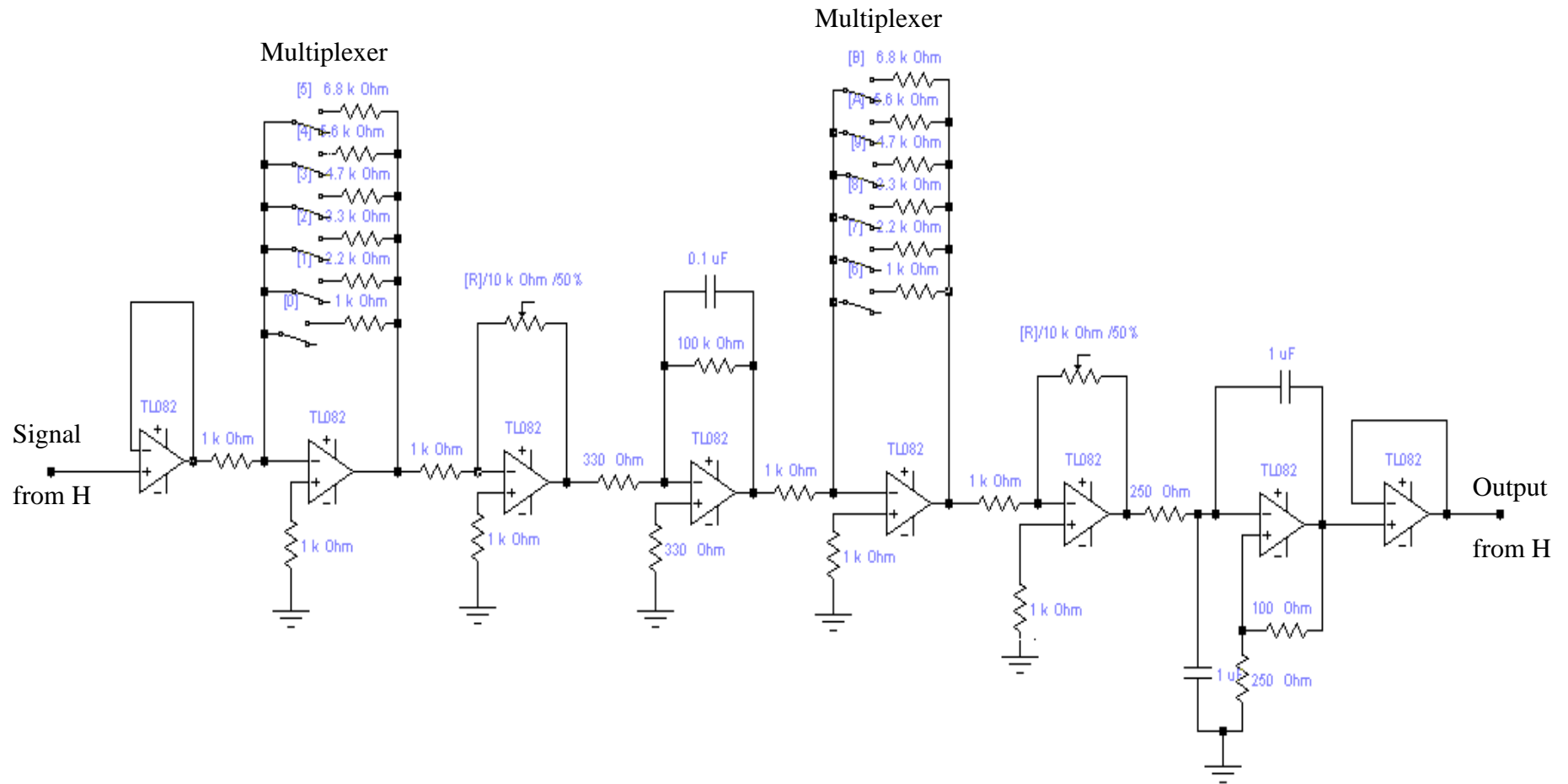


Figure 5.13 Schematic circuit diagram of H-channel circuitry

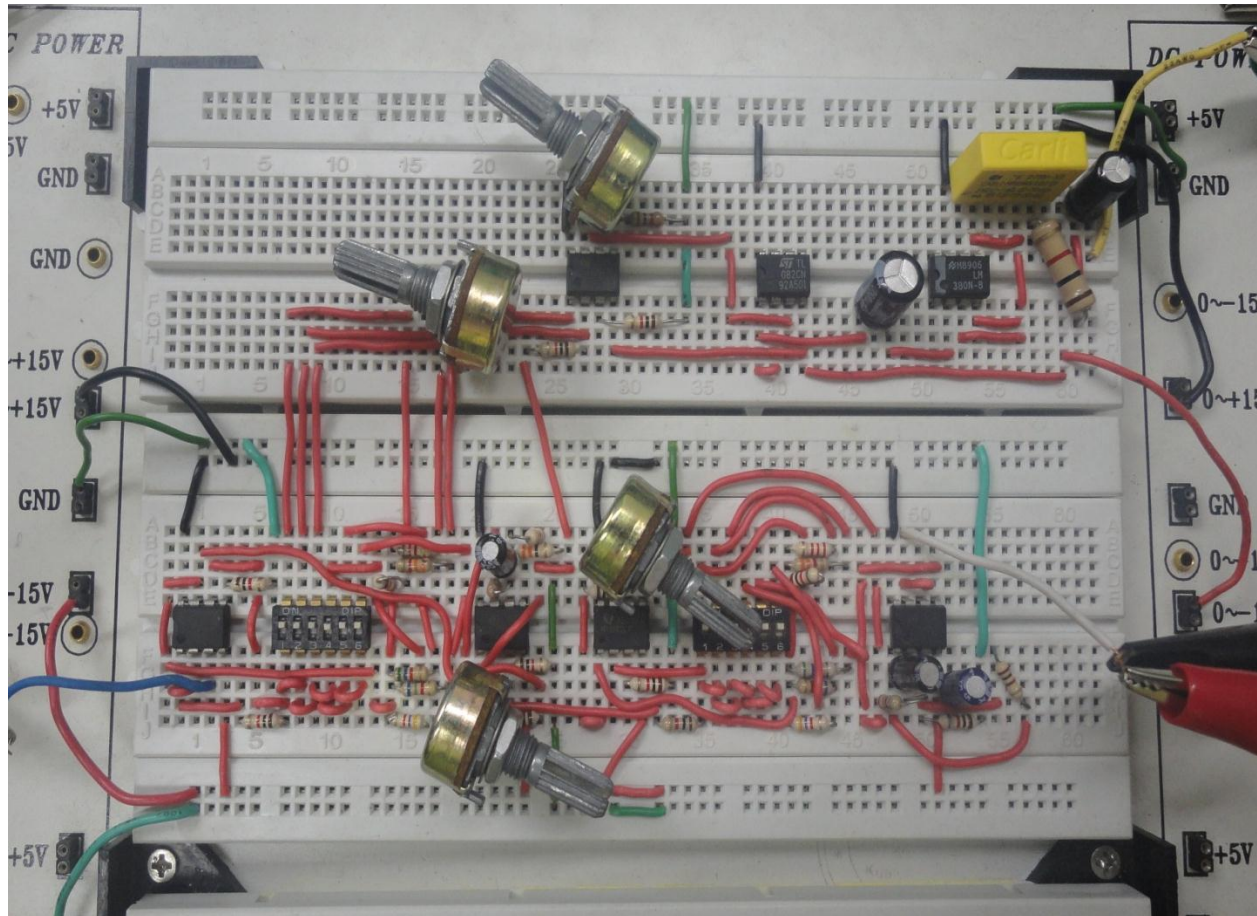


Figure 5. 14 Electronic Circuitry

## CHAPTER 6

### EXPERIMENTAL CALIBRATION

---

#### 6.0 Introduction

This chapter is concerned with the experimental calibration of H-coil and electronic circuitry. Calibration for the device under test is extremely important to ascertain the desired devices are capable in giving the reliable measurement result. The calibration of the H-coil is performed using Helmholtz coil. For electronic circuitry, the calibration is conducted using measurement based approaches.

#### 6.1 Calibration of H-Coil Sensor

The H-sensors were calibrated using Helmholtz coil as shown in Figure 6.1. It consists of two identical, thin, circular coils with 154 turns uniformly wound air cored separated by a distance of 0.20 m. Each of them was located at the centre of the circular Helmholtz coil, where the field is more homogenous and constant. The resultant e.m.f induced voltage,  $V_{e.m.f}$  of H-coil was measured using digital multimeter. Voltage induced in the H-coil is proportional to the change of magnetic flux through the coil. A different of magnetizing current,  $I$  is varying between 0.5 A to 3.0 A by adjusting the variable transformer. The magnetic field strength,  $H$  values for different magnetizing current,  $I$  can be computed using Equation 6.1 which have been derived from **Equation 2.2**.

$$H = \frac{154I}{0.4\pi} \quad (6.1)$$

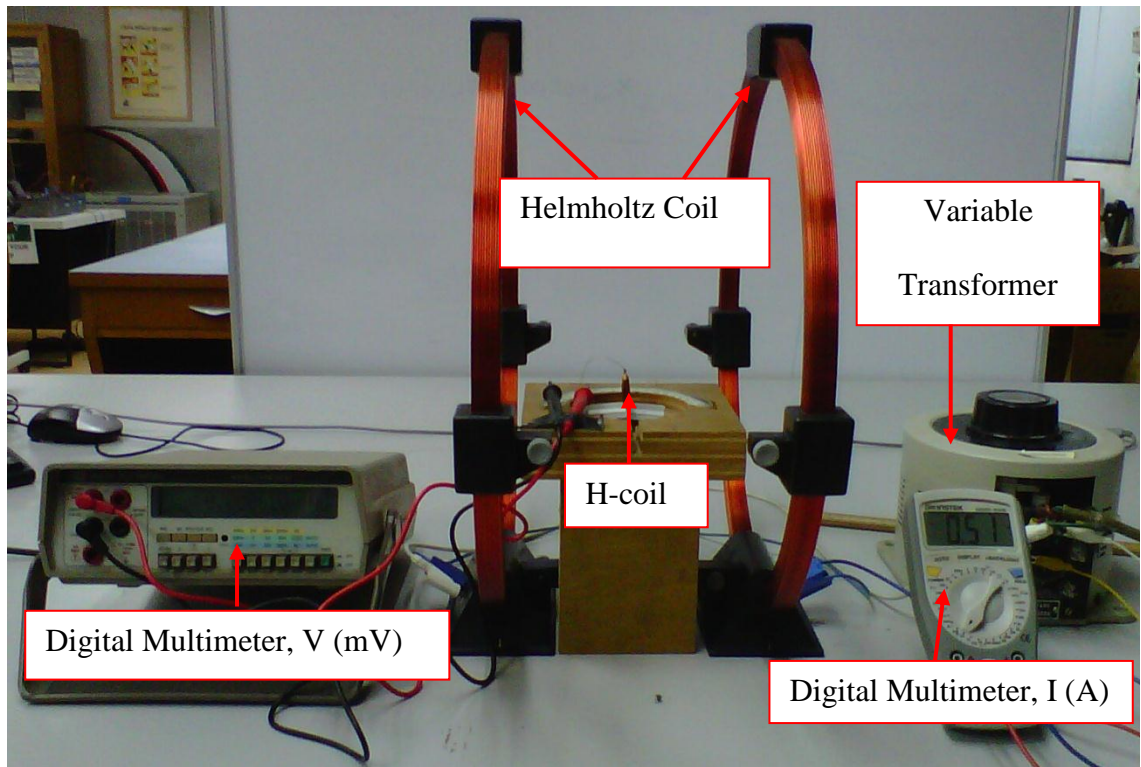


Figure 6.1 Calibration of H-coil sensor using Helmholtz coil

The sensitivity,  $S$  of the H-coil sensors can be determined by using Equation 6.2, where  $V$  is the e.m.f induced voltage and  $H$  is the magnetic field strength.

$$S = \frac{V}{H} \quad (6.2)$$

By combining Equation 2.19 and Equation 6.2 gives

$$S = -\mu_0 N(w+t_w)(t+t_w)f \quad (6.3)$$

where  $\mu_0$  is permeability of free space,  $N$  is turns of winding,  $f$  is magnetization frequency, 50 Hz and  $(w+d)(t+d)$  is cross-sectional area of H-coil sensor, A. Graph of magnetic field strength,  $H$  against voltage induced in H-coil winding,  $V_{e.m.f}$ , for H-coil was plotted. The calibration factors of H-coil,  $k$  was obtained from the slopes of the graphs. Table 6.1 summarized the sensitivities and calibration factors for different dimension of the H-coil sensors.

Table 6.1 The parameters of the H-coil sensors

	H <sub>B</sub>	H <sub>A</sub>	H <sub>C</sub>
Diameter of wire, d (mm)	0.20	0.13	0.20
Former thickness, t (mm)	0.6	0.6	0.6
Width of inner dimensions of the coil, w (mm)	20	20	20
Length of inner dimensions of the coil, l (mm)	20	20	40
Number of windings, <i>N</i>	500	500	1000
Thickness of wire, t <sub>w</sub> (mm)	0.2	0.2	0.2
Calibration factor, k (10 <sup>3</sup> (A/m)/V)	249.43	191.84	69.90
Sensitivity, <i>S</i> (μV/(A/m))	4.01	5.21	14.31

The H-coil, H<sub>A</sub> with dimensions (20 x 20) mm and inner thickness 0.6 mm wound with 500 turns of 0.2 mm wire exhibited the sensitivity at about 4.01 μV/(A/m). The H-coil, H<sub>B</sub> with the same dimension and number of turns but wound with 0.13mm diameter of wire exhibited the sensitivity at about 5.21 μV/(A/m). The sensor, H<sub>C</sub> with same dimension and diameter of wires as H<sub>A</sub> except for having 1000 turn exhibited higher sensitivity at around 14.31 μV/(A/m). A larger number of turns are essential so that higher induced e.m.f voltage can be achieved. As conclusion, the sensitivity of H-coil sensor can be increased using higher number of turns, *N*, thinner wires and having large cross-section area of the coil, *A*, as stated in **Equation 6.3**. Later, the H-coil with dimension of (20 x 20) mm and inner thickness 0.6 mm wound with 1000 turns of 0.2 mm wire is used in experiment as magnetic field sensor throughout this research.

## 6.2 Calibration of Electronic Circuitry

The calibration of the circuitry is needed to ensure the accuracy and verifiable performance of the circuit. Each stage of the circuit was individually tested by applying the input signal, *V*<sub>in</sub> and the resultant output, *V*<sub>out</sub> can be observed using Cathode-Ray Oscilloscope (CRO) and Digital Voltmeter (DVM). Figure 6.2 presents the

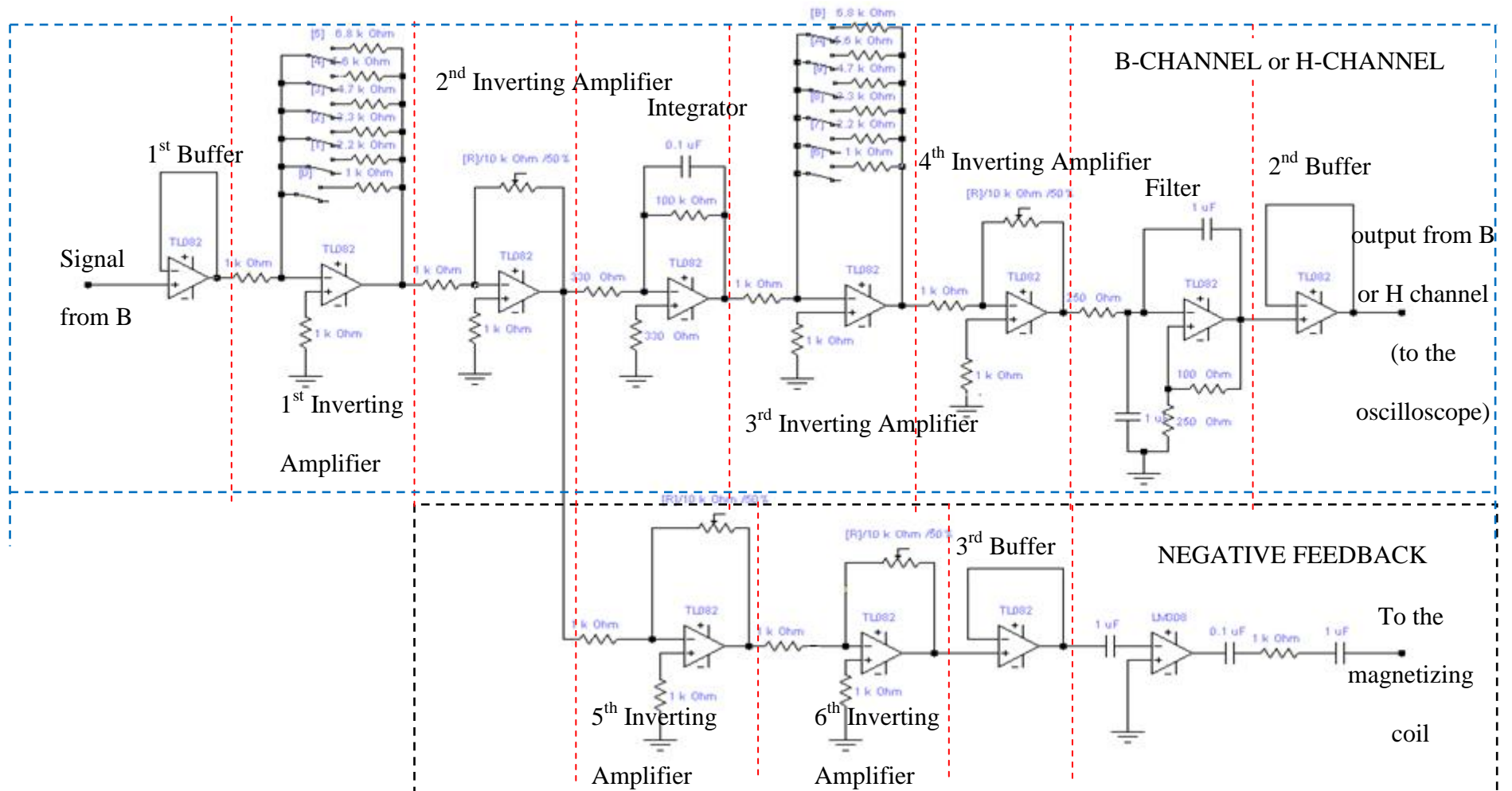


Figure 6.2 Calibration of electronic circuitry

calibration's stage of electronic circuitry. The corresponding gain values of each stage were calibrated by inserting several known a.c signal into B-channel and H-channel input and measuring the output of B-channel and H-channel by adjusting the variable resistors to achieve the required amplification. The gain of the buffer and integrator were calibrated by inputting known input signals and measuring the resulting output. The calibrated gains of each stage were found to be within 0.2%. The typical input and output for overall calibration of electronic circuitry are shown in Figure 6.3.

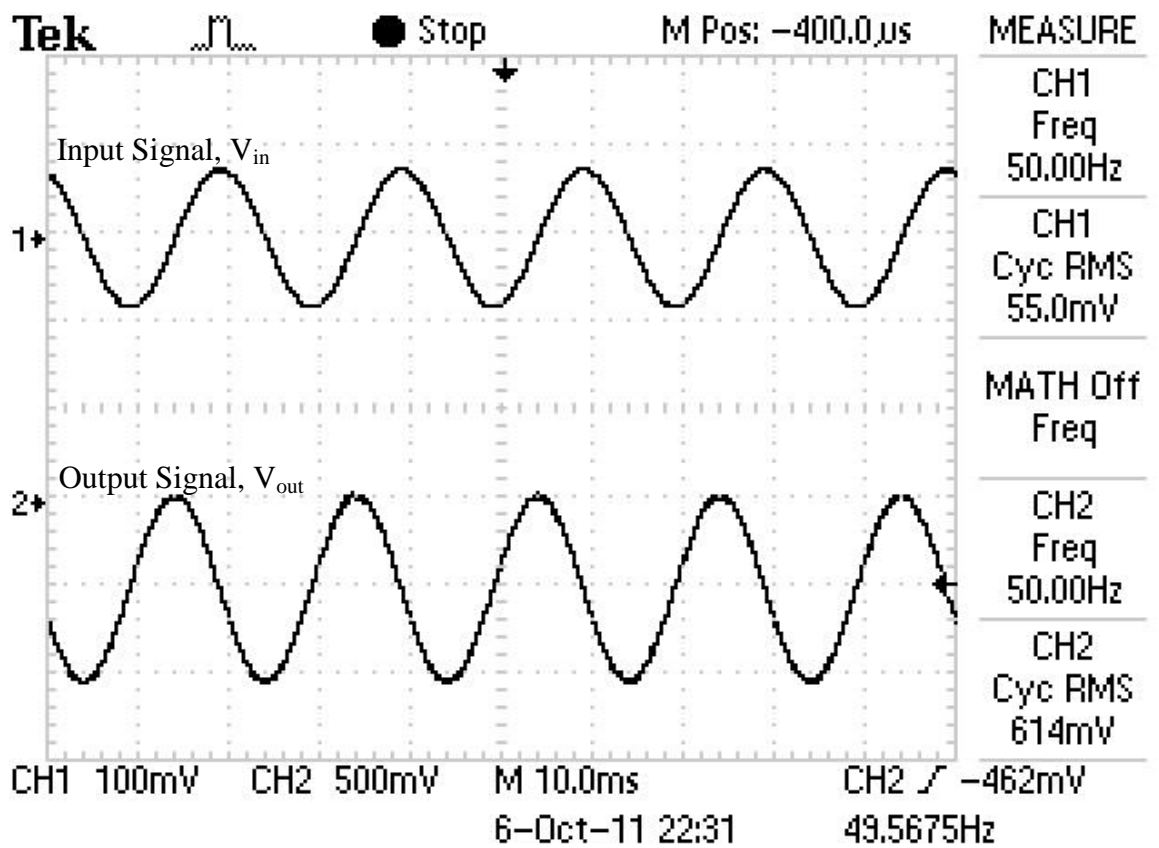


Figure 6.3 Input and output signal waveforms for the electronic circuitry calibration

## CHAPTER 7

### RESULT AND DISCUSSION

---

#### **7.0 Introduction**

This chapter presents the results of optimization on magnetizing system, magnetic sensor's positioning and evaluation on magnetic materials from the simulation and experiment. The results were evaluated in terms of their magnetic properties characteristics, field and flux distribution plots and through statistical analysis approaches. Later, these results can provide a better understanding of the effect of the Single Sheet Tester on magnetic properties of electrical steels at low frequency, 50 Hz.

#### **7.1 Finite Element Method Magnetic (FEMM) Simulation**

The assessments of electrical steel sheets were carried out using FEMM. FEMM simulation was used to optimize the design of one-dimensional magnetic measurement.

##### **7.1.1 Optimization of Magnetic Sensor's Positioning**

Magnetic sensors used for the measurement of the flux density, B-sensor, and magnetic field strength, H-sensor, play an important role in magnetic measurement since they were adopted to measure the magnetic properties of electrical steels. In Finite Element Method Magnetic (FEMM) software, the magnetic field and flux density can be measured directly by pointing the specific location on the sample under test. The positioning of these sensors is crucial factor in determine the uniform magnetization within the sample. For that reason, a horizontal double yoke single sheet tester, SST at dimension (97.2 x 93.4 x 68) mm was developed. The magnetizing winding contains 180 turn of 18 SWG copper wires. A 3% grain-oriented electrical steel, grade M4 was placed in between the right yoke and left yoke with air gap insertion at about 0.3mm.

The sensors were positioned at five different locations on the sample under test as illustrated in Figure 7.1.

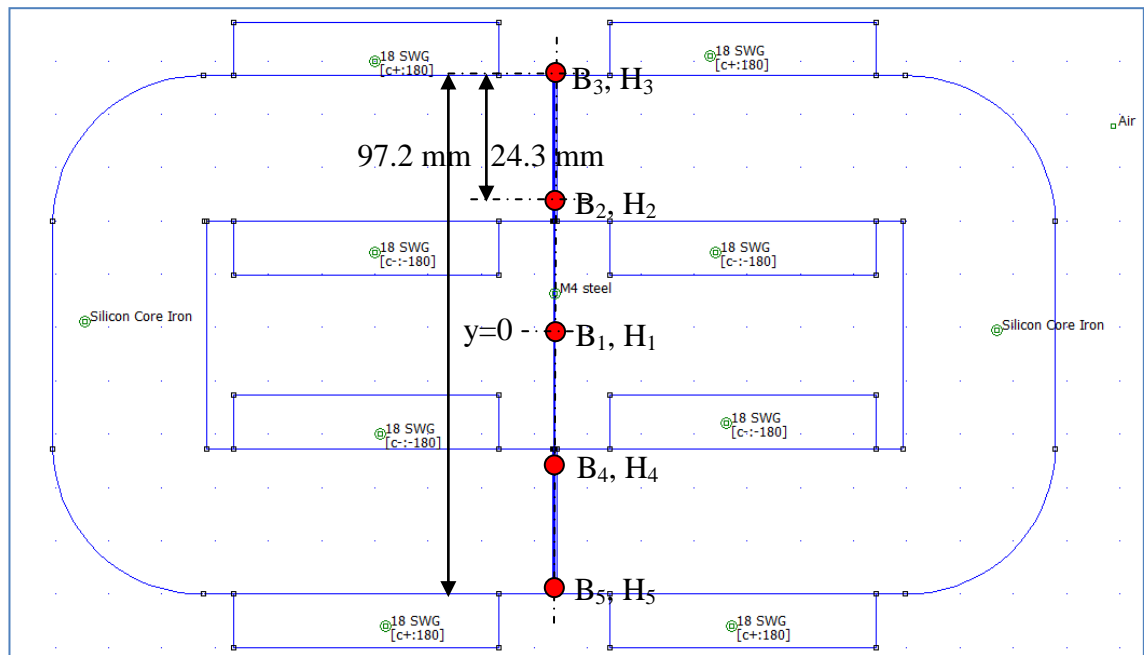


Figure 7.1 Positioning of magnetic sensors along the sample

Figure 7.2 and Figure 7.3 represent the field and flux distribution of grain oriented, M4 measured by sensors at different location at current about 1.2A. The sensors were located at different places indicated by sensor 1:  $B_1, H_1$ ; sensor 2:  $B_2, H_2$ ; sensor 3:  $B_3, H_3$ ; sensor 4:  $B_4, H_4$  and sensor 5:  $B_5, H_5$ , Figure 7.1. The zero point is the centre of the sample. Figure 7.2 and Figure 7.3 show that the magnetic field strength and flux density are distributed regularly in the middle part of the sample between yoke pole faces. This is due to a large permeability of the sample, forced all flux flows only in the area between poles of the yokes, (S. Tumanski, 2003),(F.Fiorillo, 2010).

The highest and uniform alternating field at current 1 A can be achieved at around 2.3T and 247.53 A/m when the sensor;  $B_1, H_1$  was positioned at the centre of sample. The magnetic saturation for grain oriented steel, grade M4 are given as 2.4 T. From the obtained curves, it can be seen that the side length of square are magnetized homogenously is about 20mm. As the sensors;  $B_2, H_2, B_3, H_3, B_4, H_4, B_5, H_5$  were positioned away from the middle of sample, the field and flux distribution were dropped regularly.

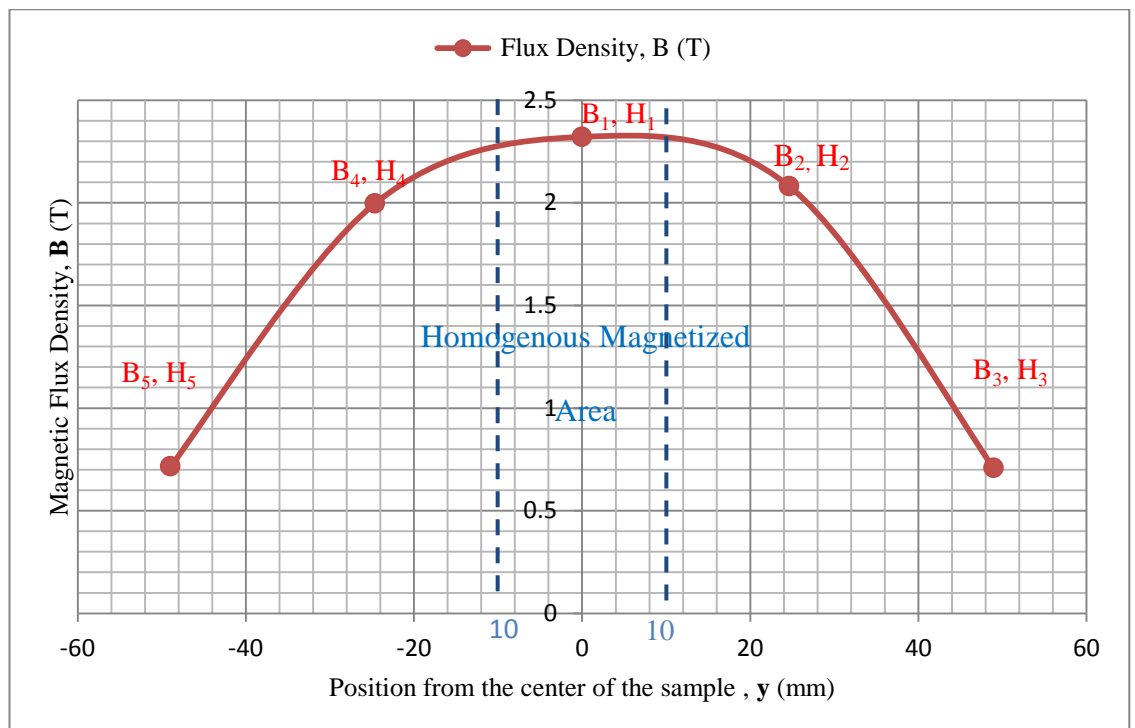


Figure 7.2 Flux distributions along grain-oriented electrical steel, grade M4

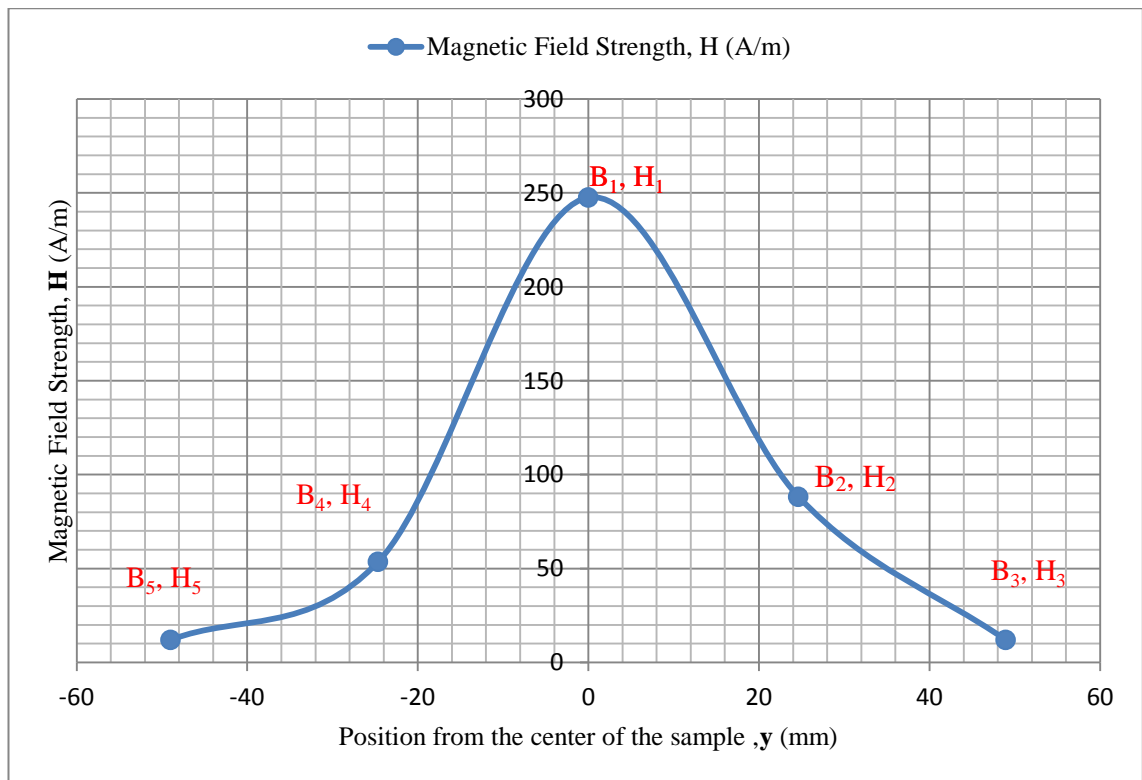


Figure 7.3 Field distributions along grain-oriented electrical steel, grade M4

It is very important to decide suitable sensors which dimensions of sensitive element that comparable with grain area. This is due to the grain size of standard electrical steel does not exceed several tens of millimetres, (Fryskowski, 2008). The B-sensor and H-sensor must be placed in the middle of sample between the poles of the yokes near the symmetry centre where the homogenous magnetized area can be achieved. The measurement should be carried out in the region of uniform magnetic field to accurately measure the magnetic properties. The finding is in agreeable with other researchers, (Zurek et al., 2008),(Miyagi, et al., 2009).

## 7.1.2 Optimization of Single Sheet Tester (SST) Set Up

### 7.1.2.1 Assessment of Air Gap

The influence of air gap between the samples under test and the C-core pole faces is investigated on 0.28 mm of 3% grain-oriented silicon iron steel, grade M4. The sample was magnetized under alternating magnetization conditions, utilizing the double yoke SST arrangement with current ranging from 0.2 A to 2.4 A, at 50 Hz at each air gap length. The magnetic sensors; B-coil and H-coil are positioned in the middle of the sample under test. The air gap was inserted between the C-core pole faces and the sample under test and was set at effective air gap, 0.3 mm, 0.5 mm, 0.8mm and 1.0 mm. An identical air gap was placed at both yoke faces as illustrated in Figure 7.4 and Figure 7.5.

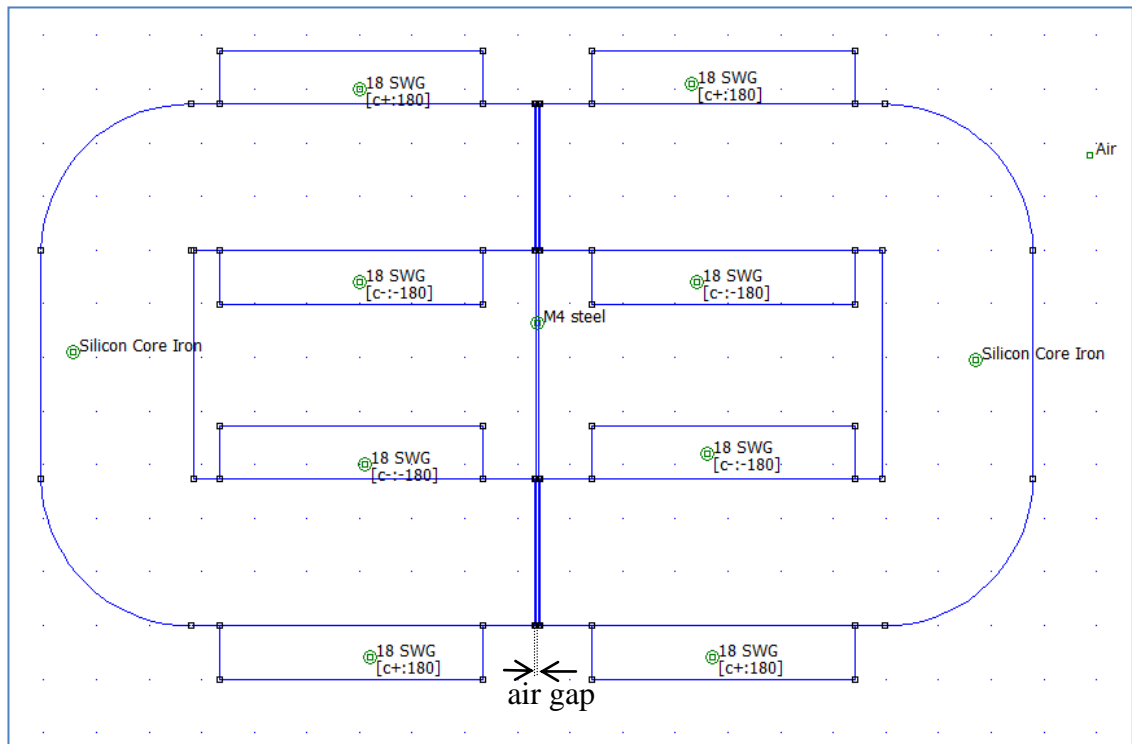


Figure 7.4 Side view plot of SST set up with air gap insertion (0 mm)

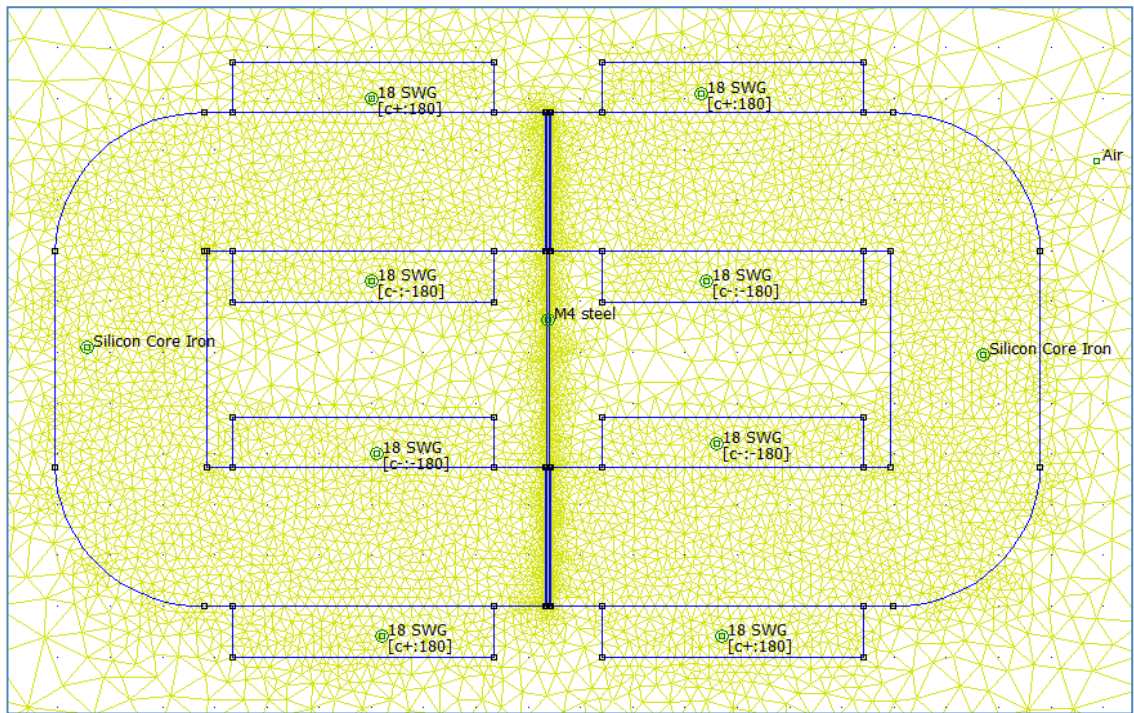


Figure 7.5 Mesh plot of SST set up with air gap insertion (0.3 mm)

Figure 7.6 demonstrates the zoomed-in view of the flux plot variation of air gap insertion to the SST set up. The corresponding solid black lines indicate as a flux line pattern flow through the sample under test and the corresponding colours indicated as magnitude of field strength. In the presence of effective air gap, the yellowish colour and solid lines show that there is a large non-uniformity of flux distribution between the yokes and sample under test, in Figure 7.6 (a). When air gap length of 0.3 mm was introduced between the yokes pole faces and the sample, the flux distribution can be clearly seen become uniform and homogenous, Figure 7.6 (b). This behaviour can be explained as due to the air gap enlarge the yokes reluctances and lessen the flux density in the yoke as well as in the gap. More energy is required to drive the same flux across the air gap than through an equal volume of the yokes due to much lower permeability of the air, (Jiles, 1991). This eventually enhanced the field homogeneity within the sample.

Figure 7.7 and Figure 7.8 shows the magnetizing curve of non-oriented sample, M4 for different air gap length at different ranges of current. Results indicate that the magnetic field strength,  $H$  is increased linearly with the current,  $I$ . However, for magnetic flux density,  $B$ , as the current is being amplified, the  $B$  is increased until it reached its saturation magnetization level. It can be seen that for air gap length at 0.3mm, it requires only 1.2 A to magnetize the sample to its saturation magnetization at 2.3 T with  $H$  at around 356 A/m. However, when the air gap was increased up from 0.5 mm to 1 mm, more deviation of magnetic properties of sample can be observed. As air gap increases, results suggest that more magnetizing current is needed to magnetize the sample to the required saturation magnetization level. This is due to the increase in the yoke reluctance which eventually leads to the flux leakages, (Chakraborty, 2005).

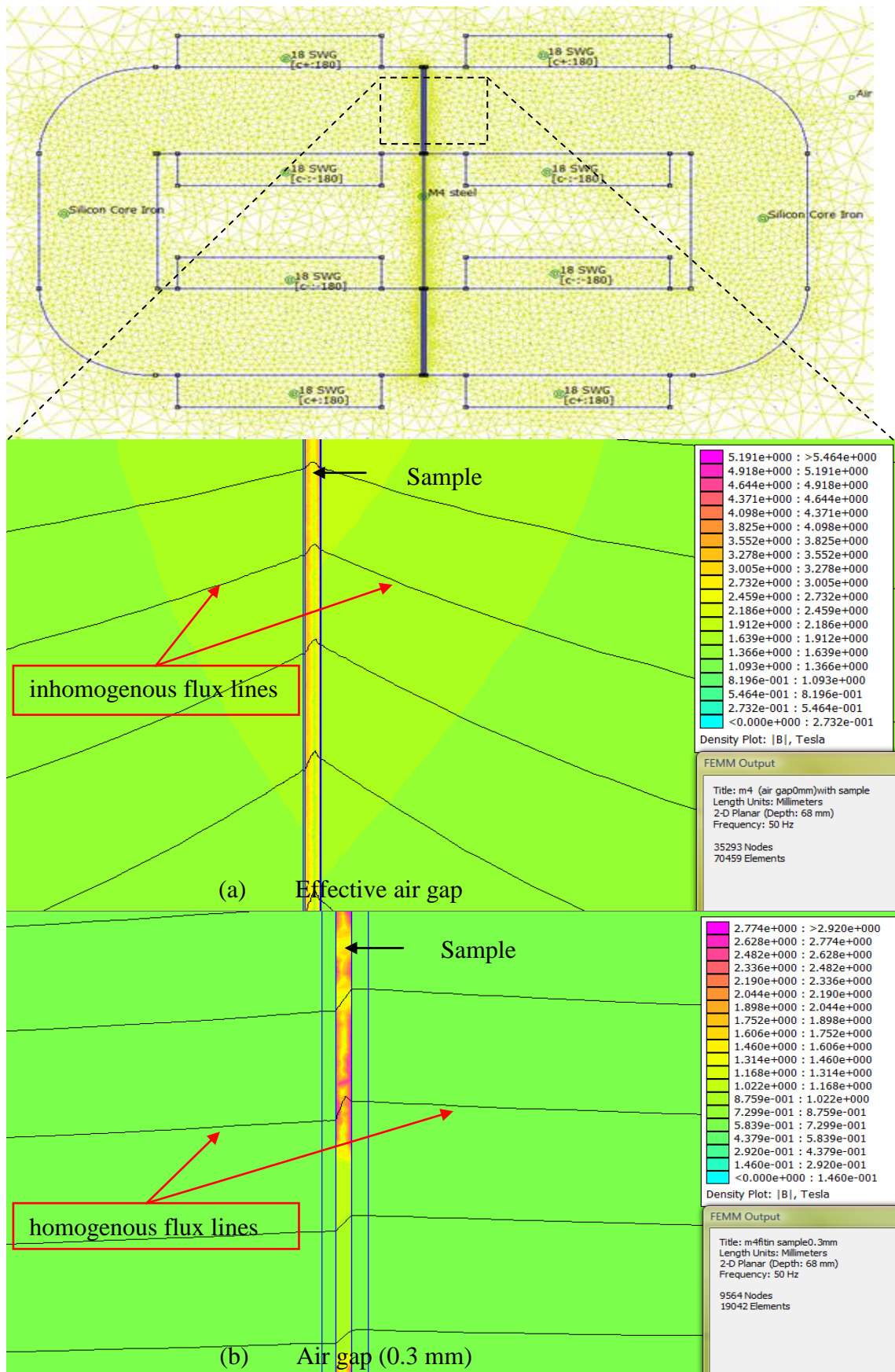


Figure 7.6 Flux plot of air gap length at (a) effective air gap and (b) 0.3 mm for grain-oriented sample, M4 (zoomed-in-view)

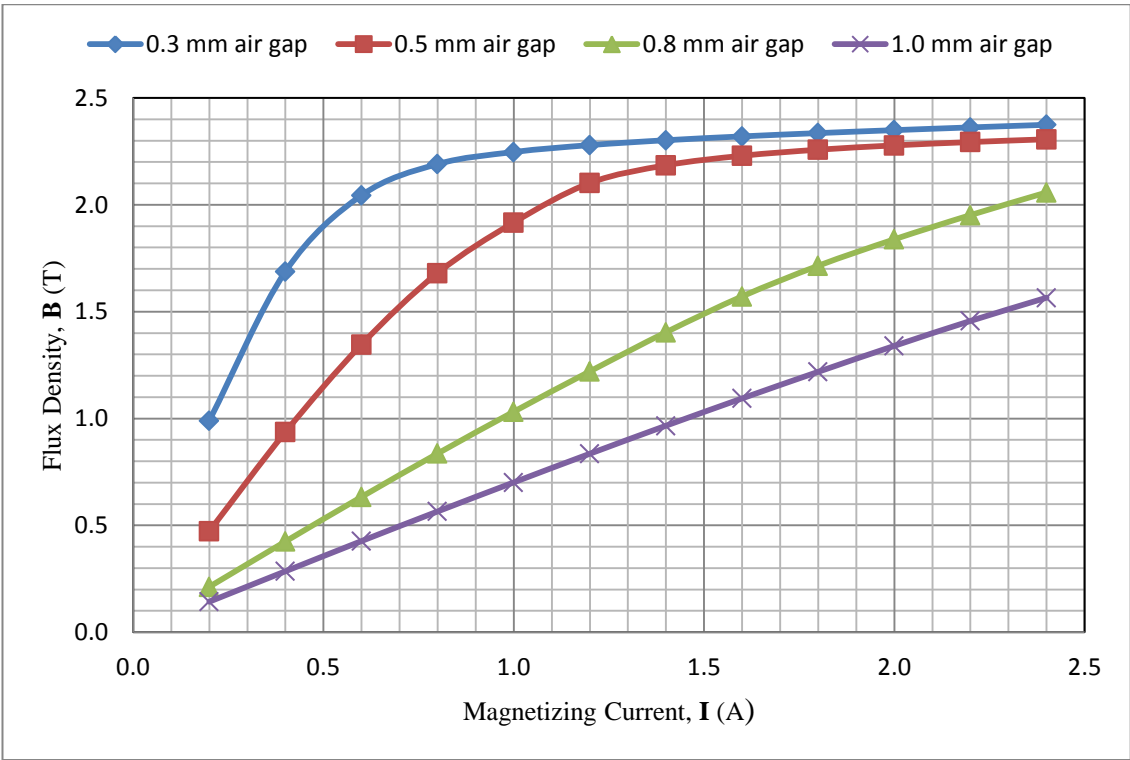


Figure 7.7 Flux density waveforms for different air gap length

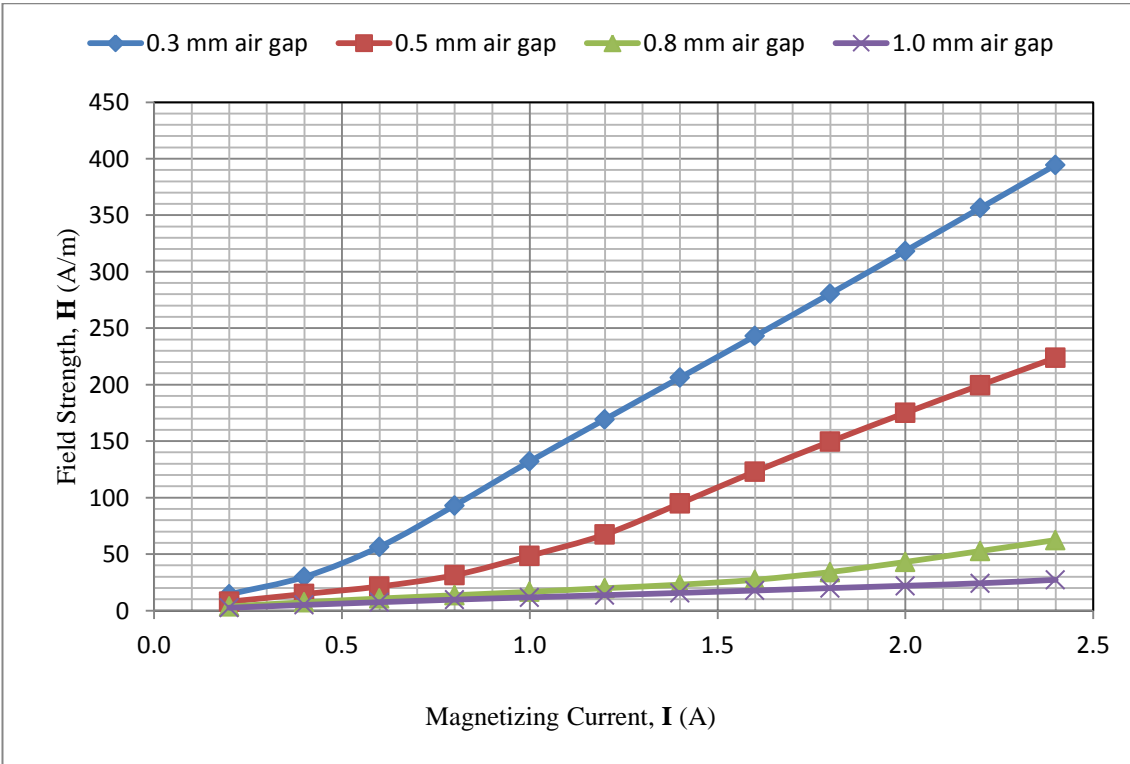


Figure 7.8 Field strength waveforms for various air gap lengths

The stray flux distribution at yokes pole faces with the different insertion of air gap is illustrated in Figure 7.9. The solid lines referred as flux lines pattern flow through the sample and the corresponding colours indicated as magnitude of field strength. For air gap length at 0.3 mm, it can be seen that more concentrated flux is flowing through the sample. The flux leakage appeared when the air gap length is increased at about 0.5 mm to 1 mm. The findings show that the lengthy air gap lead to worse conditions of the flux penetration and, hence decreasing the magnetic properties of sample, (Stupakov, 2006). Results obtained show that homogeneity of field and flux distribution of sample can be obtained by introducing an air gap length at 0.3 mm, which then applied throughout the investigation.

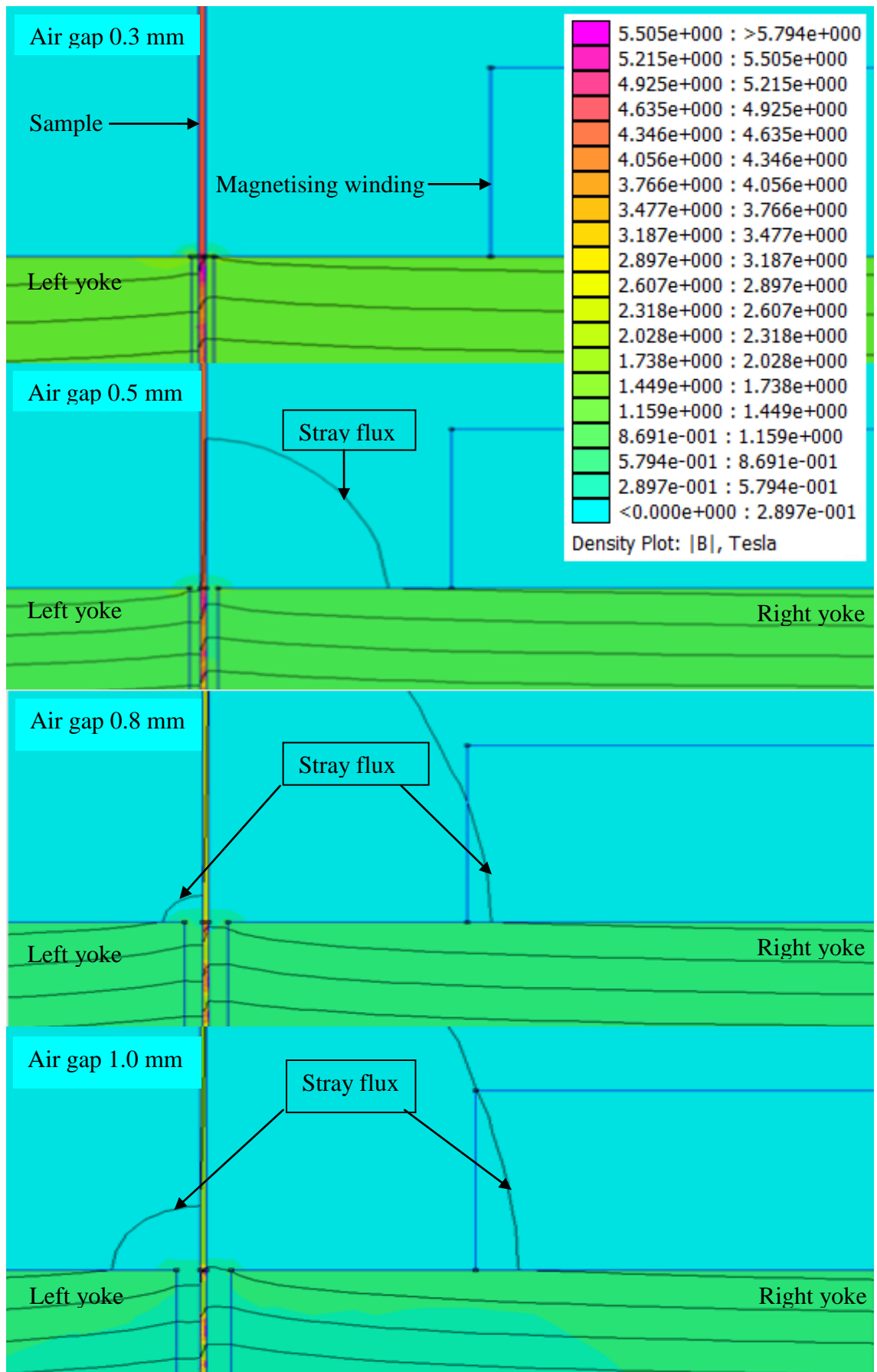


Figure 7.9 Stray flux distributions of various air gap lengths insertion

### 7.1.2.2 The Effect of Yoke's Dimension

In analysing the accuracy of magnetizing measurement, the influence of yokes (also known as C-cores) geometry was also taken into account. Two sets of magnetizing Single Sheet Tester (SST) set up were constructed to investigate the effect of core's dimension. A former double yokes SST, Yoke A with dimension of (97.2 x 93.4 x 68.0) mm is shown in Figure 7.10. The optimization of the yoke is carried out using Yoke B with dimension of (145.8 x 140.1 x 68.0) mm, Figure 7.11. A mesh view plot for different dimension of double yoke SST was displayed in Figure 7.12. The measurements were performed on the 0.28 mm thick grain-oriented sample; grade M4 at a frequency of 50 Hz. An air gap of 0.3mm was placed between the samples and yoke pole faces. The field and flux were measured in the middle of the sample under test.

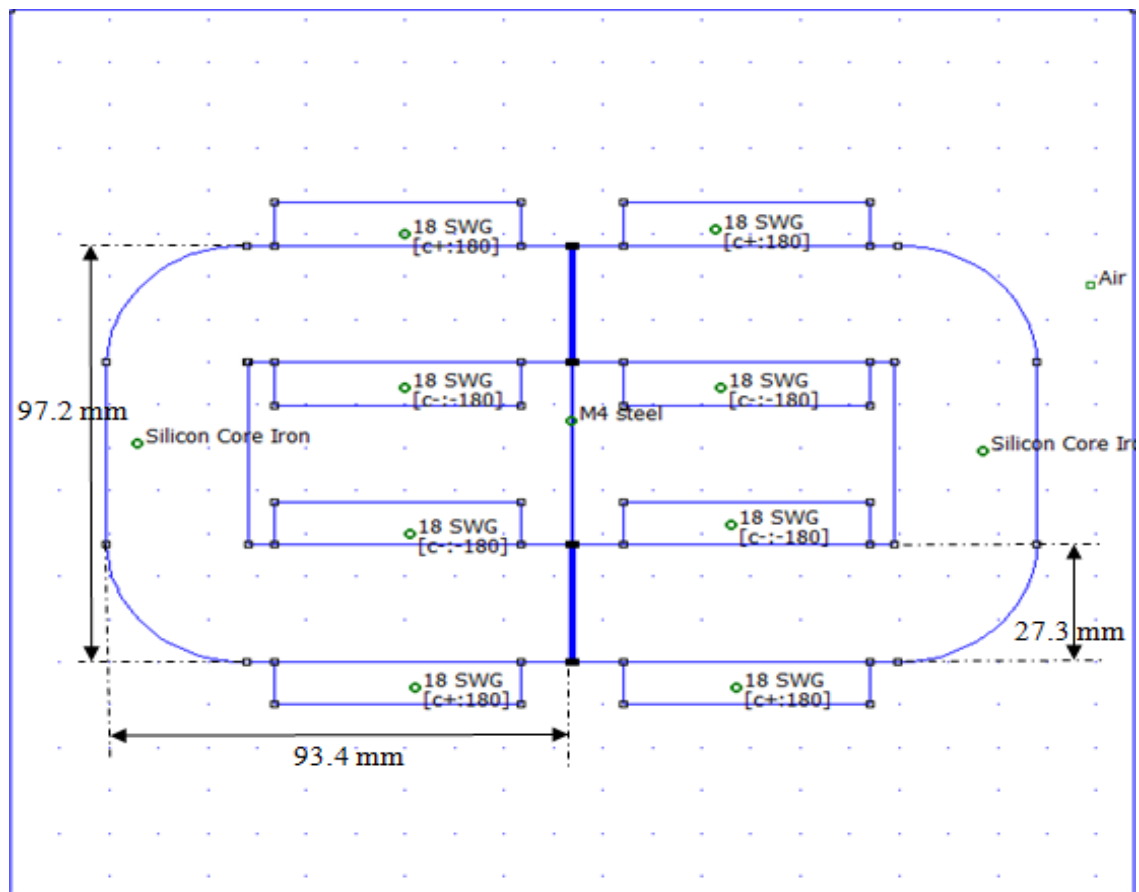


Figure 7.10 Yoke A with dimension of (97.2 x 93.4 x 68.0) mm

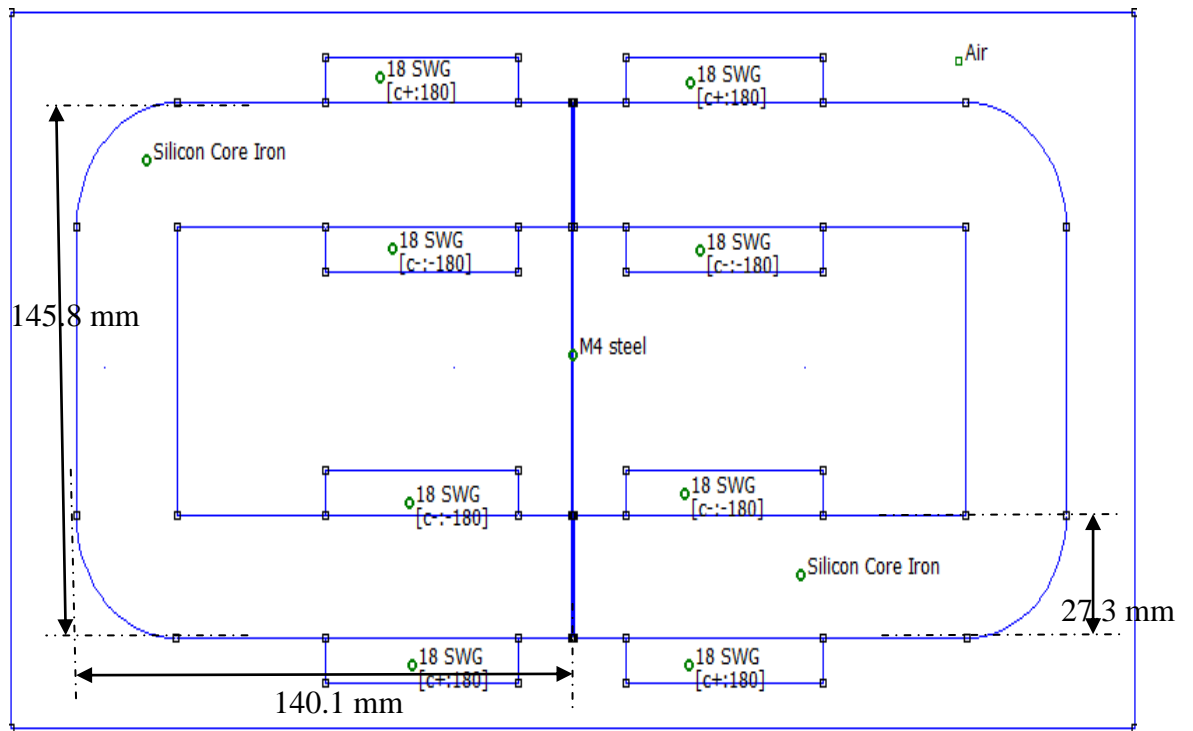


Figure 7. 11 Yoke B with dimension of (145.8 x 140.1 x 68.0) mm

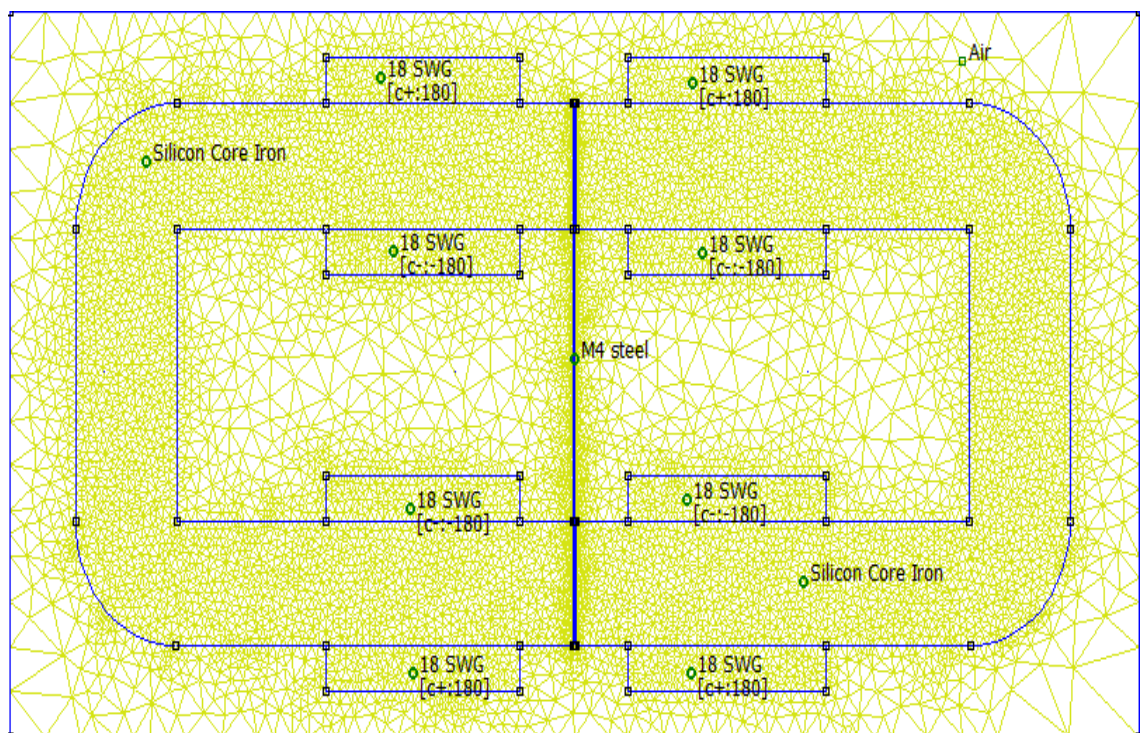


Figure 7.12 A mesh view of Yoke B

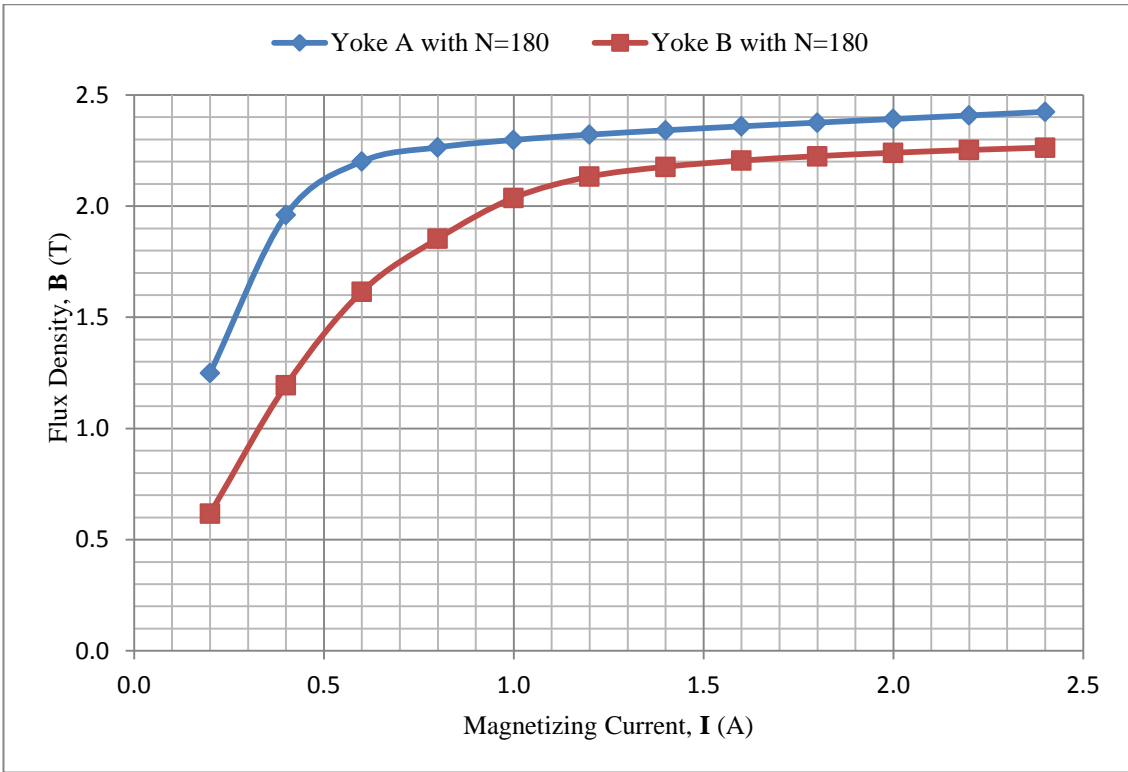


Figure 7.13 Comparison of flux density distribution for Yoke A and Yoke B

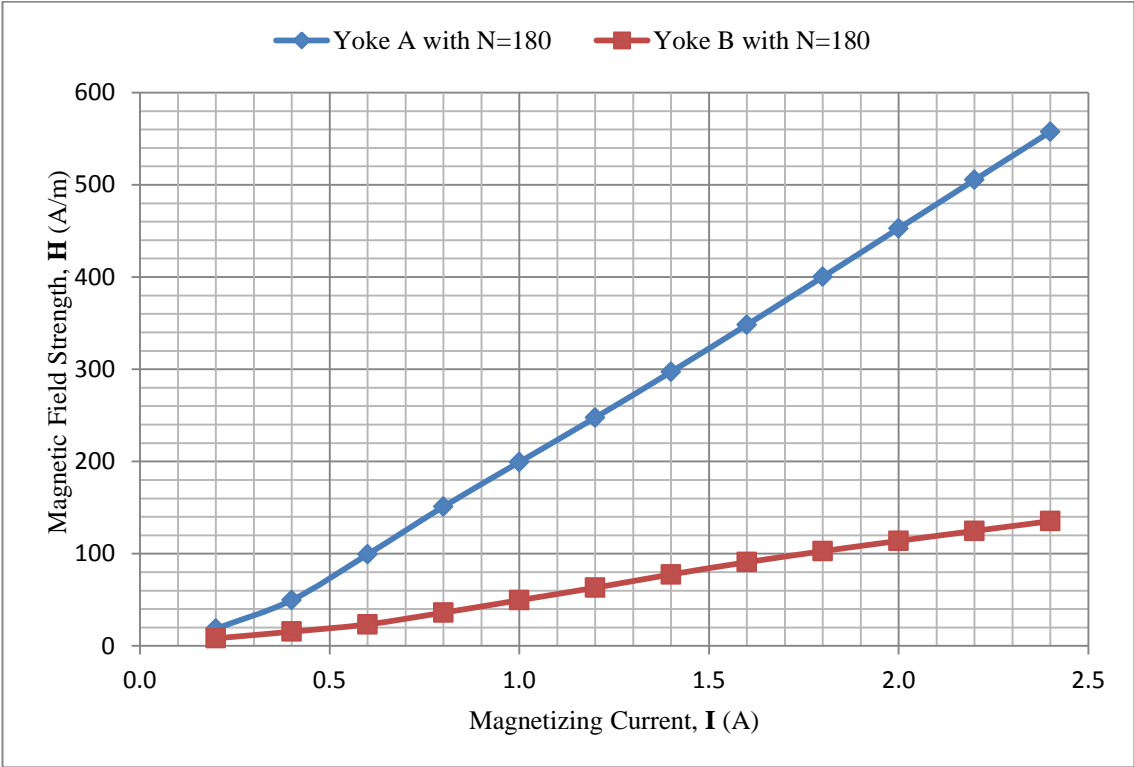


Figure 7.14 Comparison of magnetic field strength distribution for Yoke A and Yoke B

Figure 7.13 and Figure 7.14 show the graph of magnetic flux density,  $B$  and magnetic field strength,  $H$  against magnetizing current,  $I$  for two different dimensions of double yokes SST with the magnetizing winding,  $N$  of 180 turns. As it clear from the Figure 7.14, the magnetic field,  $H$  increases with the increasing current,  $I$ . On the other hand, the flux density,  $B$  is nonlinear whereby it raised linearly until it is magnetically saturated, Figure 7.13. The use of 3 % silicon core is to confine and guide the magnetic field lines to be concentrated in the core material, (Wikipedia, 2011). The presence of magnetic core can increase the strength of magnetic fields produced by a coil. In case of Yoke A with dimension of (97.2 x 93.4 x 68) mm, it only requires 0.6 A to magnetise the sample, M4 to maximum flux density at 2.20 T. In contrast, for a Yoke B with dimension of (145.8 x 140.1 x 68) mm, a higher current of 1.6 A is required to magnetize the sample to a same desired flux density.

A higher deterioration of magnetic measurement results can be observed once the Yoke B was used as a magnetic core, Figure 7.13 and Figure 7.14. For instance, at current 0.6 A, the percentage difference of flux density and magnetic field strength measured at the centre of the sample for Yoke and Yoke B were reduced at 26.6 % and 76.4%, respectively. According to Ampere's circuital law as described in **Equation 2.10**, the magnetic field,  $H$  produced by a magnetic circuit depended on the conduction path of circuit,  $L$  and the current carried,  $I$ . At current,  $I=1$  A, the magnetic field for Yoke A is about 49.60 A/m whereas for Yoke B is obtained as 199.34 A/m. With regards to these field strength values, the obtained mean length,  $L$  around the yokes is found 900 mm and 3630 mm for Yoke A and Yoke B, respectively. It can be seen that flux density is proportional linearly to current and inversely proportional to flux path length. The Yoke B with dimension of (145.8 x 140.1 x 68) mm provided a high reluctance flux closure path. Therefore, a large current and turns of wire is necessary in

order to increase the strength of magnetic fields in the core. Noticed that, an 18 SWG copper wires only can handle current up to 3 A.

The corresponding flux plot for Yoke A and Yoke B at 2.0 A is presented in Figure 7.16. The increase of yoke's dimensions have led to lower sample magnetization and causing additional flux leakage between the yoke legs, (Stupakov, 2006). This affects a deviation in magnetic field and flux density measurement.

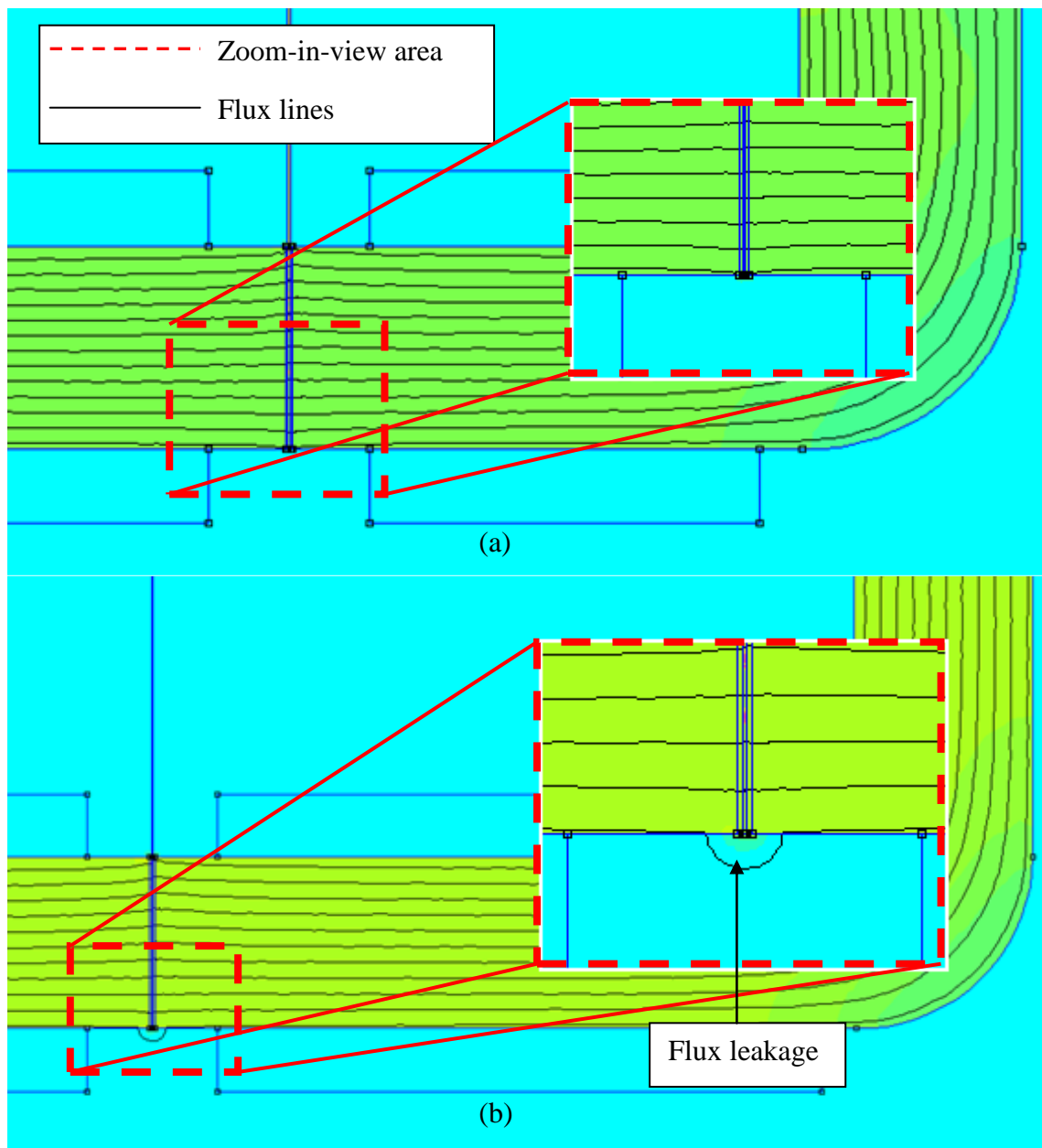


Figure 7.15 Zoom-in-view of flux plots for (a) Yoke A with  $N=180$  and (b) Yoke B with  $N=180$

Figure 7.13, Figure 7.14 and Figure 7.15 show the enhancement of field and flux distribution using Yoke B with different number of turns. It can be observed that the magnetic characteristic of sample can be improved significantly so as the flux leakages were diminished by enhancing the turns of winding, N of 720 turns on magnetic cores. In summary, the Yoke A with dimension of (97.2 x 93.4 x 68) mm is used as a magnetizing yoke because it can generate the magnetizing field with a low reluctance flux closure path.

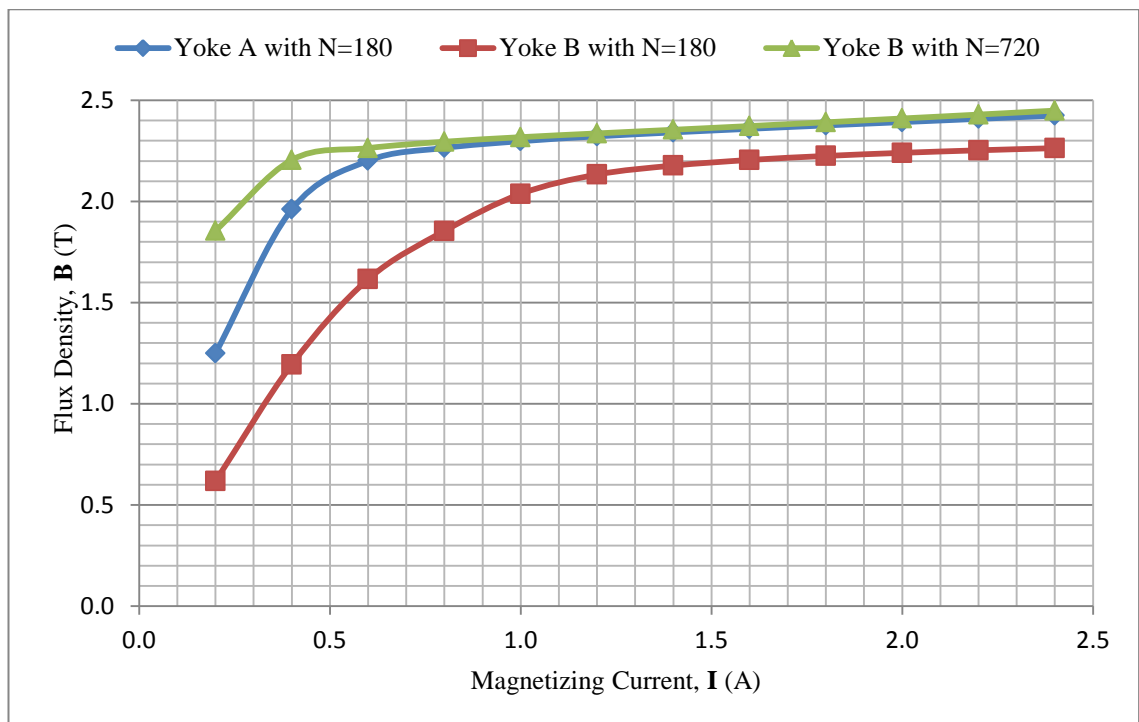


Figure 7.16 Flux distribution pattern for Yoke A and Yoke B

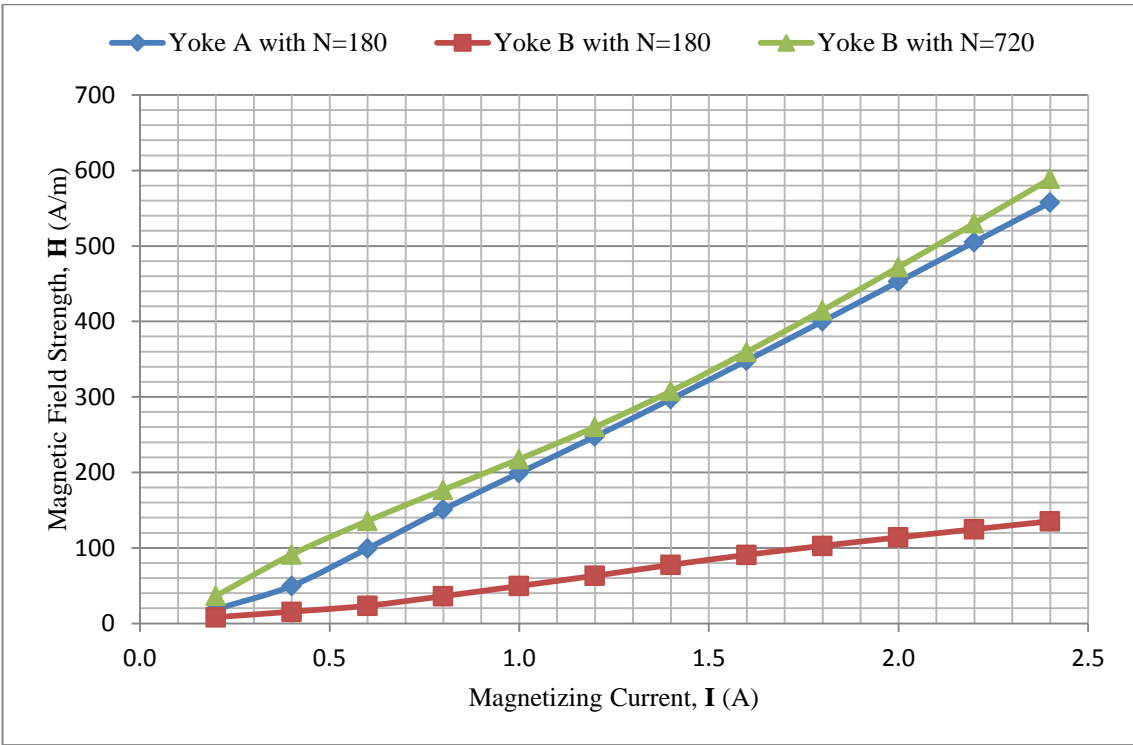


Figure 7.17 Field distribution pattern for Yoke A and Yoke B

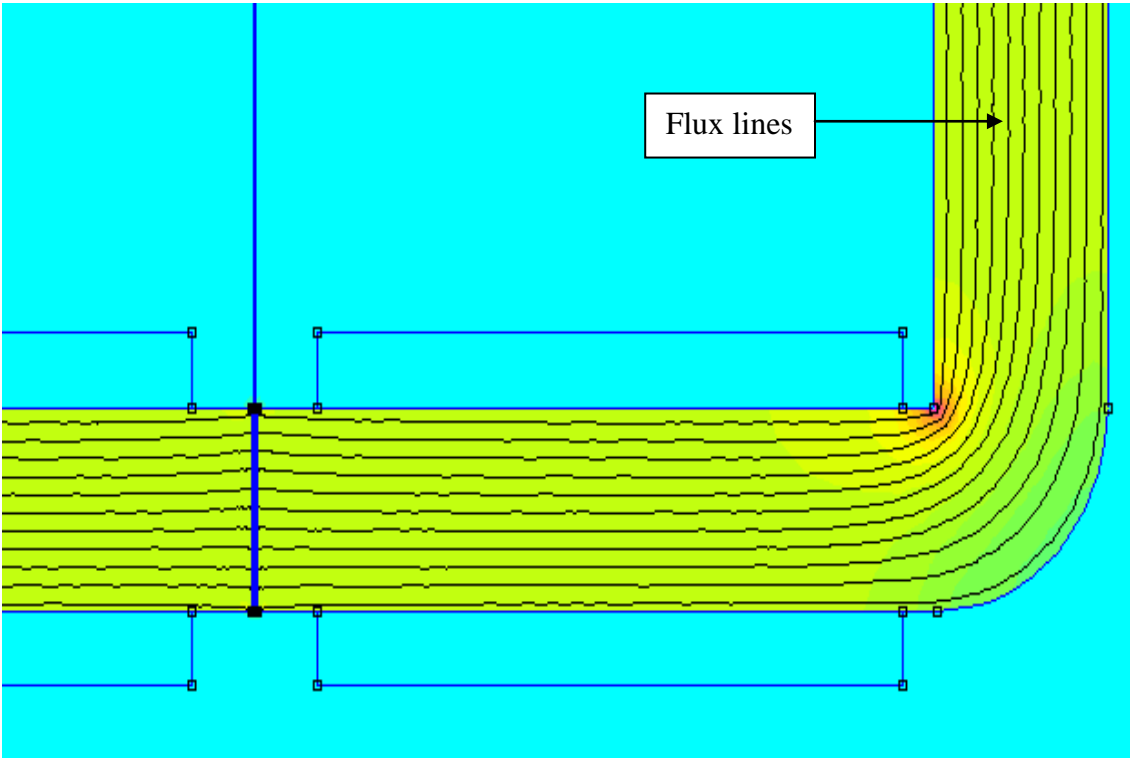


Figure 7.18 Flux plot for Yoke B with magnetizing winding, N of 720 turns

### 7.1.3 Optimization of Sample's Dimension

The effects of the sample's dimension were investigated on 0.28 mm of 3% grain-oriented silicon iron steel; grade M4. The sample was magnetised along rolling direction by utilizing the horizontal double yoke Single Sheet Tester (SST) arrangement with the current ranging from 0.6 A to 1.8 A at 50 Hz. The samples were designed with an additional length about 30 mm and 60 mm at both ends of former sample with dimension of (97.2 x 93.4 x 68) mm. The so-called overhang sample's length is denoted as LO. Figures 7.19 illustrates the mesh view design of horizontal double yokes SST with overhang sample. In order to study the effects of stray flux on the magnetic measurement, the B-coil sensors and H-coil sensors were positioned at upper end, centre and lower end on the sample under test. The sensors that appointed at the centre of sample were labelled as  $B_1H_1$ , upper end were tagged as  $B_2, H_2$  and lower end was assigned as  $B_3, H_3$ .

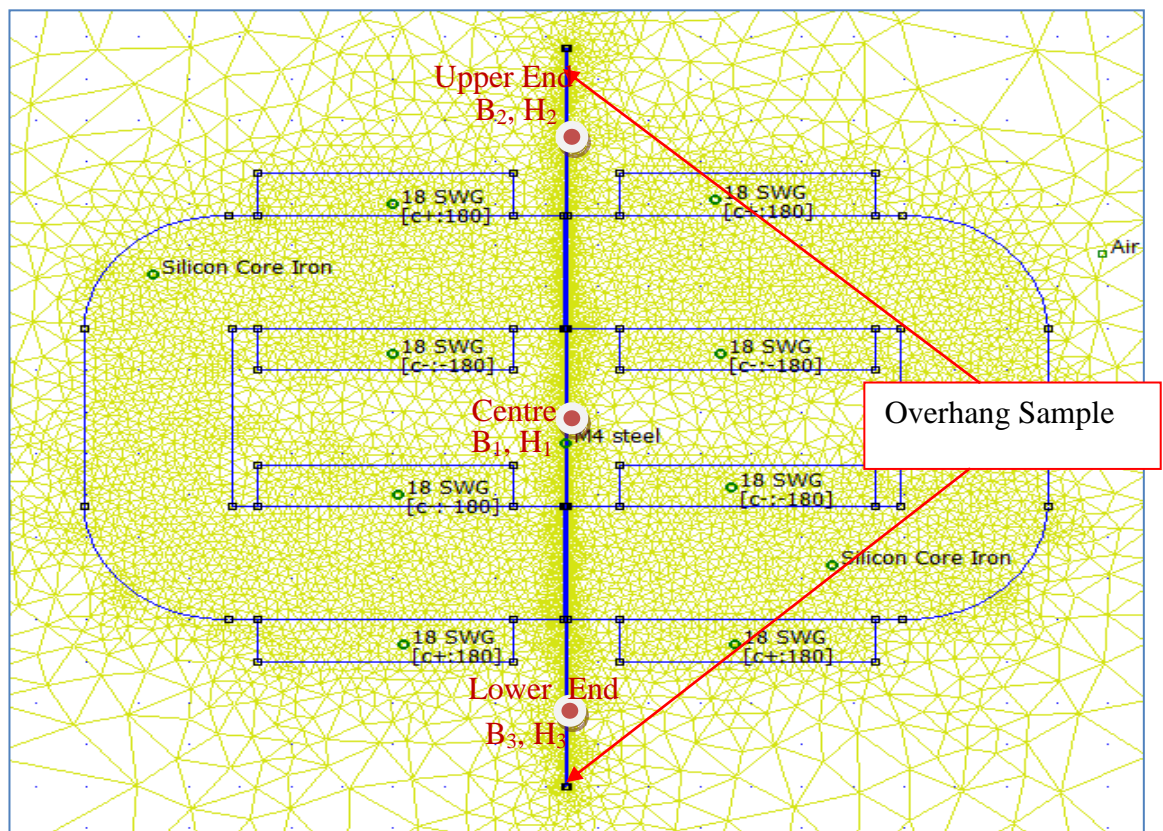


Figure 7.19 A mesh view of horizontal double yokes SST with overhang sample

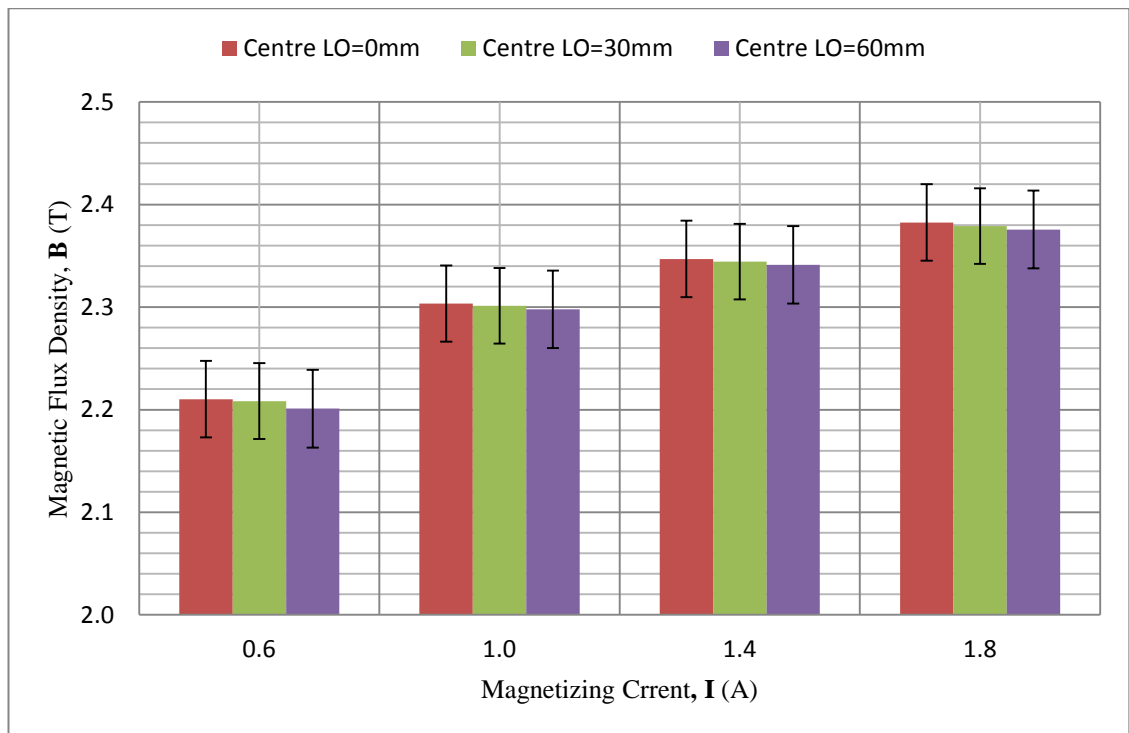


Figure 7.20 Comparison of flux density distribution for different sample's dimension at the centre of sample

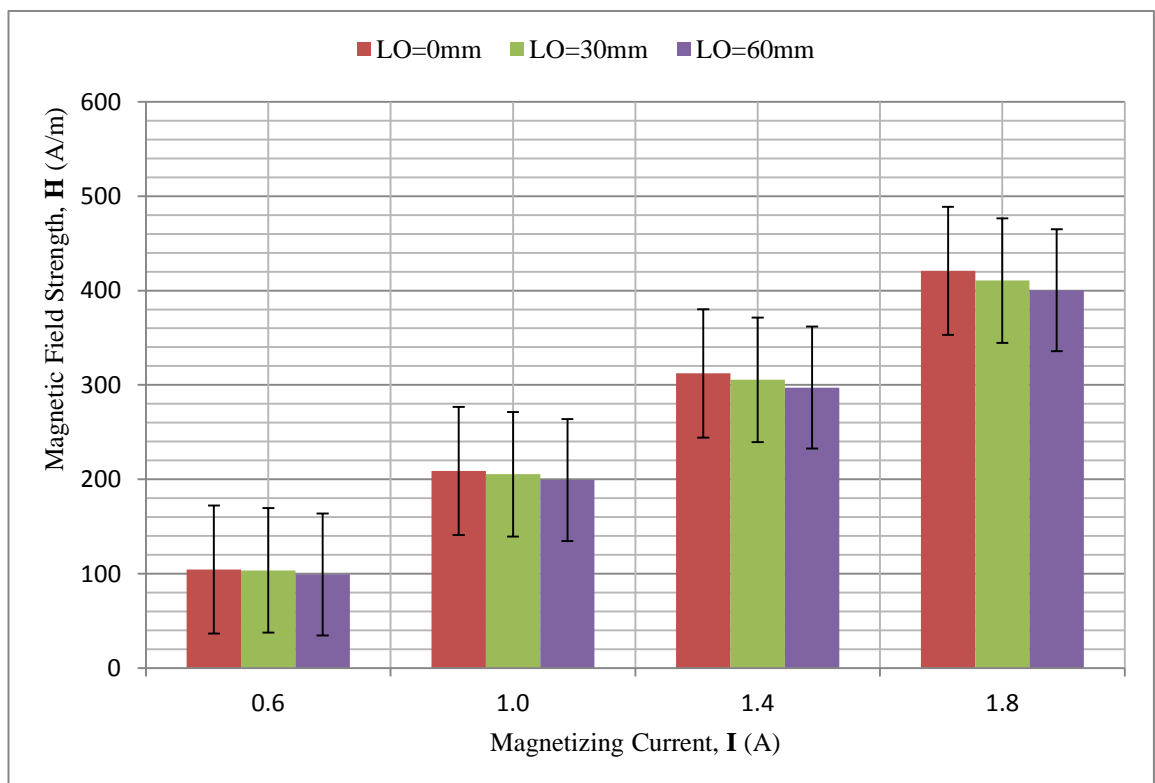


Figure 7.21 Comparison of field distribution for different sample's dimension at the centre of sample

Figure 7.20 and Figure 7.21 show the magnetic field and flux densities in the centre of the sample for different geometry of sample with respect to the rolling direction. It can be observed that magnetic flux densities of overhang sample are slightly decreased in the range of 0.1 to 0.2 % with sample without overhang. The flux density,  $B$  for sample with  $LO=0$  mm,  $LO=30$  mm and  $LO=60$  mm measured by the B-coil sensor at 1 A are obtained as 2.3034 T, 2.3012 T and 2.2978 T, respectively. The magnetic field strength,  $H$  for sample  $LO=0$  mm,  $LO=30$  mm and  $LO=60$  mm at 1 A are found at around 208.90 A/m, 205.39 A/m and 199.34 A/m, respectively. The percentage difference between these overhang samples with so-called fit-in sample is in the range of 1.7 to 4.6 %. The findings indicated that the magnetic properties are slightly deteriorated by overhang samples. It can be noted that as sample sizes is increased, the magnetic characteristic are worsen. This is due to the flux distribution near the H-coil of the tester with a long overhang approaches uniformity more rapidly than that with a short overhang, (T. Nakata, 1989).

Figures 7.22 and Figure 7.23 present a comparison of the field and flux distribution in the upper end and lower end of the overhang sample of the double yoke SST, respectively. Results indicate that overhang sample,  $LO=30$ mm and  $LO=60$ mm have the same linear trend where the stray flux proportionally increase with the increasing of current,  $I$ . The amount of stray flux increases with longer overhang sample. Although the value of stray flux is small, it affected the field and flux measured in the centre of sample, Figure 7.21. In case of overhang sample, the under yoke sample region is magnetized first, and only then the magnetization of the adjacent overhanging part takes places, (Stupakov, et al., 2009). It leads to inhomogeneous of sample magnetization and the flux leakage between the yoke legs which can influence the measurement of magnetic properties, (Stupakov, 2006). Therefore, fit-in sample is chosen as a standard sample size throughout this research.

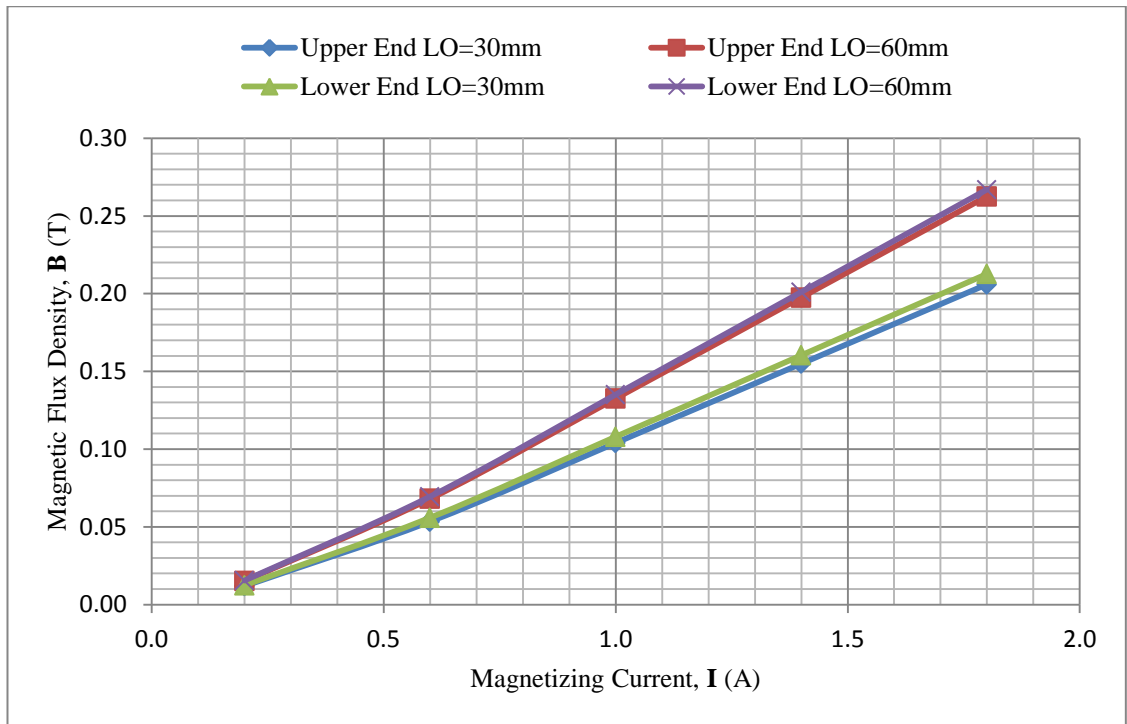


Figure 7.22 Comparison of flux distribution for different sample's dimension measured at the upper and lower end of the samples

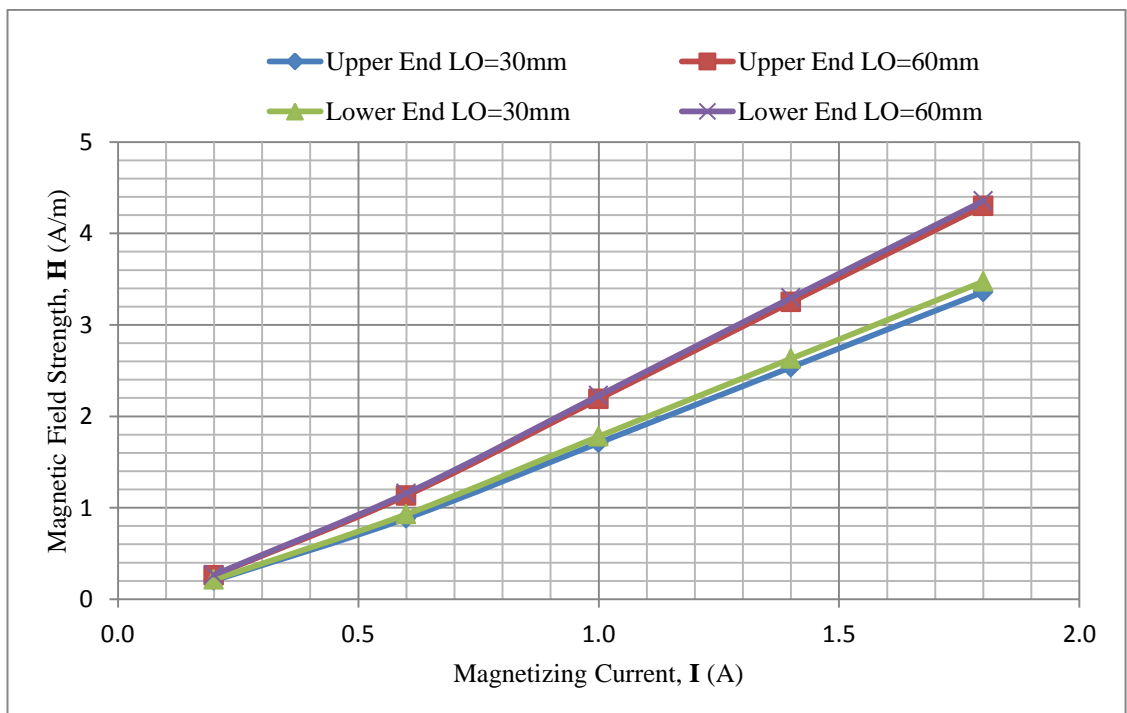


Figure 7.23 Comparison of field distribution for different sample's dimension measured at the upper end and lower end of the samples

#### 7.1.4 Evaluation of Sample under Test

The effect of different types of electrical steels was investigated on grain oriented and non-oriented silicon steels with different grades which are 0.5 mm non-oriented silicon iron steels; grade M19 and M27 and 0.28 mm and 0.27 mm of 3% grain-oriented silicon iron steel, grade M4 and M3. The samples were magnetized under 50 Hz magnetization conditions, employing the double yoke SST arrangement with the current ranging from 0.2 A to 2.4 A. The magnetic sensors; B-coil and H-coils are located in the middle of the sample under test. The 0.3 mm air gap was inserted between the C-core pole faces and the sample under. Figure 7.24 shows the assembly of SST where the sample is placed between the symmetrical C-cores.

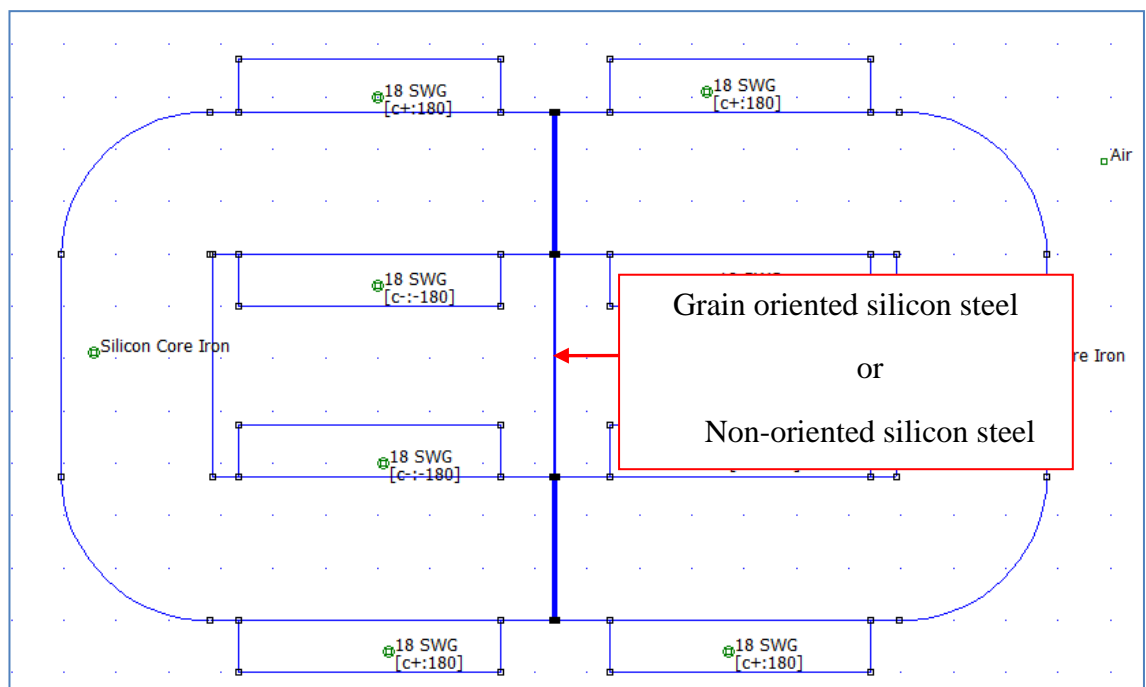


Figure 7.24 Side view of the assembly for grain-oriented silicon steel or non-oriented silicon steel

i) **Non-oriented silicon steel sheet**

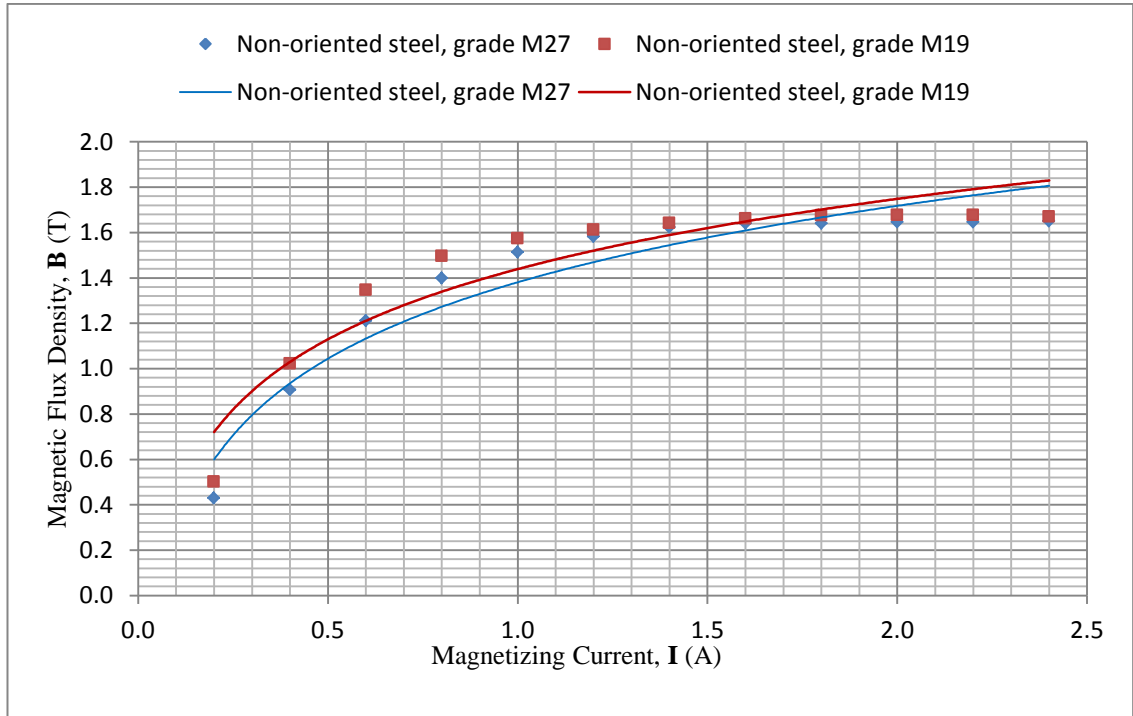


Figure 7.25 Magnetic flux distributions on different grade for non-oriented silicon steels, M27 and M19

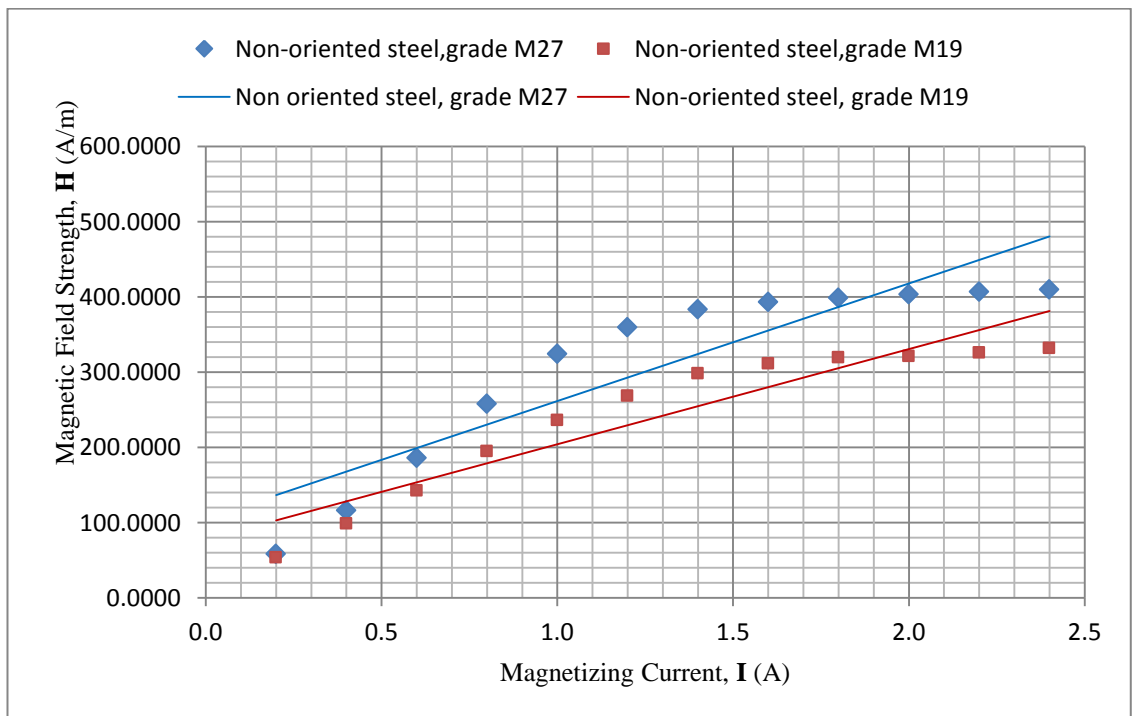


Figure 7.26 Magnetic field strength distributions for non-oriented silicon steels, grade M19 and M27

Figure 7.25 and Figure 7.26 represent the flux and field distribution for non-oriented steel samples, grade M19 and grade M27. It can be seen that the magnetic field is vary linearly with the current,  $I$ , Figure 7.26. Meanwhile the flux distribution curves are increased gradually as the magnetizing current is being amplified. As the  $H$  increases, the  $B$  approaches a saturation level for the material asymptotically. At saturation stage, all magnetic domains are practically lined up. Therefore additional increases in applied field are not able to cause further alignment of the domains, Figure 7.25. Results show that at a frequency of 50 Hz, the flux density range for 0.5 mm non-oriented steels, grade M27 is between 0.4 to 1.7 T. On the contrary, for 0.5 mm non-oriented steels, grade M19; the flux density is around 0.5 to 1.7 T. Results indicate that for current,  $I=0.4$  A, the flux density for non-oriented steel, M19 is about 1.02 T while non-oriented steels grade M27 only magnetize the sample at 0.91 T. In conclusion, less current is needed to magnetize the non-oriented sample, grade M19 to the required flux density compared to non-oriented, grade M27.

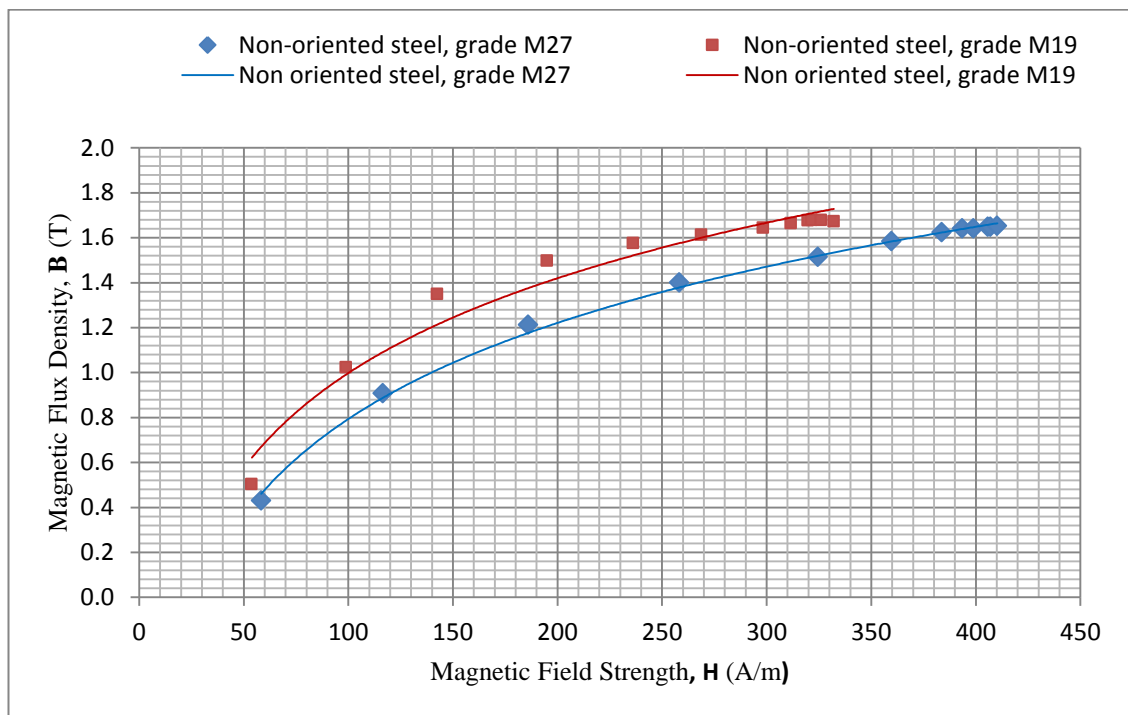


Figure 7.27 Magnetization curves for non-oriented steels, grade M19 and M27

Figure 7.27 shows the magnetizing curve for different grades of non-oriented steels. Different grades of non-oriented magnetic materials have different magnetic properties as each grade was assigned according to its core loss, (Steel, 2007). The permeability of non-oriented samples can be determined using **Equation 2.7** which defined as the ratio of the flux density,  $B$  to the magnetic field strength,  $H$ . A good grade of soft magnetic materials must have high permeability, which requires less magnetic field strength,  $H$  as stated in **Equation 2.8**. Furthermore, a better grade of electrical steel only requires a less current to obtain a higher flux. Thereby, it can be concluded that the non-oriented steel, grade M19 has a better magnetic properties than non-oriented steel, grade M27. The finding is in agreement with the manufacturer data, (JFE, 2007),(Steel, 2007) .

**ii) Grain oriented silicon steel sheet**

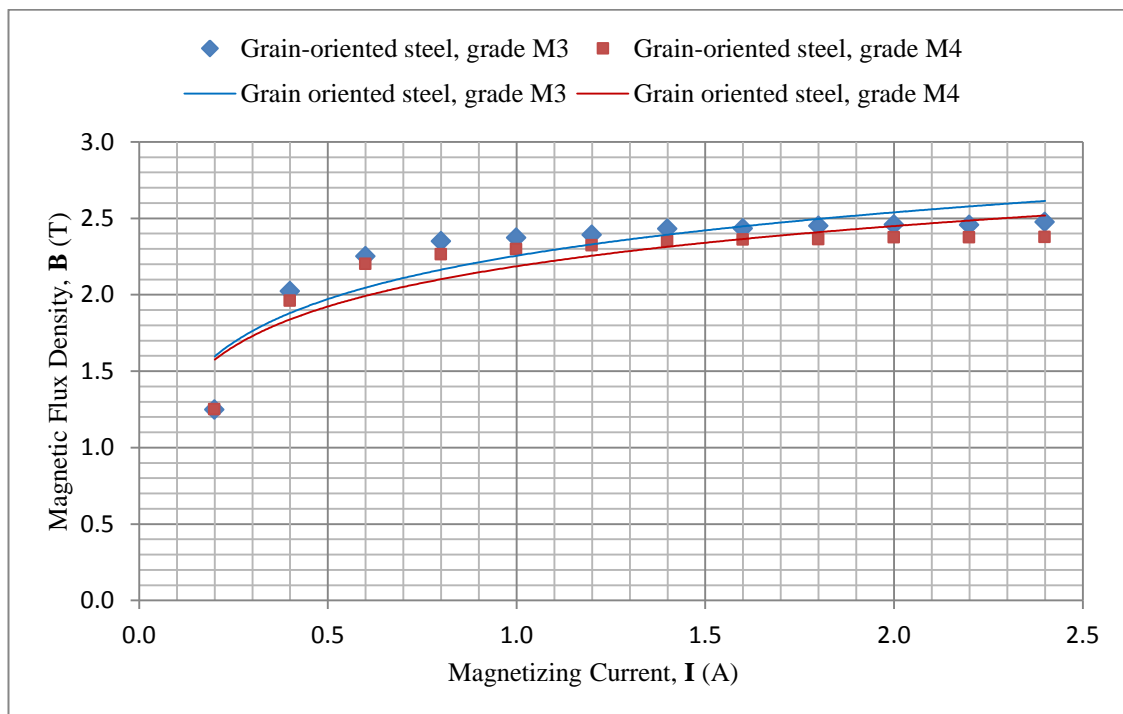


Figure 7.28 Flux distributions for grain-oriented steels, grade M3 and M4

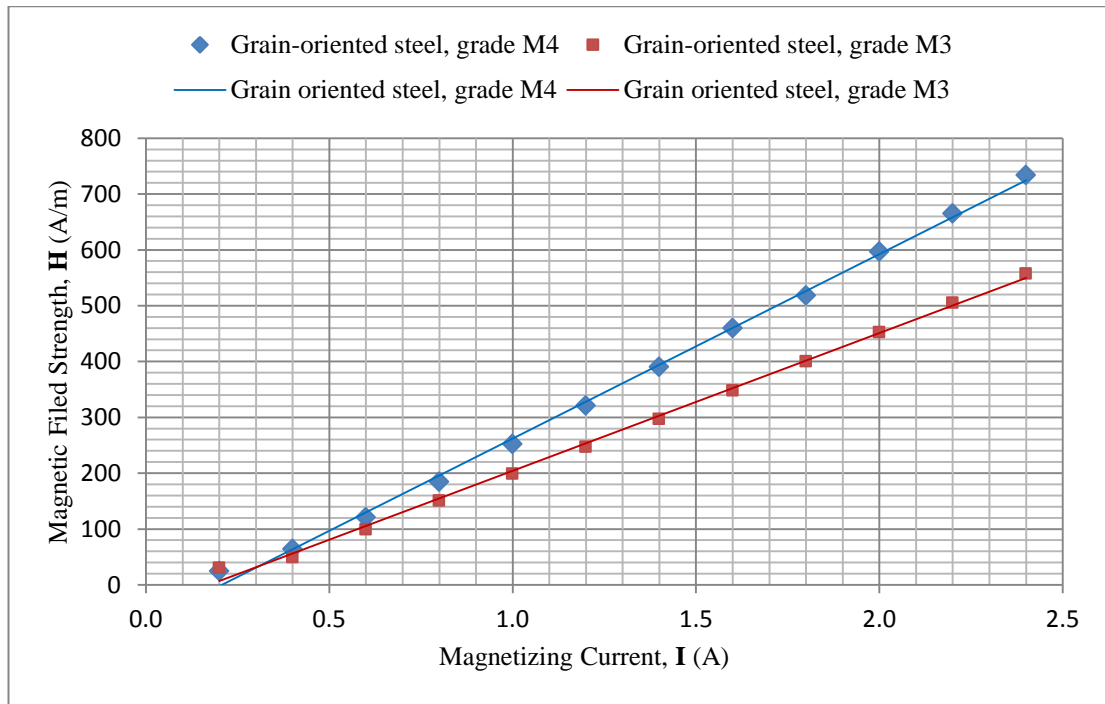


Figure 7.29 Field distributions for grain-oriented steels, grade M3 and M4

Figure 7.28 and Figure 7.29 represent the flux and field distribution for grain oriented samples, grade M3 and grade M4. In general, the magnetic field is increasing linearly with magnetizing current. In case of flux distribution, it can be seen that below the magnetization knee at about 1.9T, both grade of grain oriented electrical steels can be treated as a quasi linear until the magnetic material met its saturation level. Result shows that flux density range for 0.27 mm grain oriented steel, grade M3 is between 1.3 to 2.5 T at a frequency of 50 Hz. In contrast, for 0.28 mm grain oriented steel, grade M4; the flux density, B is around 1.3 to 2.4 T. For the field distribution, it requires about 1.2 A for grain oriented steel, grade M3 to magnetise the sample at 247.53 A/m while grain oriented steel, grade M4 needs 1 A to magnetise the sample at 252.26 A/m. It can be observed that the grain oriented steel, grade M3 has high value of B and less of H but vice versa for grain oriented steel, grade M4.

The direction of magnetization is limited to the easy axis rolling direction in order to achieve optimum magnetic properties. This is due to the anisotropic structures formed in grain oriented which have been controlled so that all crystal is identically aligned to one preferred direction, (Buschow and Boer, 2004). Based on **Equation 2.7**, it can be predicted that grain oriented steel; grade M3 has higher permeability than grade M4. Electrical steel which has highly anisotropic structures and possess high permeability, only requires less current to get the higher magnetic flux.

Figure 7.30 shows the magnetization curves for different grades of grain oriented steels, M3 and M4. As the magnetic field increases, the flux density approaches a saturation level asymptotically. Based on calculated permeability and magnetizing curve as in Figure 7.30, it can be seen that grain oriented steel, grade M3 has better magnetic properties compared to grade M4 which is in agreement with the manufacturer data, (JFE, 2007),(Steel, 2007) .

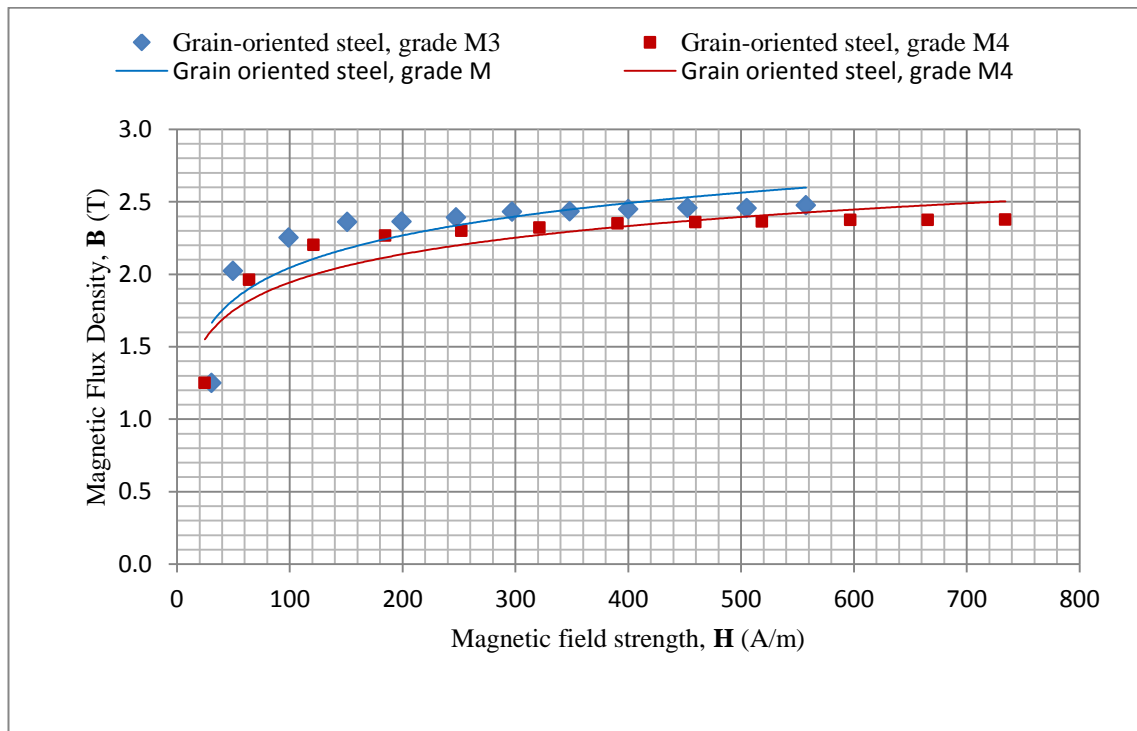


Figure 7.30 Comparison of magnetization curves for grain oriented electrical steels, grade M3 and M4

iii) Differences between Grain oriented silicon steel sheet, M4 and Non-oriented silicon steel sheet, M19

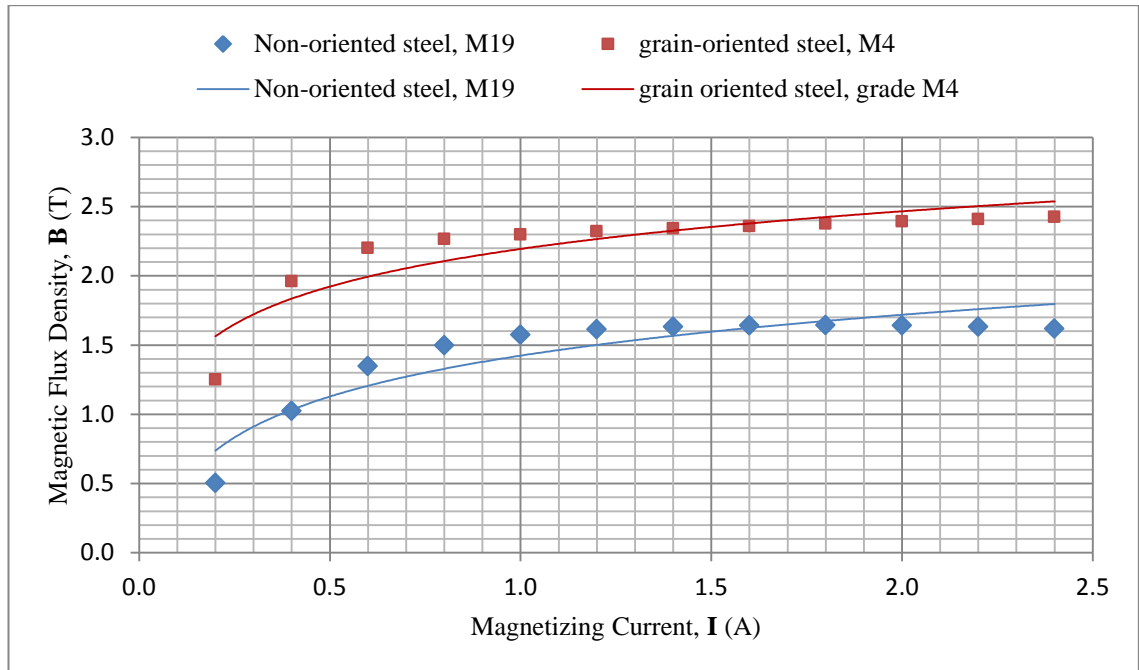


Figure 7.31 Comparison of magnetic flux density distribution for electrical steels, grade M4 and M19

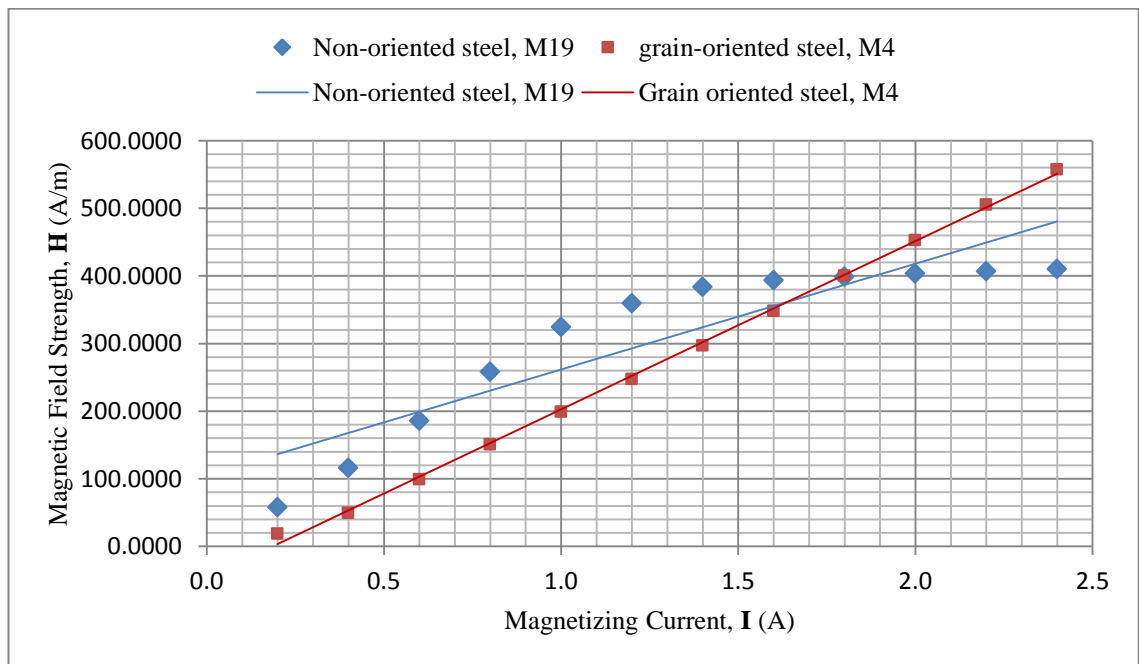


Figure 7.32 Comparison of magnetic field strength distribution for electrical steels, grade M4 and M19

Figure 7.31 and Figure 7.32 show the analysis results on distribution of amplitude of magnetic flux density,  $B$  and magnetic field strength,  $H$  for grain oriented and non-oriented steels. It can be seen that the magnetic flux density for grain oriented steel, M4 and non-oriented steel, grade M19 are gradually increased with the current,  $I$  until it reached saturation level. In case of magnetic field strength, the field distribution is increased linearly with the current. The intersection between the two graphs at about 1.8A in Figure 7.32 indicates that the non-oriented steel, M19 already reached the saturation at about 1.8A whereas for grain oriented steel, M4, it is still has not been saturated . The experimental results show that at a frequency of 50 Hz, the flux density range for 0.27 mm thick grain oriented, grade M4 is between 1.2 to 2.4 T. In contrast, for 0.5 mm non-oriented silicon iron steels grade M19, the flux density is around 0.5 to 1.6 T.

It have been reported that non-oriented steels can be tested up to 1.6T whereas for grain oriented steels, the normal range extends to 1.8 T ,(ASTM, 2000). For the grain oriented steel sheet; grade M4 , a less current about 1 A is needed to achieve the maximum flux density of 2.3 T in centre of sample while the non-oriented steel, at 1 A, it only can magnetise the sample up to 1.6 T. These differences of their magnetic properties due to grain size and thickness of these samples, which grade M4 and M19 with the thickness of 0.28 mm and 0.50 mm, respectively. An optimum grain size is not only defined for given magnetization but also depended on the texture and silicon content (A.J. Moses, 2012). In addition, this is also due to the fact that the grain oriented silicon steel are specially designed to have a large anisotropic crystallographic orientation along the  $(110)\{001\}$  or  $(100)\{001\}$  direction which have a dominant and excellent excitation characteristics in the rolling direction, (Michiro, et al., 2002),(Tamaki et al., 2010) . Meanwhile, the crystal domains in the non-oriented steel sheet are normally much smaller, and the observed domain structure very much more

complicated because of surface closure domains that form to reduce the local surface demagnetizing fields, (Graham, 1982).

Permeability,  $\mu$  is the most important parameter for soft magnetic material since it indicates how much magnetic induction is generated by the material in a given magnetic field. In general, the better materials have higher permeability, (Jiles, 1991). Figure 7.33 displays the magnetization curves for different types of electrical steels, grade M4 and M19. The magnetizing curve was found to vary nonlinearly with the applied field. A good grade of electrical steel must have high permeability and require fewer magnetic fields to obtain higher flux. Based on permeability which is due to material grade and magnetizing curve as in Figure 7.30, it can be summarized that grain oriented electrical steel is having excellent magnetic characteristics than non-oriented electrical steel.

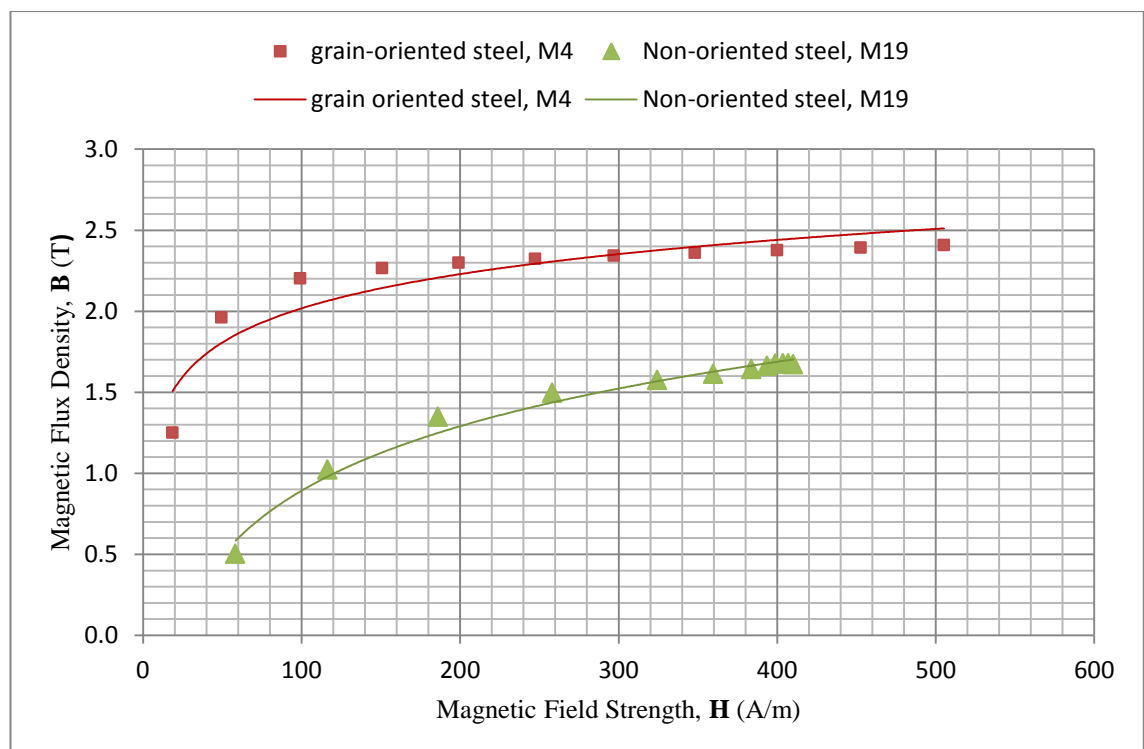


Figure 7.33 Magnetization curves of electrical steels, grade M4 and M19

## 7.2 Magnetic Hardware Set up

The typical output signal of magnetic field above the steel sample using 1000 turns of H-coil sensor with dimension of (20x20) mm is shown in Figure 7.34. The output signal of H-sensor is similar with signal obtained from other researchers, (Slawomir Tumanski and Baranowski, 2004). The non-sinusoidal shape is due to nonlinear behaviour of magnetic materials. The signal from H-coil sensor is much clearer after being buffered, amplified and filtered using H-channel circuit.

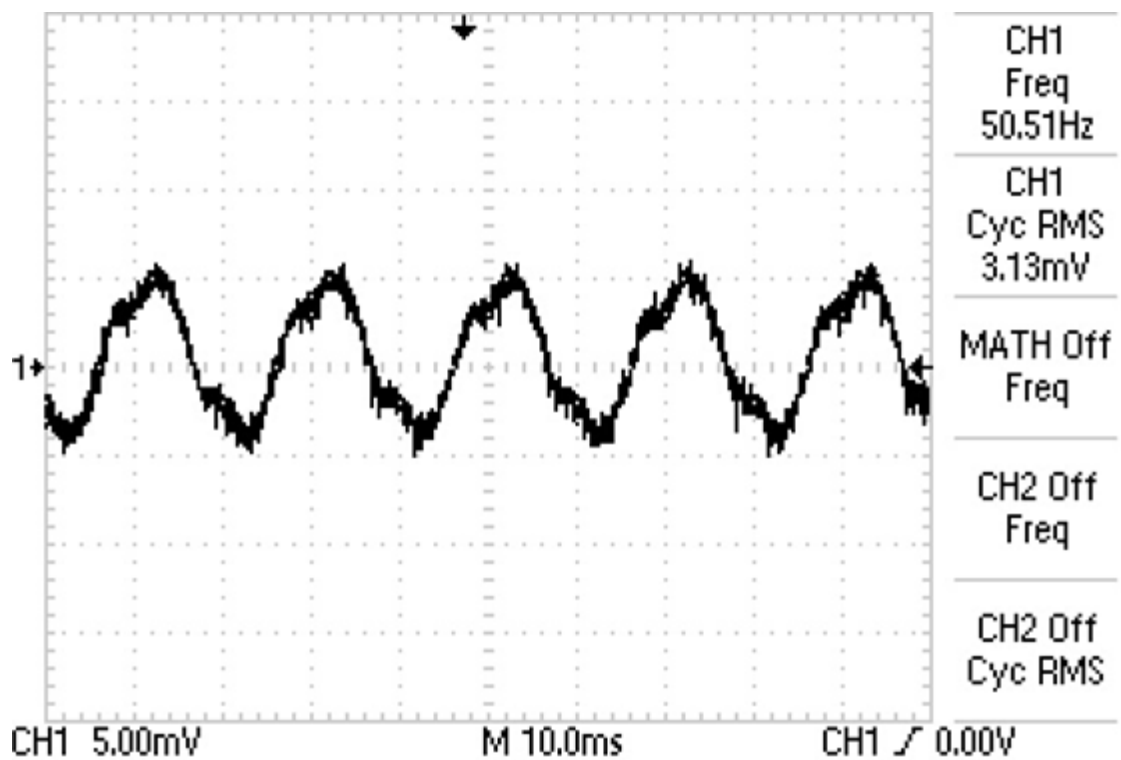


Figure 7.34 Induced voltage waveform from H-coil sensor

Figure 7.35 shows the output signal from B-coil sensor after being buffered, amplified and filtered using B-channel circuit. As it can be seen from Figure 7.35, the output voltage of the B-coil sensor tends to be in sinusoidal shape. This is due to negative feedback system which controls the magnetization conditions by keeping the

sinusoidal waveform of flux density using suitable combination of exciting waveform and the sensor output signal (Stupakov, et al., 2009), (Mahadi, 1996).

The magnetic flux density,  $B$  for the magnetic material is calculated using **Equation 2.21** as per stated in Chapter 2. Whereas the magnetic field intensity,  $H$  for the steel sample is determined by multiplying the e.m.f induced voltage with the calibration factor,  $k=69.90 \times 10^3 \text{ (A/m)/V}$ .

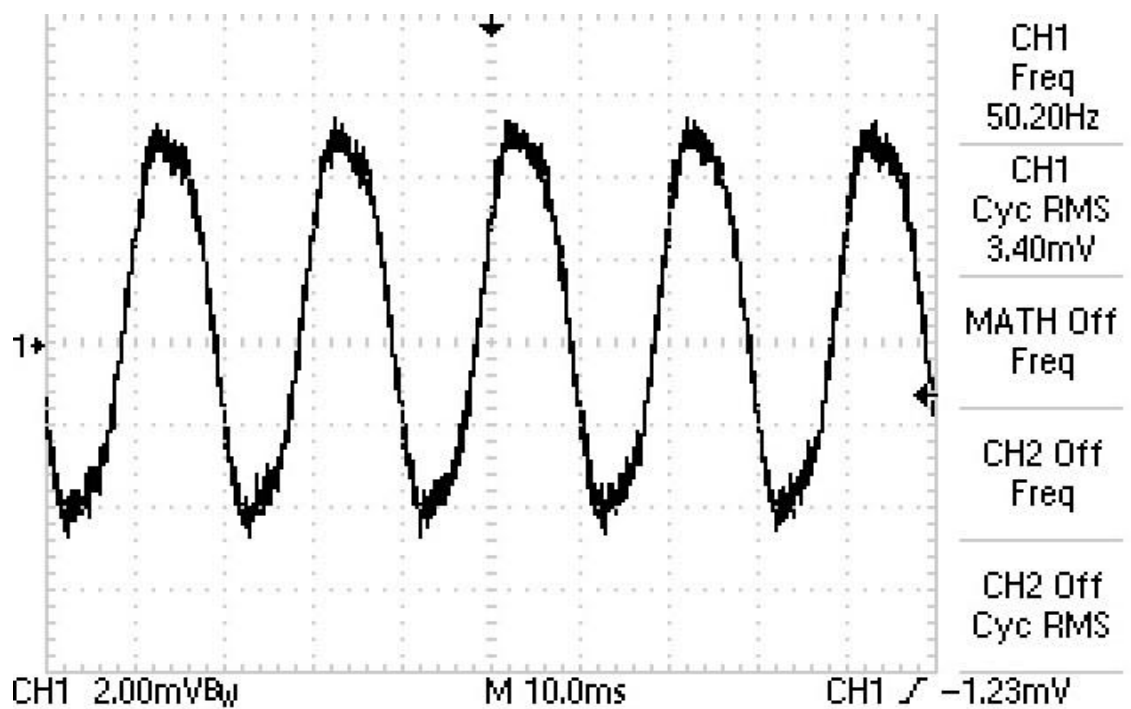


Figure 7.35 Induced voltage waveform from B-coil sensor

### 7.2.1 Evaluation of Sample under Test

The effect of anisotropy of electrical steels was investigated on non-oriented and grain oriented silicon steels with different grades which are 0.5 mm non-oriented silicon iron steels; grade H60 and H18 and 0.3 mm of grain-oriented silicon iron steel; grade M5 and Z6H. The samples were magnetised under 50 Hz magnetisation conditions, employing the double yoke SST arrangement with the current ranging from 0.2 A to 1.8 A. The magnetic sensors; B-coil and H-coils are placed in the central region of the sample. The 0.3 mm air gap was inserted between the C-core pole faces and the sample under.

#### i) Non-oriented (NO) silicon steel sheet

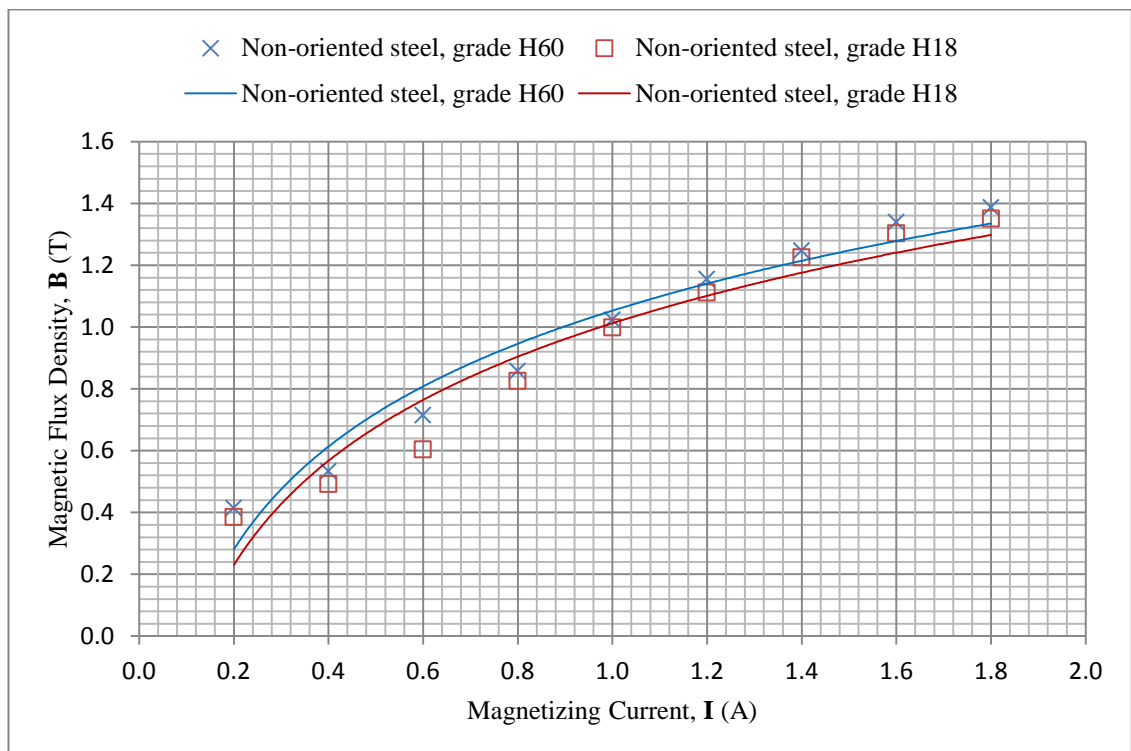


Figure 7.36 Flux density distribution for non-oriented steels, grade H18 and H60

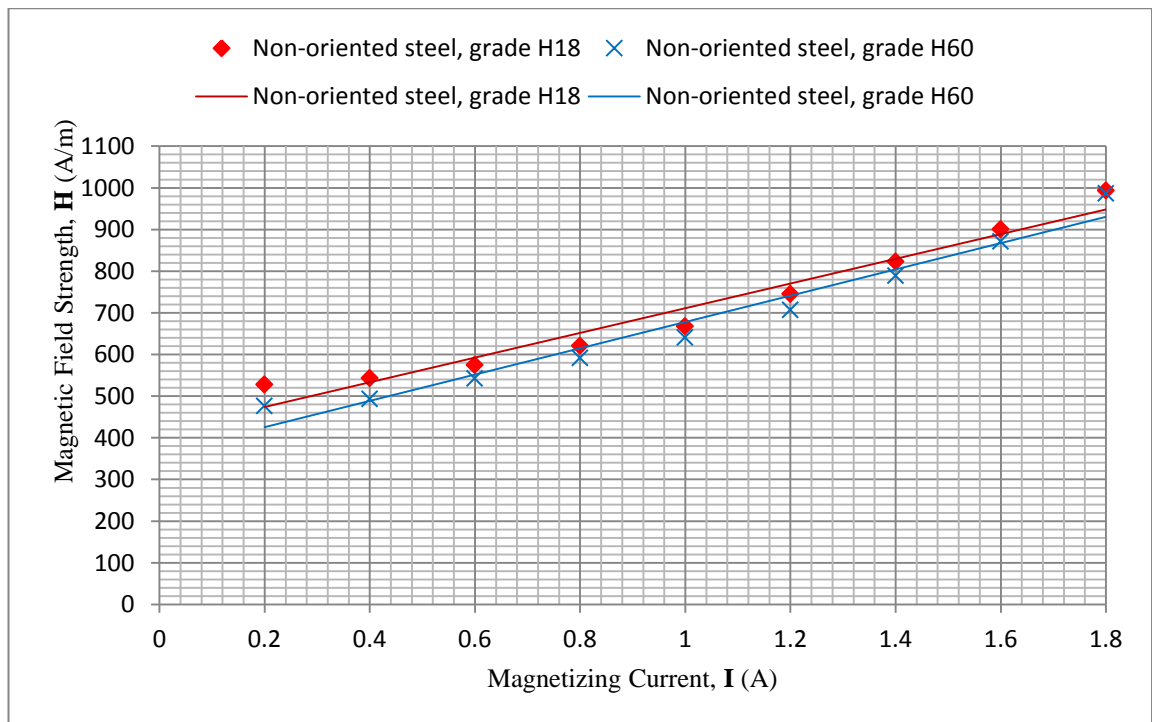


Figure 7.37 Field strength distributions for non-oriented steels, grade H18 and H60

Figure 7.36 and Figure 7.37 present the field and flux distributions for non-oriented steels, grade H18 and H60. It can be seen that the magnetic flux density for both non-oriented steel samples are nonlinear with the current, I. Figure 7.36 indicates that the non-oriented steel, H60 and H18 will reach magnetization saturation at about 1.4 T and 1.35 T, respectively. In case of magnetic field strength, the field distribution is increased linearly with the current, I, Figure 7.37. Results show that at a frequency of 50 Hz, the flux density range for 0.5 mm thick non-oriented, grade H60 is between 0.3 T to 1.4 T. For 0.5 mm thick non-oriented silicon iron steel, grade H18, the flux density is around 0.25 T to 1.35 T. It can be seen that the non-oriented steel, grade H60 has high value of B and less of H but vice versa for non-oriented steel, grade H18.

ii) Grain oriented (GO) silicon steel sheet

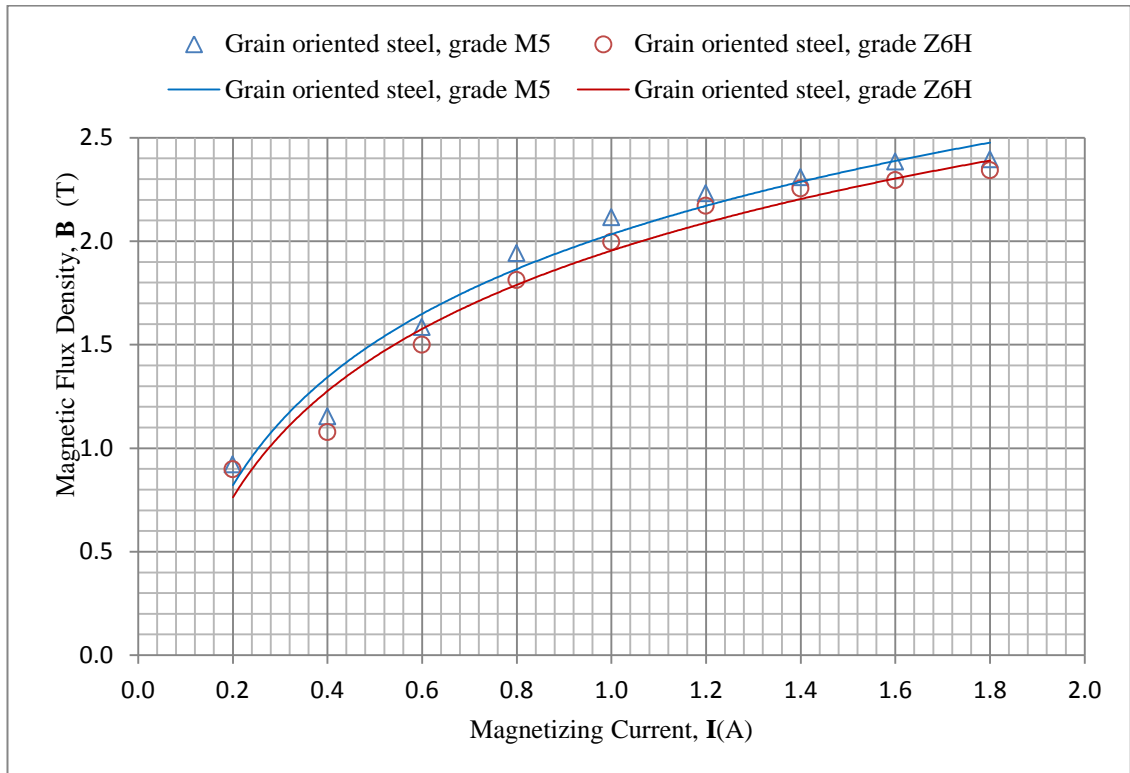


Figure 7.38 Flux density distribution of grain oriented steels, grade M5 and Z6H

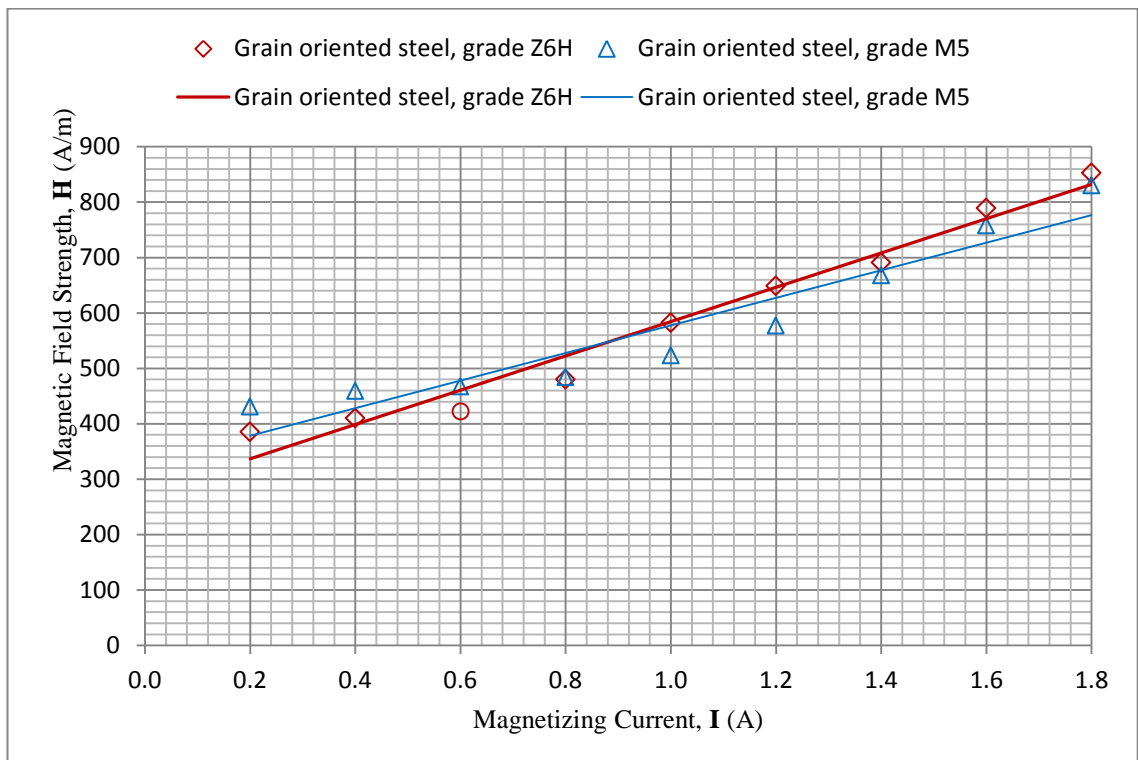


Figure 7.39 Field strength distributions of grain oriented steels, grade Z6H and M5

Figure 7.38 and Figure 7.39 show the flux and field distribution for grain oriented steels, grade M5 and grade Z6H. Results show that the magnetic field is increasing linearly with magnetizing current,  $I$ . However, for the magnetic flux density distributions curve, it can be treated as nonlinear with increasing of current,  $I$ . The magnetic saturation level for grain oriented steels, grade M5 and Z6H are about 2.4 T and 2.3 T, respectively. For grain oriented steel, grade M5 and grade Z6H, the field distribution at current,  $I=1.2$  A are 620 A/m and 640 A/m. It can be observed that the grain oriented steel, grade M5 has high value of  $B$  and less of  $H$  but vice versa for grain oriented steel, grade Z6H.

**iii) Grain oriented (GO) silicon steel sheet and Non-oriented (GO) silicon steel sheet**

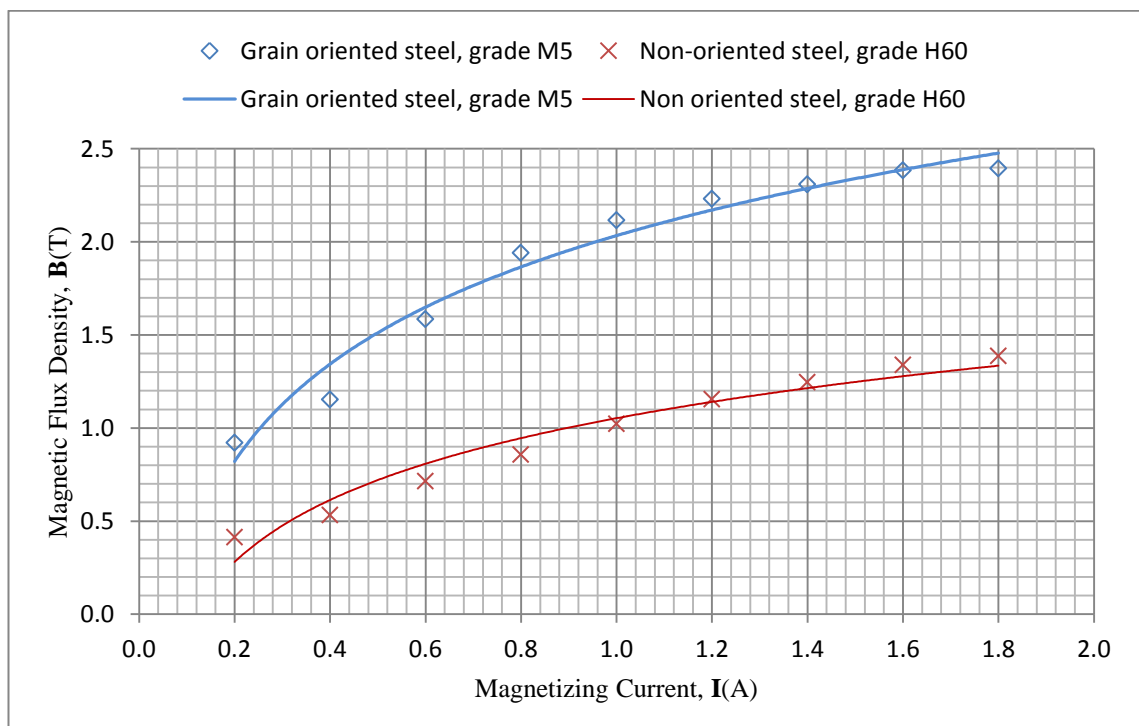


Figure 7.40 Comparison of flux density distribution for GO and NO steels, grade M5 and H60

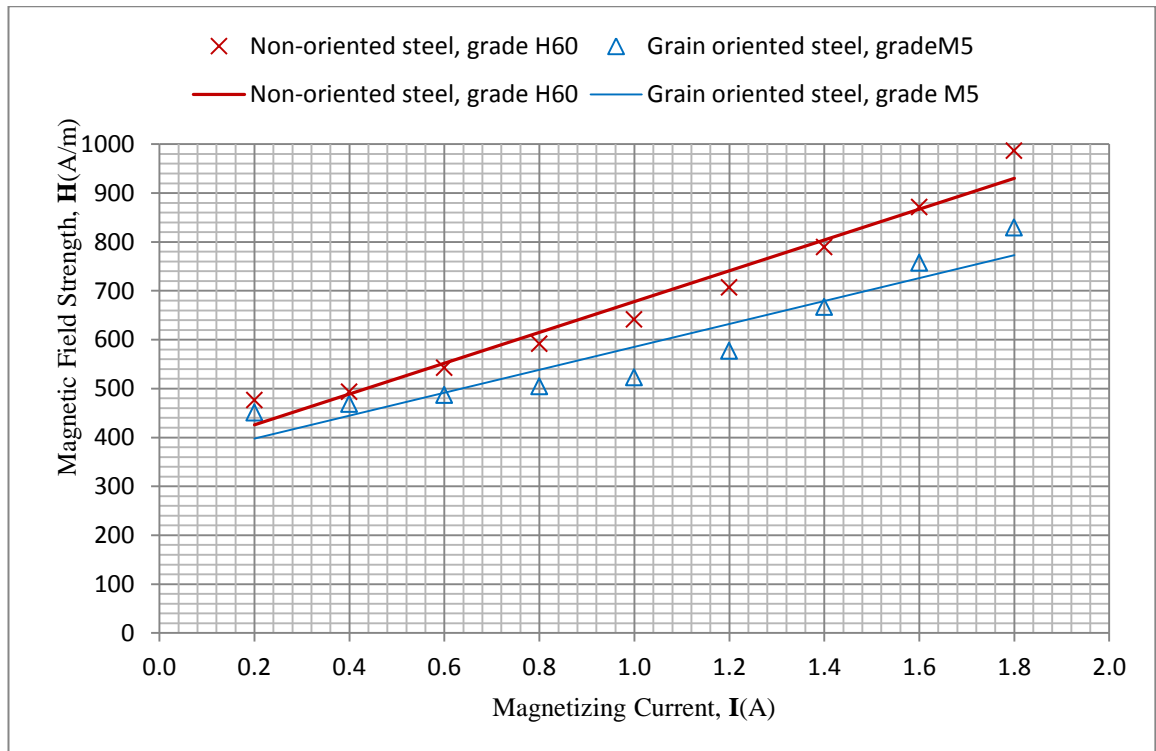


Figure 7. 41 Comparison of magnetic field distribution for grain oriented and non-oriented steels, grade M5 and H6O

Figure 7.40 and Figure 7.41 show the analysis results on distribution of amplitude of magnetic flux density,  $B$  and magnetic field strength,  $H$  for grain oriented and non-oriented steels. It can be seen that the magnetic flux density for grain oriented steel, M5 and non-oriented steel, grade H60 are nonlinear with the current,  $I$ . In case of magnetic field strength, the field distribution is vary linearly with the current,  $I$ . The non-oriented steels can be tested up to 1.6T while for grain oriented steels, the normal range extends to 1.8 T, (ASTM, 2000). For the grain oriented steel, grade M5, at current,  $I=1$  A, it can magnetize the sample at about 2.2 T while the non-oriented steel, at 1 A only magnetize the sample up to 1.2 T. These differences of their magnetic properties due to grain size and thickness of these samples, which grade M5 and H60 with the thickness of 0.3 mm and 0.5 mm, respectively. This also due to the fact that the grain oriented silicon steel are specially designed to have unique crystal structure that

have excellent excitation characteristics in the rolling direction, (Michiro, et al., 2002),(Tamaki, et al., 2010) .

Permeability,  $\mu$  of the material is defined as the ease which a material allows flux to be created. In general, the better material has the higher permeability, (Jiles, 1991). The permeability of grain oriented steels, grade M5 is obtained as 0.00404 H/m while for non-oriented steels, grade H60, the calculated permeability is 0.0016 H/m which is in agreement with manufacturer data, (Nippon). Figure 7.42 displays the magnetization curves for different types of electrical steels, grade M5 and H60. The magnetizing curve was found to vary nonlinearly with the applied field. Results show that when the value of H is low, small increase in the magnetic field will produce large increases in the value of flux density, B. For higher values of H and B, it can be perceived that increases in H will produce progressively smaller increases in B. It is obvious that stage of magnetization will be reached where an increase in magnetic field will have negligible effect on magnetic flux density. Based on calculated permeability and magnetizing curve as in Figure 7.42, it can be summarized that grain oriented electrical steel is having excellent magnetic characteristics than non-oriented electrical steel.

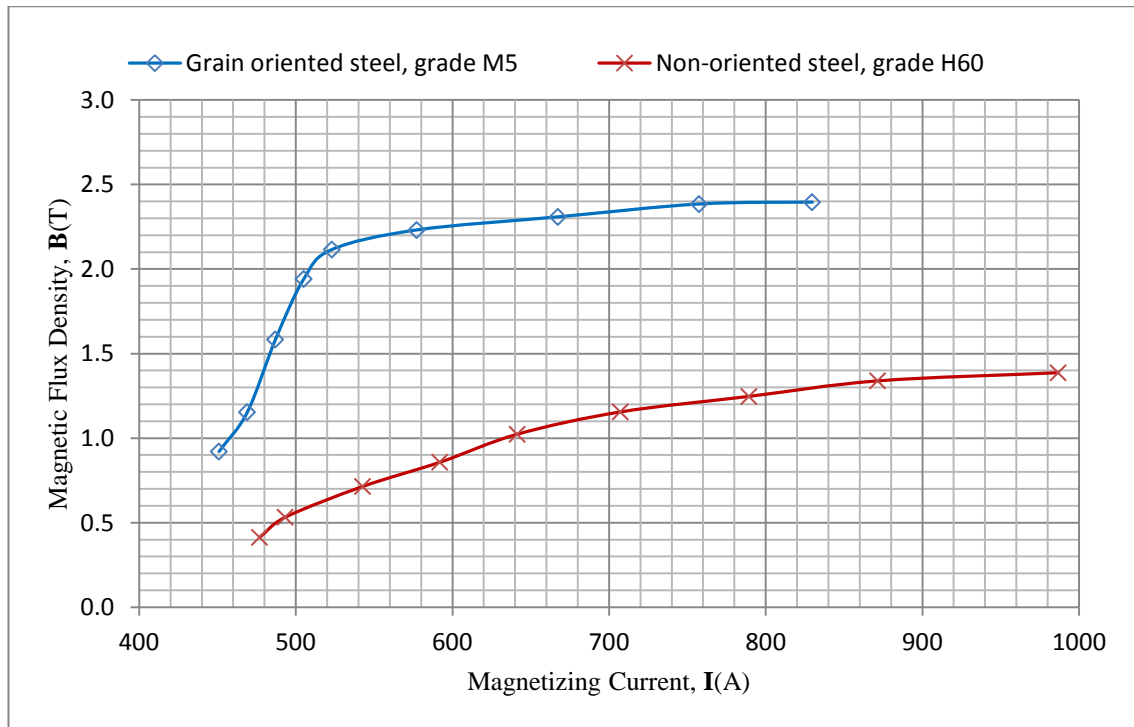


Figure 7. 42 Comparison of magnetization curves for GO and NO steels, grade M5 and H60

Grain oriented electrical steels are commonly utilized in power transformers and large motors since they exhibits highly anisotropic magnetic characteristics due to their unique crystal structure, (H.G. Kang et al., 2011). On the contrary, non-oriented electrical steels sheet are widely used for power generators and large capacity rotating machines where having high performances but low production costs. This is due to the more isotropic nature of the non-oriented material and at least ten times smaller of its grains compared to grain oriented materials, (Rashid et al., 2008).

## 7.2.2 Evaluation on Stray Flux

### i) Direct stray flux from the sample's surface

The stray flux was measured using square formed search coil, (30 x 30) mm in dimension constructed with five-turn coils of 0.2mm diameter enamelled copper wire located on the surface of non-oriented steel, grade H60. The so-called overhang sample having an additional length about 30mm at both ends of formerly fit in sample referred as LO=30mm was magnetized under frequency of 50 Hz with the current,  $I=1.6A$ . The search coil was aligned with the rolling direction of the sample and varied at different angle at  $\Theta=0^\circ$  to  $90^\circ$  to the sample's surface. Figure 7.43 illustrates the normal search coils to detect normal flux entering the sample surface. In order to examine the effect of stray flux detected in the middle of sample, this normal search coil was positioned in the central region of the overhang and fit in sample.

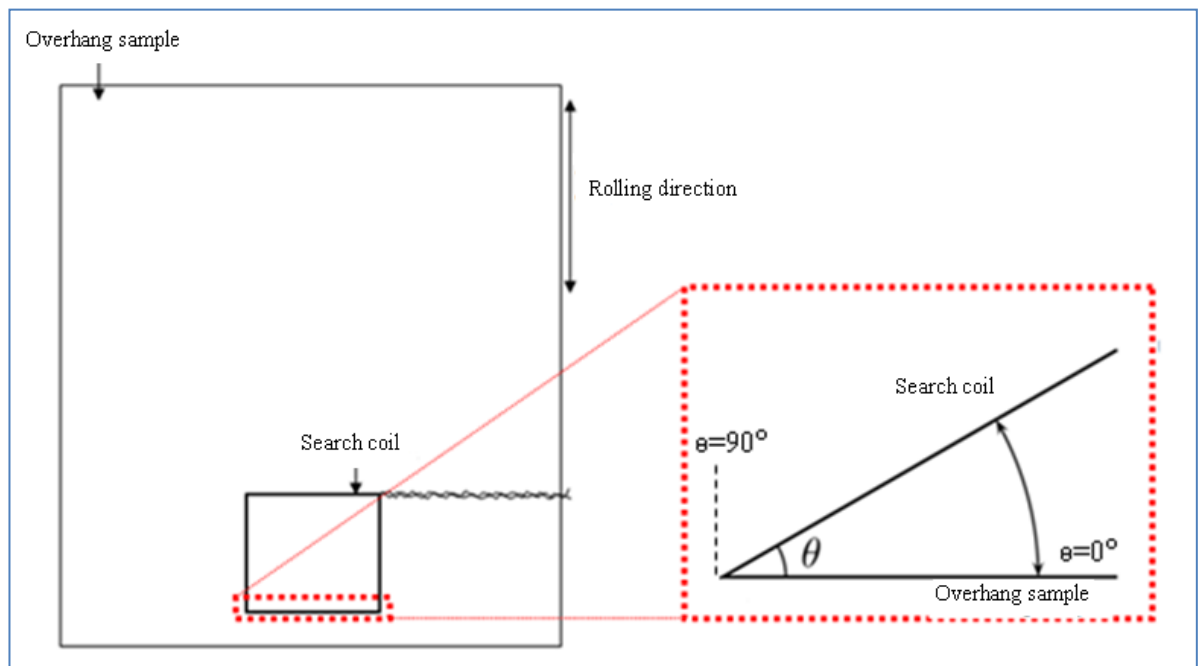


Figure 7.43 Arrangement of search coil placed on the surface of overhang sample

Result of stray flux measurement on non-oriented electrical steel, grade H60 taken at constant current,  $I$  at 1.6 A against angle between rolling direction is shown in Figure 7.44. The obtained result shows that the stray flux is decreases gradually as the angle of search coil increases at  $90^\circ$ . It can be seen that, the highest stray flux is obtained at angle of search coil axis to the sample surface,  $\Theta=0^\circ$ . This is due to the fact that crystalline structures of anisotropic magnetic material lead the easy direction of magnetization along the rolling direction,  $\Theta=0^\circ$ , (J. Liu and Shirkoohi, 1993).

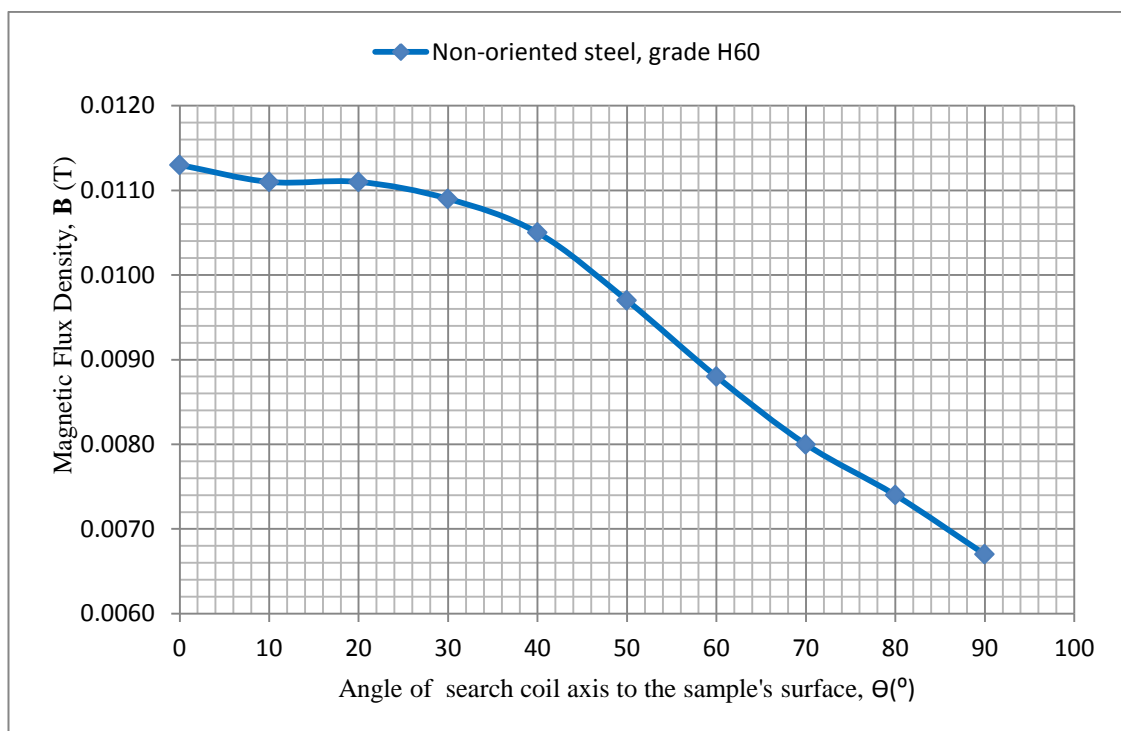


Figure 7.44 Flux density distributions of normal flux with variation of angle,  $\Theta$  of search coil axis to the sample's surface

Figure 7.45 presents the normal flux density detected at the centre of overhang and fit in non-oriented sample, grade H6. The graph shows that the normal stray flux is vary linearly with the current, I. It can be perceived that the stray flux is much higher for overhang sample compare to fit in sample. This is due to inhomogeneous of sample magnetization as in overhang sample, the flux tend to magnetize the sample under yoke followed by the neighbouring overhang part. For instance, the stray flux measured at I=1.2 A for overhang and fit in sample are 8.10 mT and 7.15 mT, respectively. The calculated percentage difference of stray flux between overhang sample with so-called fit in sample at I=1.2 A is about 13.3%. Even though, the value of stray flux is small which is around 6 to 10 mT, it can affect the field and flux measurement as a whole, Figure 7.47. Result obtained suggests that the stray flux can be minimized using fit in sample.

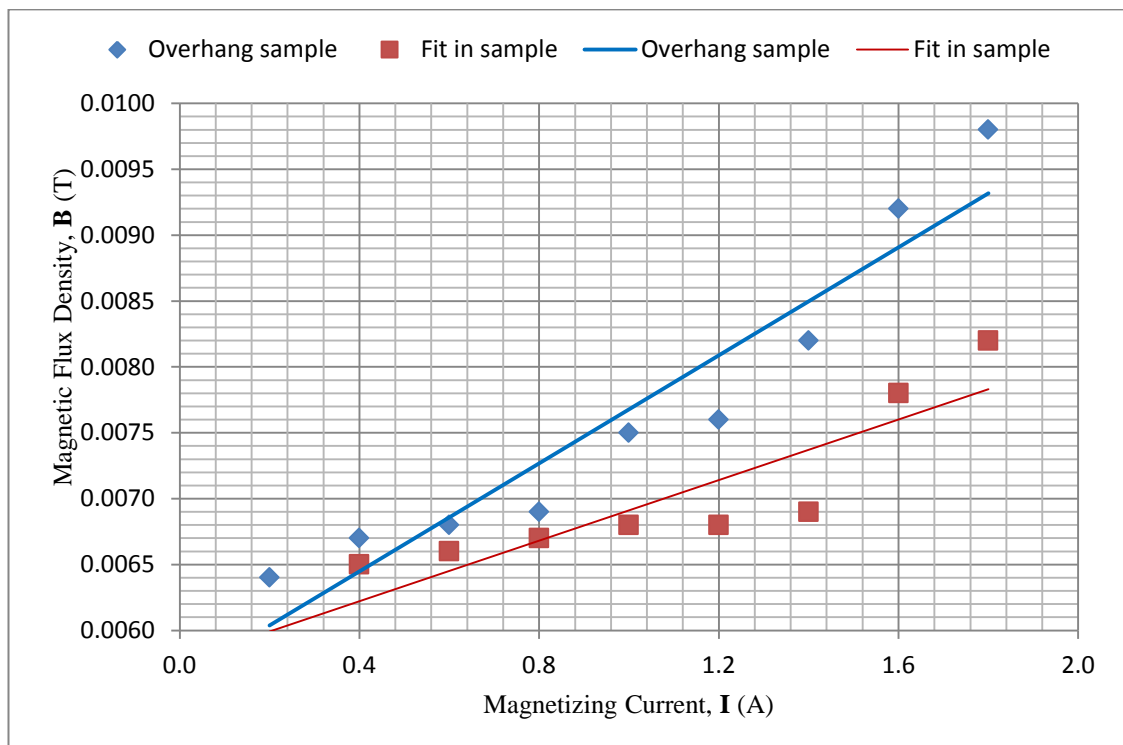


Figure 7.45 Flux distributions of normal flux measured at the centre of non-oriented sample, grade H6

ii) **The effect of sample dimension on stray flux**

The effect of variation of sample's dimension was investigated on the 0.5 mm thick non-oriented steel, grade H60. The fit in and overhang samples were assigned as LO=0mm and LO=30mm, respectively. The samples were magnetized at current ranging of 0.2 A to 1.8A, at frequency of 50 Hz. B-coils were constructed using 0.2mm diameter of enamelled copper wire wound about 20 mm apart in the middle of samples which enclosed the sample under test. The sensors were positioned at upper end, centre and lower end on the sample under test as shown in Figure 7.46.

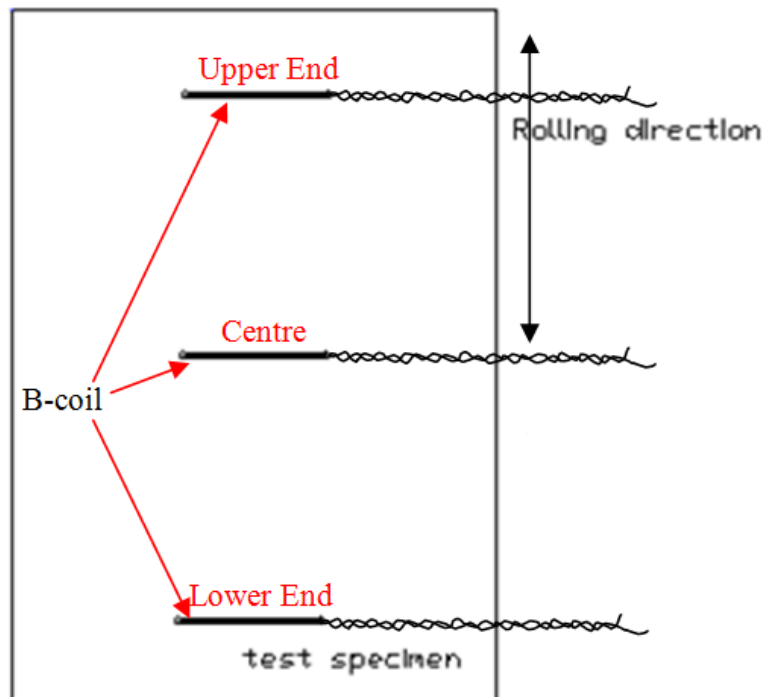


Figure 7.46 Location of B-coil sensor on the sample surface

Figure 7.47 presents the influence of sample dimension on the measurement results. Results show that the flux distributions measured in the central region of sample, LO=0 mm and Lo=30 mm are treated as nonlinear curve. The magnetic flux density for non-oriented steel, grade H60 is proportionally increased with the current, I until it reached

saturation level at around 1.4 T for fit in sample, LO=0 mm and 1.2 T for overhang sample, LO=30 mm. The flux distributions detected in the upper end and lower end of overhang sample are increase linearly with increasing of current, I. The contrast between magnetic flux density measured in the upper end and lower end with the central region of overhang sample is about 5.3% to 15.1% which is to be considered as quite high. This is due to non-uniformity of sample magnetization and flux leakage at the core end which can influence the measurement of field and flux distribution of sample, Figure 7.47. The effect of stray flux can be reduced using sample that is fitted nicely within the yoke pole faces. Results indicate that the field and flux measurement are mainly affected by the variation of sample dimension.

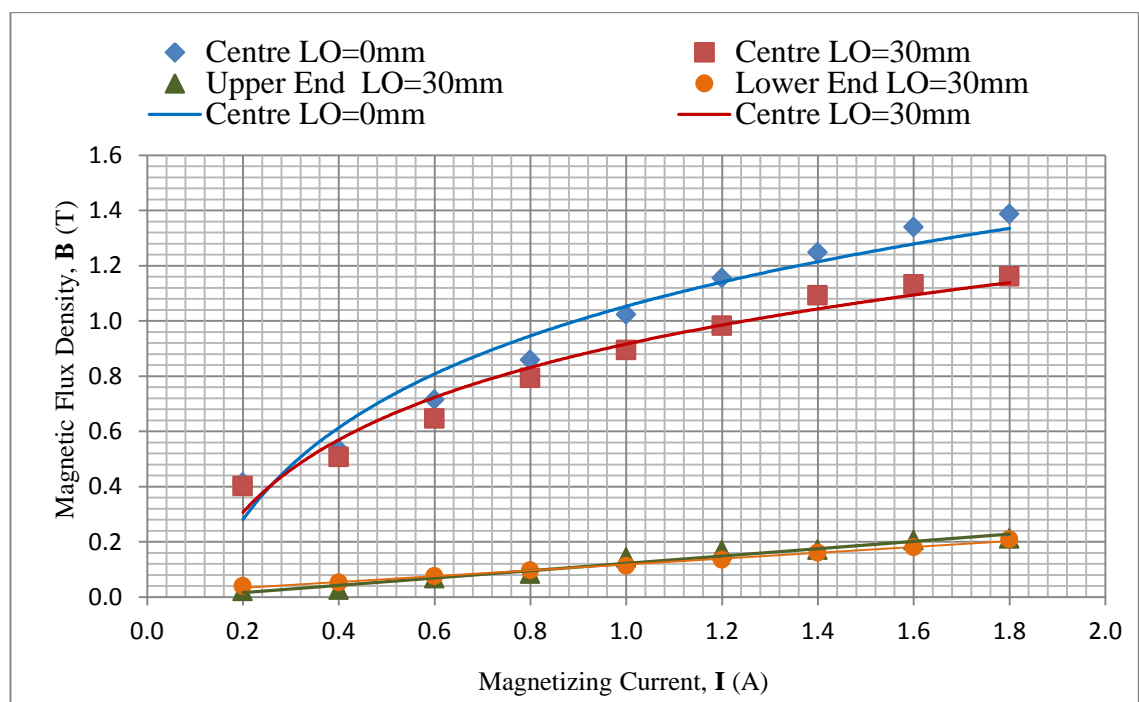


Figure 7.47 Flux density distributions measured at the centre, lower end and upper end of overhang and fit in sample

### 7.3 Statistical Analysis

Statistical analysis is performed to interpret statistical significance as a causal relationship of influential factor of Single Sheet Tester to the magnetic properties of electrical steels. One-way ANOVA and pooled T-Test as per described in subsection 2.6 were chosen as statistical method and the test is executed at the 5% significance level. Tukey post hoc test was then implemented as a multiple comparison in order to obtain the relation among all the population means.

#### 7.3.1 Normality of Data

In order to utilize one-way ANOVA and T-Test, the population of data must be normally distributed. Normal distribution of data can be examined by performing a correlation test for normality. A hypothesis test for normality is based on the linear correlation coefficient. If the variable under consideration is normally distributed, the correlation between the sample data and their normal scores should be near 1 because the normal probability plot should be roughly linear, (Weiss, 2005). The null and alternative hypotheses are executed at the 5% significance level.

Null hypothesis,  $H_0$ : The variable is normally distributed

Alternative hypothesis,  $H_a$ : The variable is not normally distributed

The critical value,  $R_p^*$  is obtained using Table IX (appendix), N is number of data and the value of test statistic is denoted as  $R_p$ . Table 7.1, Table 7.2, Table 7.3, Table 7.4 and Table 7.5 show the summary of the correlation test for normality for each analysis of data.

In general, all the tables (Table 7.1, Table 7.2, Table 7.3, Table 7.4 and Table 7.5) indicated that the test results are of the normal distribution due to the fact that the test statistic,  $R_p$  is more than the critical value,  $R_p^*$ . Therefore, it can be stated that at 5% significance level, the data provide sufficient evidence to conclude that the variable data are normally distributed. Hence, One-way ANOVA and pooled T-test can be executed.

Table 7.1 Correlation test for normality for H-coil analysis

Variable	H-coil	N	$R_p^*$	$R_p$	Judgment	Conclusion
Magnetic Field Strength, H (A/m)	$H_A$	6	0.889	0.987	Accept $H_0$	Normal Distribution
	$H_B$	6	0.889	0.993	Accept $H_0$	Normal Distribution
	$H_C$	6	0.889	0.996	Accept $H_0$	Normal Distribution

Where  $H_A$  : inner thickness 0.6 mm wound with 500 turns of 0.20 mm wire  
 $H_B$  : inner thickness 0.6 mm wound with 500 turns of 0.13 mm wire  
 $H_C$ : inner thickness 0.6 mm wound with 1000 turns of 0.20 mm wire

Table 7.2 Correlation test for normality for air gap length analysis

Variable	Air Gap Length (mm)	N	$R_p^*$	$R_p$	Judgement	Conclusion
Flux density, B (T)	0.3	6	0.889	0.895	Accept $H_0$	Normal Distribution
	0.5	6	0.889	0.983	Accept $H_0$	Normal Distribution
	0.8	6	0.889	0.996	Accept $H_0$	Normal Distribution
	1.0	6	0.889	0.997	Accept $H_0$	Normal Distribution
Field strength, H (A/m)	0.3	6	0.889	0.983	Accept $H_0$	Normal Distribution
	0.5	6	0.889	0.973	Accept $H_0$	Normal Distribution
	0.8	6	0.889	0.998	Accept $H_0$	Normal Distribution
	1.0	6	0.889	0.995	Accept $H_0$	Normal Distribution

Table 7.3 Correlation test for normality for yokes dimension analysis

Variable	Yokes Dimension (mm)	$R_p^*$	$R_p$	Judgement	Conclusion
Flux density, B (T)	Yoke A	0.889	0.981	Accept $H_0$	Normal Distribution
	Yoke B	0.889	0.958	Accept $H_0$	Normal Distribution
Field strength, H (A/m)	Yoke A	0.889	0.991	Accept $H_0$	Normal Distribution
	Yoke B	0.889	0.986	Accept $H_0$	Normal Distribution

Where Yoke A with dimension of (97.2 x 93.4 x 68.0) mm  
Yoke B with dimension of (145.8 x 140.1 x 68.0) mm

Table 7.4 Correlation test for normality for sample dimension analysis

Variable	Sample Dimension (mm)	N	Rp*	Rp	Judgement	Conclusion
Flux density, B (T)	97.2 x 68.0	5	0.880	0.971	Accept H <sub>0</sub>	Normal Distribution
	127.2 x 68.0	5	0.880	0.970	Accept H <sub>0</sub>	Normal Distribution
	157.2 x 68.0	5	0.880	0.954	Accept H <sub>0</sub>	Normal Distribution
Field strength, H (A/m)	97.2 x 68.0	5	0.880	0.990	Accept H <sub>0</sub>	Normal Distribution
	127.2 x 68.0	5	0.880	0.990	Accept H <sub>0</sub>	Normal Distribution
	157.2 x 68.0	5	0.880	0.989	Accept H <sub>0</sub>	Normal Distribution

Table 7.5 Correlation test for normality for anisotropy analysis

Variable	Types of samples	N	Rp*	Rp	Judgement	Conclusion
Flux density, B (T)	Grain Oriented steel, M4	6	0.889	0.891	Accept H <sub>0</sub>	Normal Distribution
	Non Oriented steel, M19	6	0.889	0.929	Accept H <sub>0</sub>	Normal Distribution
Field strength, H (A/m)	Grain Oriented steel, M4	6	0.889	0.991	Accept H <sub>0</sub>	Normal Distribution
	Non Oriented steel, M19	6	0.889	0.987	Accept H <sub>0</sub>	Normal Distribution

### 7.3.2 The Effect on H-Coil Dimension

T-Test was performed to obtain a probability statement about differences in means e.m.f induced voltage,  $V_{e.m.f}$  in H-coil windings. Three H-coils were constructed using the same dimension (20 x 20) mm and labelled as H<sub>A</sub>, H<sub>B</sub> and H<sub>C</sub>. The first sensor, H<sub>A</sub> having the inner thickness 0.6 mm wound with 500 turns of 0.2 mm wire, second sensor, H<sub>B</sub> having the inner thickness 0.6 mm wound with 500 turns of 0.13 mm wire and third spring, H<sub>C</sub> having the inner thickness 0.6 mm wound with 1000 turns of 0.2 mm wire. The null hypothesis and alternative hypothesis test are performed as:

Null hypothesis,  $H_0: \mu_1 = \mu_2 = \mu_3$  (The e.m.f induced voltages have the same means)

Alternative hypothesis,  $H_a$ : Not all the means are equal

The symbols  $\mu_1$ ,  $\mu_2$  and  $\mu_3$  are indicated as the mean e.m.f induced voltage,  $V_{e.m.f}$  in H-coil windings. The test is performed at the 5% significance level. The response variable in this testing was induced voltage and the factor was H-coil geometry dimensions which are number of turn, N and area, A. Table 7.6 displays the output acquired by applying the pooled T-test to the data distribution.

Table 7.6 Summary of T-Test with  $\alpha=0.05$  for the different specification of H-coil

Response Variable	Factor	H-coil	Mean Difference	Sig. (2-tailed)	Decision	Conclusion
e.m.f induced voltage, $V_{e.m.f}$ (V)	Area, A	H <sub>A</sub>	.001088	.002	Reject H <sub>0</sub>	Highly significance difference between yoke dimension
		H <sub>B</sub>	.001357	.003	Reject H <sub>0</sub>	Highly significance difference between yoke dimension
	Number of Turns, N	H <sub>A</sub>	.001088	.002	Reject H <sub>0</sub>	Highly significance difference yoke dimension
		H <sub>C</sub>	.011310	.000	Reject H <sub>0</sub>	Highly significance difference yoke dimension

The Table 7.6 above shows that the P-value for the hypothesis test is less than the specified significance level of 0.05, therefore null hypothesis, H<sub>0</sub> is declined. The test results are statistically significant at the 5% level. Thus, it can be concluded that, at the 5% significance level, the data provide sufficient evidence that the e.m.f induced voltages among the three sets of H-coil are different. From the statistical result, it confirms that the number of turns and area influenced the effectiveness of magnetic sensor (in term of their sensitivities).

One-way ANOVA test was carried out to analyze the significance different of the three H-coils. The null hypothesis and alternative hypothesis are as follows:

Null hypothesis,  $H_0: \mu_1 = \mu_2 = \mu_3$  (The e.m.f induced voltages have the same means)

Alternative hypothesis,  $H_a: \mu_1 \neq \mu_2 \neq \mu_3$  (Not all the means are equal)

The response variable in this testing was e.m.f induced voltages and the factor was geometric parameters of the H-coil sensors. Table 7.7 displays the output obtained by applying one- way ANOVA at the 0.05 significance level.

Table 7.7 One-way ANOVA summary test for the H-coil dimension analysis

Response Variables		F	P-value	Decision	Conclusion
V <sub>e.mf</sub> induced voltage (V)	Between different H-coil	194.76 0	.000	Reject H <sub>0</sub>	There is a significance difference among the H-coils

The Tukey multiple-comparison method was conducted to find specifically which geometric parameters of H-coils differ from which others. Table 7.8 shows the simultaneous 95% confidence intervals for the differences between the e.m.f induced voltage means.

Table 7.8 Homogenous subsets H-coil dimension analysis for Tukey post hoc tests

H-Coil	Subset for alpha, $\alpha = 0.05$	
	1	2
H <sub>A</sub>	.0010883	.0113100 1.000
H <sub>B</sub>	.0013578	
H <sub>C</sub>		
Sig.	.892	

A homogenous subset is a set of groups for which no pair of group means differs significantly. From the Table 7.8, it can be seen that, H<sub>A</sub> and H<sub>B</sub> are in the first column homogenous subsets which means they do not differ significantly. The second column

homogenous subsets contain only  $H_C$ , which means that the  $H_C$  is differs from each of the others. Hence, it can be concluded that e.m.f induced voltages in the H coil having the inner thickness 0.6 mm, wound with 1000 turns of 0.2 mm wire exceeds than in the other H-coils, and that no other means can be declared different at the 95% family confidence level.

### 7.3.3 The Effect of Air Gap

One-way ANOVA test was carried out to evaluate the significance different for the lengths of air gap at 0.3 mm, 0.5 mm, 0.8 mm and 1.0 mm to the magnetic properties of sample using SST set up. The null hypothesis and alternative hypothesis test are performed as below:

Null hypothesis,  $H_0: \mu_1 = \mu_2 = \mu_3 = \mu_4$  (field or flux distributions have the same means)

Alternative hypothesis,  $H_a$ : Not all the means are equal

The response variable in this testing was magnetic properties of sample and the factor was length of air gap. Table 7.9 shows the output obtained by applying one- way ANOVA at the 0.05 significance level.

Table 7.9 One-way ANOVA summary test for the lengths of air gap analysis

Response Variables		F	P-value	Decision	Conclusion
Flux density, B (T)	Between different air gap length	11.881	.000	Reject $H_0$	Highly significance difference between the air gap length
Field strength, H (A/m)	Between different air gap length	6.686	.003	Reject $H_0$	Highly significance difference between the air gap length

P-value which less than 0.05 was indicated that there is a highly significant difference between lengths of air gap introduced in the magnetizing set up. Therefore, it can be statistically proven that the field and flux concentrations within the samples are affected by the lengths of air gap introduced.

In order to evaluate which mean sample's dimensions vary from which others, post hoc testing was executed using Tukey's method. Table 7.10 displays the homogenous subsets result for Tukey post hoc test.

Table 7.10 Homogenous subsets lengths of air gap for Tukey post hoc test

Length of air gap (mm)	Flux Density, B (T)		Magnetic Field Strength, H (A/m)		
	Subset for alpha, $\alpha=0.05$		Subset for alpha, $\alpha=0.05$		
	1	2	1	2	3
Air gap 1.0	0.883		14.727		
Air gap 0.8	1.241		26.188	26.188	
Air gap 0.5		1.834		103.103	
Air gap 0.3		2.124			191.198
Sig.	0.364	0.549	0.983	0.081	1.000

Notice that a homogenous subset is a set of groups that are not significantly different. It summarized the result by ranking the sample means from smallest to largest and by connecting with lines those whose population means were not declared different, (Weiss, 2005). It can be seen that almost all lengths of air gap insertion differs in their magnetic properties and those with lengthy air gap produces less magnetic properties. Therefore, it can be concluded that magnetic properties of the air gap with length of 0.3 mm surpass that in the other length of air gap, and that no other means can be affirmed different at the 95% family confidence level.

### 7.3.4 The Effect of Yokes Dimension

T-Test was performed to obtain a probability statement about differences in means between two dimensions of the C-core (also known as yoke) which are Yoke A with dimension of (97.2 x 93.4 x 68.0) mm and Yoke B with dimension of (194.4 x 186.8 x 68.0) mm. The null and alternative hypotheses are:

Null hypothesis,  $H_0: \mu_1 = \mu_2$  (mean field or flux distributions are the same)

Alternative hypothesis,  $H_a: \mu_1 \neq \mu_2$  (mean field or flux distributions are different)

The symbols  $\mu_1$  and  $\mu_2$  are indicated as the mean field or flux distributions of the Yoke A and Yoke B, respectively. The test is performed at the 5% significance level. Table 7.11 displays the output acquired by applying the pooled T-test to the data distribution.

Table 7.11 Summary of T-Test with  $\alpha=0.05$  for the different yoke dimension

Magnetic Properties	Dimension of yokes (mm)	Mean Difference	Sig. (2-tailed)	Decision	Conclusion
Flux density, B (T)	Yoke A	2.3195	.000	Reject $H_0$	Highly significance difference between yoke dimension
	Yoke B	1.5753	.001	Reject $H_0$	Highly significance difference between yoke dimension
Field strength, H (A/m)	Yoke A	127.5849	.016	Reject $H_0$	Highly significance difference yoke dimension
	Yoke B	32.6788	.012	Reject $H_0$	Highly significance difference yoke dimension

The output in Table 7.11 reveals that the P-value for the hypothesis test is of 0.000. Since the P-value less than the specified significance level of 0.05, the null hypothesis,  $H_0$  is rejected. At the 5% significance level, the data provide sufficient evidence to conclude that a difference exists between the mean field and flux

distribution of two dimensions of yokes, Yoke A : (97.2 x 93.4 x 68.0) mm and Yoke B : (194.4 x 186.8 x 68.0) mm.

### 7.3.5 The Effect of Sample Dimension

One-way ANOVA test was carried out to analyse the significance different of the field and flux data distribution between the dimensions of sample which (97.2 x 68) mm, (127.2 x 68) mm and (157.2 x 68) mm. The null hypothesis and alternative hypothesis are as follows:

Null hypothesis,  $H_0: \mu_1 = \mu_2 = \mu_3$  (field or flux distributions have the same means)

Alternative hypothesis,  $H_a$ : Not all the means are equal

The response variable in this testing was magnetic properties of samples and the factor was sample's dimensions. Table 7.12 displays the output obtained by applying one- way ANOVA at the 0.05 significance level.

Table 7.12 One-way ANOVA summary test for the different sample dimensions

Response Variables		F	P-value	Decision	Conclusion
Flux density, B (T)	Between sample dimensions	.288	.755	Accept $H_0$	No significance difference between sample dimensions
Field strength, H (A/m)	Between sample dimensions	.013	.987	Accept $H_0$	No significance difference between sample dimensions

P-value which higher than 0.05 was indicated that there is a no significant difference between the dimensions of samples. At the 5% significance level, the data do not provide enough evidence to conclude that a difference exists in field and flux distributions among the sample's dimensions. Although, the field and flux distribution on sample's dimension is not significantly difference, the precaution step should be

taken into consideration. This is due to the amount of stray flux increases with longer overhang sample and lead to inhomogeneous of sample magnetization, (Stupakov, 2006). Thus, it can affect the measurement of field and flux in the middle of the sample.

### 7.3.6 The Effect of Anisotropy

T-Test was executed to analyse the mean of magnetic properties, flux density and field strength for different types of samples which are non-oriented silicon steels and grain oriented silicon steels. The null hypothesis and alternative hypothesis test are executed as below:

Null hypothesis,  $H_0: \mu_1 = \mu_2$  (mean field or flux distributions are the same)

Alternative hypothesis,  $H_a: \mu_1 \neq \mu_2$  (mean field or flux distributions are different)

The symbols  $\mu_1$  and  $\mu_2$  denoted as the mean field or flux distributions of the grain oriented and non-oriented silicon steel, respectively. The test is done at the 5% level of significance. Table 7.13 shows the summary of the T-test for the variation types of samples analysis.

Table 7. 13 T-Test summary test for the different types of samples

Magnetic Properties	Types of electrical steel	Mean Differences	Sig. (2-tailed)	Judgement	Conclusion
Flux density, B (T)	Grain Oriented steel, M4	2.0819	.000	Reject $H_0$	Highly significance difference between sample types
	Non-oriented steel, M19	1.2949	.001	Reject $H_0$	Highly significance difference between sample types
Field strength, H (A/m)	Grain Oriented steel, M4	127.5849	.016	Reject $H_0$	Highly significance difference between sample types
	Non-oriented steel, M19	217.2220	.006	Reject $H_0$	Highly significance difference between sample types

From the Table 7.13, it shows that there is a significant difference between the anisotropy of samples since the P-value less than the specified significance level of 0.05. At the 5% significance level, the data provide adequate proof to conclude that a difference exists between the mean field and flux distribution of two type of samples which are non-oriented steel, grade M19 and grain oriented silicon steel, grade M4.

#### **7.4 Validation on FEMM Simulation Analysis and Experiment Analysis**

The model validation is carried out by a comparison of trend analysis on magnetic properties for electrical steels obtained by FEMM simulation and hardware results. Figure 7.48, Figure 7.49, Figure 7.50 and Figure 7.51 show the magnetic flux density,  $B$  and magnetic field strength,  $H$  distribution for grain oriented and non-oriented steel measured under FEMM simulation and hardware.

It can be seen in Figure 7.48 and Figure 7.49, both simulation and hardware result show the similar pattern trend for the flux distribution curve of grain oriented and non-oriented steel where the flux distribution curves are non-linear with increasing of current,  $I$ . The flux is increasing with the current until the materials tend to become magnetically saturated. Further increases of magnetizing current,  $I$  will produce only a small increase in flux density,  $B$ . For the magnetic materials, the magnetic field strength,  $H$  varies directly with the current,  $I$ . It can be observed that both simulation and hardware result show the similar trend of field distribution as the  $H$  is proportionally linear with the current,  $I$ .

It is known that grain oriented steel has the better magnetic properties than non-oriented steel. A good grade of soft magnetic material must have a high permeability and only requires a smaller amount of current,  $I$  (less of magnetic field strength,  $H$ ) to gain higher flux density,  $B$ . Results show that grain oriented steels have higher value of  $B$  and lesser of  $H$  and vice versa for non-oriented steels. `

In general, the simulation results are in good accordance with the experimental results. The relatively small discrepancy of magnetic field between the experimental and the simulations can be due to the uncertainty of the effective air gap width in simulation. Besides that, in FEMM simulation, the magnetic field strength is obtained by pointing at the centre of sample by assuming H-coil is placed in the central region of

sample. However in hardware, the H-coil is placed tangentially about 1mm to 3 mm on top of specimen. This might lead to discrepancy of measurement results.

Some journal highlighted that stresses and deformation also contribute to inconsistency of magnetic measurement of electrical steel,(S. Tumanski, 2000),(Miyagi et al., 2010),(Senda et al., 2006) . Compression on the yoke, drilling the holes and shearing the electrical steel would deformed the domain structure of sample and affect the magnetic properties of electrical steel. Therefore, a precaution step should be taken during the preparation of the magnetic circuit and sample so that the stress can be avoided.

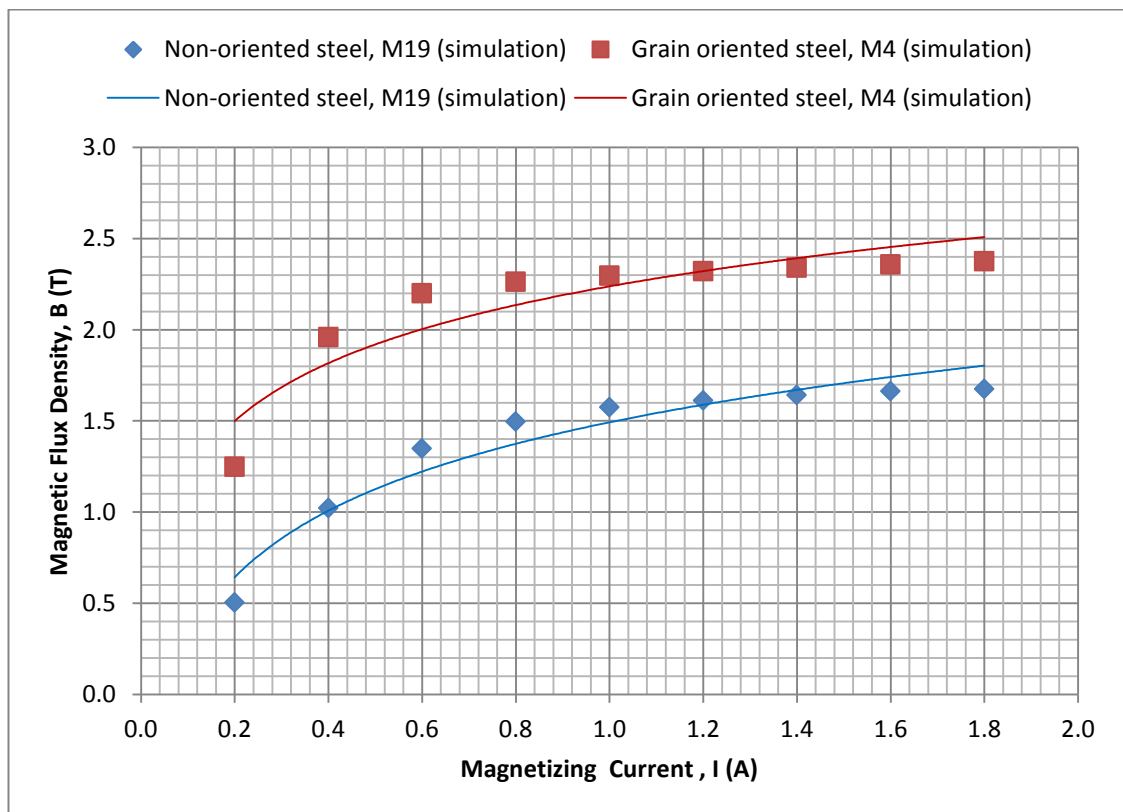


Figure 7.48 Flux distributions for different types of silicon steel using FEMM software

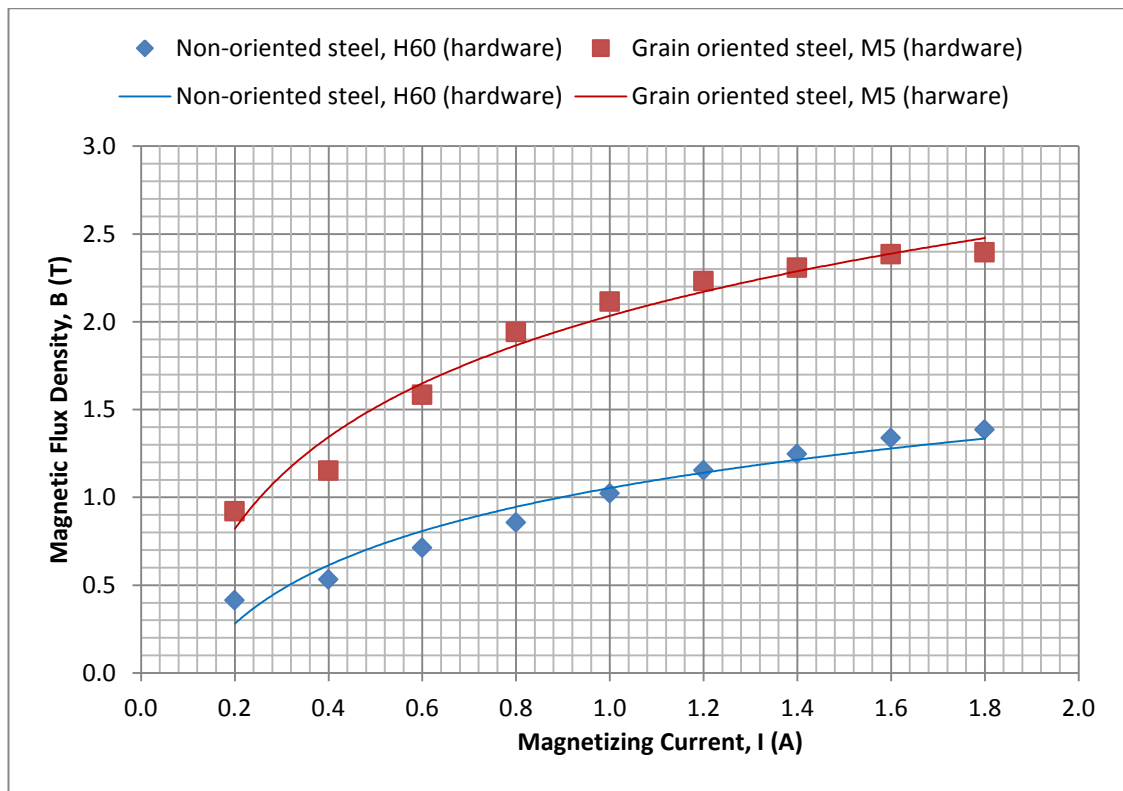


Figure 7.49 Flux distributions for different types of silicon steel using hardware

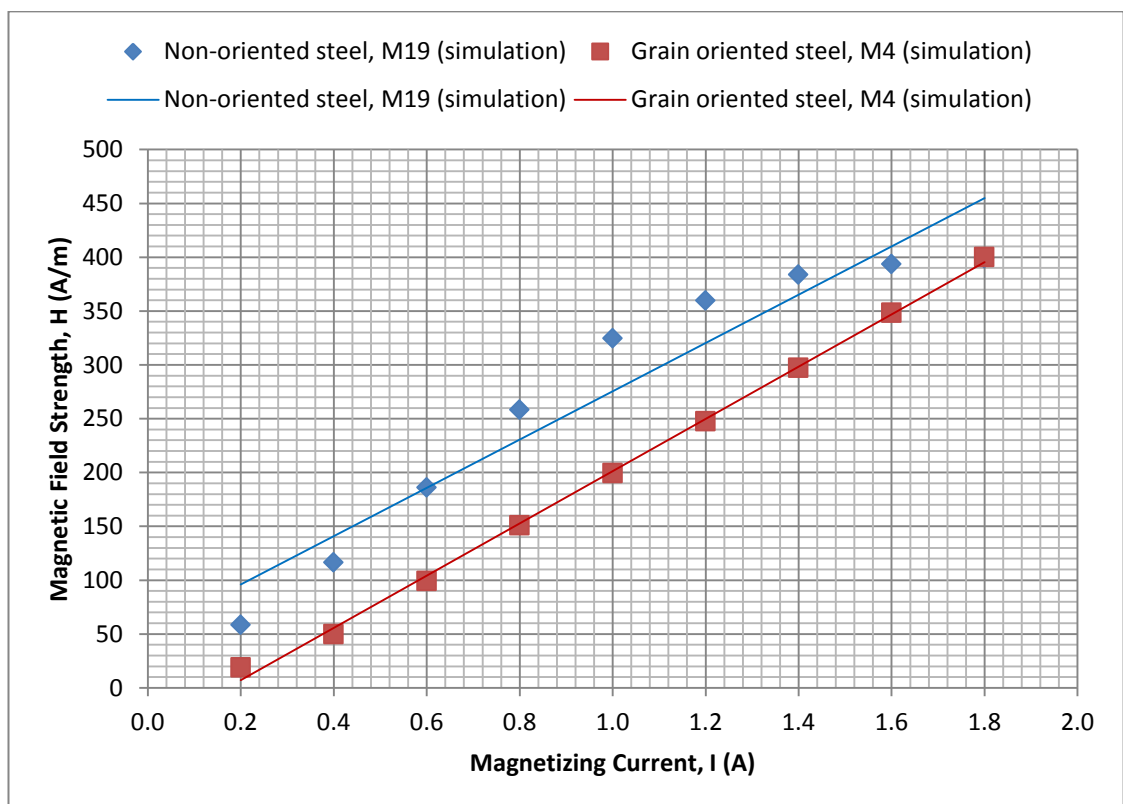


Figure 7.50 Field distributions for different types of silicon steel using FEMM software

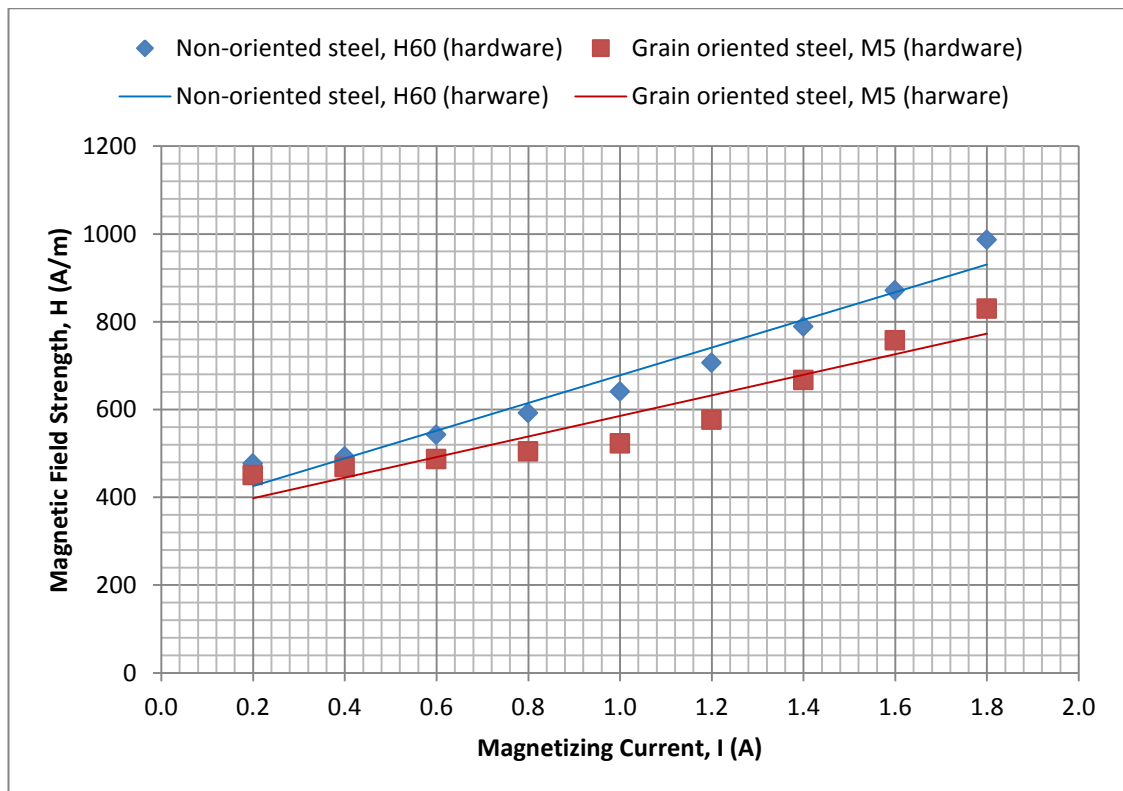


Figure 7.51 Field distributions for different types of silicon steel using hardware

## CHAPTER 8

### CONCLUSION AND RECOMENDATION

---

#### 8.0 Conclusion

Single Sheet Tester (SST) has been successfully designed, simulated and developed. The magnetic properties of grain oriented and non-oriented steel sheet under 50 Hz magnetization condition in the rolling direction were investigated. The effects of design factors of SST such as an air gap length, yoke's dimension, sample dimension and positioning of sensor were addressed and optimized with the aid of Finite Element Method Magnetic (FEMM) simulation. The experimental results were verified with simulation outcomes. The statistical analysis was conducted to interpret statistical significance of effect factor of SST to the magnetic properties of electrical steels. The conclusion of the finding can be summarized as follows:

- The positioning of the magnetic sensors which are B-coil and H-coil is crucial factor in magnetic measurement. From the simulation result, it is found that the magnetic fields and flux densities are distributed uniformly in the central of the sample due to sample's high permeability which forces the flux to flow only in the area between poles of yokes. Therefore, for accuracy and reliable of magnetic measurement, the sensors must be placed in the central region of sample where the homogenous magnetized area can be obtained. The H-coil is positioned about 1 mm to 3 mm away from the sample surface in order to evade disturbance of stray field from domain and grain boundaries.
- The effect of air gap in SST has been studied on grain oriented silicon steel, grade M4. In the presence of effective air gap, the solid flux lines show a large non-uniformity of the flux distribution between the yoke poles and sample. The more concentrated flux flows through the sample were observed when air gap of 0.3 mm was introduced to the SST. Air gap enlarges the yokes reluctances and lessen the flux

density in the yoke as well as in the gap which requires more energy to drive the same flux across the air gap than through an equal volume of the and improve the field homogeneity within the sample. However, as the air gap lengths were increased from 0.5 mm to 1 mm, the more leakage fluxes were seen. This is due to the increase in the yoke reluctances which lead to worse condition of the flux penetration within the sample and yokes. Therefore, the homogeneity of flux and field distribution of sample can be achieved at air gap length of 0.3 mm.

- The influence of yoke's dimension also has been investigated. The use of yoke is to confine and guide the magnetic field lines to be concentrated in the core material. The presence of magnetic core can increase the strength of magnetic fields produced by a coil. It can be seen that flux density is proportionally increase with current and inversely proportional with the flux path length. The increases of yoke's dimension at (145.8 x 140.1 x 68.0) mm lead to lower sample magnetization due to a high reluctance flux closure path which caused flux leakage between the yoke legs. The yoke dimension of (97.2 x 93.4 x 68.0) mm was used as a magnetizing yoke as it can generate the magnetizing field with a low reluctance flux closure path.

- The effects of the sample dimension on magnetic measurement were investigated on grain oriented and non-oriented silicon steels. The fit in sample,  $L_0=0$ mm is defined as sample which is fitted nicely within the yoke end poles and overhang sample is described as sample which have additional length at both ends of fit in sample. The sensors were located at three different positions which are upper end, centre and lower end of sample. The flux distributions measured in the centre of sample were treated as non-linear curve whereas the flux distribution measured in the upper end and lower end of sample were considered as linear with current. The findings also showed that the magnetic flux distribution for fit in sample is slightly higher than overhang sample. The stray flux also increased with the longer overhang sample. This

is due to non-uniformity of sample magnetization as in overhang sample, the flux tend to magnetize the sample under yoke followed by the neighbouring overhang part. This attributed to the flux leakage between the yoke legs which affected the magnetic measurement of sample.

- The effect of anisotropy of electrical steels which are grain oriented and non-oriented silicon steel also have been investigated in this research. It can be seen that for both types of electrical steels showed the similar trend of curve. The magnetic field distributions are increased linearly with the current whereas the magnetic flux density distributions are treated as non-linear with the current. Result also indicated that the grain oriented silicon steels have better anisotropy and magnetic properties than non-oriented steels. It is observed that the magnetizing curve for grain oriented silicon steels were higher compared to non-oriented steels. The electrical steel which has high anisotropic structures and high permeability will require fewer magnetic fields to obtain high magnetic flux density. However, the magnetizing curve for each grade of electrical steels is different due to grain size and thickness of the sample.

- One –way ANOVA, T-test and Tukey post hoc were performed to evaluate the statistical significance for effect factor of SST to the magnetic properties of electrical steels. The tests were executed at the 0.05 significance level. As overall, it can be seen that the statistical results are in good accordance with the simulation and experimental analysis. The data provided sufficient evidence that the number of turns, N and area of H-coil influenced the effectiveness of magnetic sensor. It also concluded that the magnetic properties of the air gap of 0.3 mm surpass that in the other air gap length. It statistically proven that the field and flux concentrations within the samples are affected by the lengths of air gap. The data also provide sufficient evidence to conclude that the yoke's dimension affect the magnetic measurement. As for the effect of anisotropy, the data gave adequate evidence to conclude that there is significance different between the

mean field and flux distribution of grain oriented and non-oriented steels. However for sample dimension, the data do not provide enough evidence to conclude that a different exist in field and flux distribution among the sample dimension. This is due to the percentage different between the overhang and fit in sample is in the range of 1.7 % to 4.6 %. However, the precaution step must be taken into consideration. This is due to longer overhang sample will increase stray flux and flux leakage at the core end and sample and might lead to in homogenous of sample magnetization.

## **8.1 Recommendation**

A mechanical strain caused by shearing stresses occurring during the process of cutting electrical steel sheets will cause deterioration of the magnetic characteristics of the sheet (Miyagi, et al., 2010). Therefore, it is necessary to clarify the magnetic properties of the electrical steel sheet under compressive stress for improving the efficiency of the electrical machinery.

## REFERENCES

---

E. Antonelli, et al. (2005). Single Sheet Tester Efficiency Macromagnetic Analysis.

*Journal of Applied Physics* 97(10E103), 1-3. doi: 10.1063/1.1851956

An American National Standard ASTM. (2000). Standard Test Methods for Alternating-Current Magnetic Properties of Materials at Power Frequencies Using Sheet-Type Test Specimens A804/A804M-99 *Annual Book of ASTM Standards* (pp. 170-177): ASTM An American National Standard

P. Beckley. (2002). *Electrical Steel For Rotating Machines*. United Kingdom: The Institution Of Electrical Engineers.

F. Brailsford. (1968). *An Introduction To The Magnetic Properties Of Materials* (1 ed.). Britain: Longmans, Green and Co. Ltd.

K. H. J. Buschow, & F.H. De Boer (Eds.). (2004). *Physics of Magnetism and Magnetic Materials*: Kluwer Academic Publishers.

Prantosh Chakraborty. (2005). *Electricity and Magnetism* (2nd Edition ed.). India: New Age International (P) Ltd.

F. Fiorillo. (2010). Measurement of magnetic materials. *Metrologia*(47), S114-S142. doi: 10.1088/0026-1394/47/2/S11

Bernard Fryskowski. (2008). Experimental Evaluation of Magnetic Anisotropy in

Electrical Steel Sheet. *Journal of Magnetism and Magnetic Materials*, 320, 515-522.

C.D. Graham. (1982). Physical origin of losses in conducting ferromagnetic materials (invited). *J. Appl. Phys.*, 53(11), 8276-8280.

J. Liu, & G. H. Shirkoohi. (1993). Anisotropic Magnetic Material Modelling Using Finite Element Method. *IEEE Transactions on Magnetics*, 29(6), 2458-2460.

A. H. Jahidin, & W. N. L. Mahadi. (2007). *The Influence of Different Core Arrangements on Magnetic Properties of Electrical Sheets under One-Dimensional Magnetizing System*. Paper presented at the Asia-Pacific Conference on Applied Electromagnet Proceedings (APACE 2007), Melaka, Malaysia.

Steel JFE. (2007) Electrical Steel Sheets (pp. Technical Report on electrical steels). Japan: JFE Steel Corporation.

David Jiles. (1991). *Introduction to Magnetism and Magnetic Materials*: Chapman & Hall.

Marcelo S. Lancarotte, & Aderbal de Arruda Penteadó Jr. (2004). Improving the magnetizing device design of the single sheet tester of two dimensional properties. *Journal of Magnetism and Magnetic Materials*, 160(269), 346-351.

J. Liu, et al. (1994). A method of anisotropic Steel Modelling Using Finite Element Method With Confirmation By Experimental Results. *IEEE Transactions on Magnetics*, 30(5).

Wan Nor Liza Wan Mahadi. (1996). *Design and Development of A Novel Two Dimensional Magnetic Measurement System for Electrical Steels*. University of Wales College of Cardiff.

K. Michiro, et al. (2002). Kawasaki Steel Corporation.

D. Miyagi, et al. (2010). Influence of Compressive Stress on Magnetic Properties of Laminated Electrical Steel Sheets. *IEEE Transactions on Magnetics*, 46(2), 318-321.

D. Miyagi, et al. (2009). Development of Measurement System of Magnetic Properties at High Flux Density Using Novel Single Sheet Tester. *IEEE Transactions on Magnetics*, 45(10), 3889-3892.

T. Nakata, et al. (1990). Effects Of Eddy Currents In The Specimen In A Single Sheet Tester On Measurement Errors. *IEEE Transactions on Magnetics*, 26(5), 1641-1643.

N. Nencib, et al. (1996). Experimental Analysis on the Field Distribution in a Large RSST. *Journal of Magnetism and Magnetic Materials* (160), 171-173.

Steel Nippon. Datasheet Properties of electrical sheet steels. *Magnetic Properties of TOA's electrical sheet steels* (pp. 34-35): Nippon Steel.

N. Normann, et al. (1982). The Influence of Grain Orientation On the Domain Structure and Stray Field Behaviour of Fe-Si Sheets. *Journal of Magnetism and Magnetic Materials*, 26, 29-34.

W. A. Pluta. (2010). Some Properties of Factors of Specific Total Loss Components in Electrical Steel. *IEEE Transactions on Magnetics*, 46(2).

N.A.M. Rashid, et al. (2008, 16-19 Jun 2008). *Evaluation of Magnetic Field and Flux Using Single Sheet Tester*. Paper presented at the Proceeding of the 2nd International Conference on Functional Materials and Devices (ICFMD 2008), Kuala Lumpur, Malaysia.

K. Senda, et al. (2006). Influence of shearing process on domain structure and magnetic properties of non-oriented electrical steel. *Journal of Magnetism and Magnetic Materials*(304), e513-e515. doi: 10.1016/j.jmmm.2006.02.139

J. Sievert. (2000). The Measurement of Magnetic Properties of Electrical Sheet Steel- Survey on Methods and Situation of Standards. *Journal of Magnetism and Magnetic Materials* (215-217), 647-651.

Inc. SPSS. (2002). *Statistical Analysis Using SPSS*. United States of America: SPSS Inc. .

AK Steel. (2007) Product Data Bulletin: Selection of Electrical Steels For Magnetic Cores. AK Steel Corporation

O. Stupakov. (2006). Investigation of applicability of extrapolation method for sample field determination in single-yoke measuring set up. *Journal of Magnetism and Magnetic Materials*, 307, 279-287.

O. Stupakov, et al. (2009). Applicability of local magnetic measurements.

*Measurements*, 42, 706-710.

(2011, 11/5/2011). Magnetic Circuit Analysis, from

[http://services.eng.uts.edu.au/cempe/subjects\\_JGZ/eet/eet\\_ch4.pdf](http://services.eng.uts.edu.au/cempe/subjects_JGZ/eet/eet_ch4.pdf)

J. E. Thompson. (1968). *The Magnetic Properties of Materials* (1 ed.). Britain: Newnes Books.

S. Tumanski. (2000). The experimental verification of the condition of the magnetic material caused by different technological process. *Journal of Magnetism and Magnetic Materials*(215-216), 749-752.

S. Tumanski. (2002). A multi-coil sensor for tangential magnetic field investigations *Journal of Magnetism and Magnetic Materials*(242-245), 1153-1156.

S. Tumanski. (2003). Investigations of the Anisotropic Behaviour of SiFe Steels. *Journal of Magnetism and Magnetic Materials* (254-255), 50-53.

S. Tumanski. (2007). Induction Coil Sensors - A Review. *Measurement Science and Technology*, 18, R31-R46. doi: 10.1088/0957-0233/18/3/R01

Slawomir Tumanski, & Slawomir Baranowski. (2004). Single Strip Tester with Direct Measurement of Magnetic Field Strength. *Journal of Electrical Engineering* 55(10/S), 41-44.

N. Katahashi T. Nakata, K. Fujiwara and M. Nakano (1989). Effects of the Overhang of a Specimen on the Accuracy of a Single Sheet Tester. *Physica Scripta*, 40, 529-531.

Neil A. Weiss. (2005). *Introductory Statistics*. United States of America: Pearson Education Inc.

(2011). Magnetic Core Retrieved 1/2/2011, 2011, from [http://en.wikipedia.org/magnetic\\_core](http://en.wikipedia.org/magnetic_core)

S. Zurek, et al. (2008). Analysis of Twisting of Search Coil Leads As A Method Reducing The Influence Of Stray Fields On Accuracy Of Magnetic Measurements. *Sensors and Actuators A*(142), 569-573.

E. Usak, et al. (2008). Analysis of Capabilities of Small Double-Yoke Single Sheet Tester. *Journal of Electrical Engineering* 59(7/S), 21-24.

Y. Muri, et al. (2011). Measurement of Magnetic Properties of Grain-Oriented Electrical Steel Sheet Using 2D Single Sheet Tester. *Przegląd Elektrotechniczny (Electrical Review)*, ISSN 0033-2097, R87, 9b

A. Saito, et al. (2000). Magnetization Properties and Domain Structures of Grain Oriented Silicon Steel Sheets Due to Bending Stress. *IEEE Transactions on Magnetics*, 36(5).

- R. Rygal, et al. (2000). Influence of Cutting Stress on Magnetic Field and Flux Density Distribution in Non-Oriented Electrical Steels. *Journal of Magnetism and Magnetic Materials*, 215-216, 687-689.
- A. J. Moses, et al. (2000). Aspects of the Cut-Edge Effect Stress on the Power Loss and Flux Density Distribution in Electrical Steel Sheets. *Journal of Magnetism and Magnetic Materials*, 215-216, 690-692.
- K. Senda, et al. (2006). Influence of Shearing Process on Domain Structure and Magnetic Properties of Non-Oriented Electrical Steel. *Journal of Magnetism and Magnetic Materials*, 304, e513-515.
- S. Tumanski. (2000). The Experimental Verification of The Condition of the Magnetic Material Caused by Different Technological Processes. *Journal of Magnetism and Magnetic Materials*, 215-216, 749-752.
- N. Hihat, et al. (2010). Experimental Method for Characterizing Electrical Steel Sheets in the Normal Direction. *Sensors*, 10, 9053-9064. doi:10.3390/s101009053
- H.G. Kang, et al. (2011). Qualification of Magnetic Flux Density in Non-Oriented Electrical Steel Sheets by Analysis of Texture Components. *Journal of Magnetism and Magnetic Materials*, 323, 2248-2253.
- A. J. Moses (2012). Energy efficient electrical steels: Magnetic performance prediction and optimization. *Scripta Mater.* <http://dx.doi.org/10.1016/j.scriptamat.2012.02.027>

Teruyuki Tamaki, et al. (2010). Comparison of Magnetic Field Analysis Methods Considering Magnetic Anisotropy. *IEEE Transactions on Magnetics*, 46(2), 187-190.

O. Stupakov. (2012). System for controllable magnetic measurement with Direct Field Determination. *Journal of Magnetism and Magnetic Materials*, 324, 631-636.

## LIST OF PUBLICATIONS

---

### Journal

N.A. Rahman, **N.A. Rashid**, W.N. Mahadi and Z. Rasol, (2011) Magnetic Field Exposure Assessment of Electric Power Substation in High Rise Building, Journal of Applied Sciences, Volume 11, Number 6, 953-961 (ISI-Cited Publication)

### Publications and Conference Proceedings

**N.A Rashid**, W. N. L. Mahadi, (2012) Simulation and Statistical Approaches on Field and Flux Distribution of Electrical Steels in a Single Sheet Tester, International Conference on Solid State Science and Technology (ICSST 2012), Melaka, Malaysia. (abstract submitted)

**N.A.Rashid**, A.H. Jahidin, W.N.L Mahadi, (2008) Evaluation of Magnetic Field and Flux Using Single Sheet Tester, International Conference on Functional Materials and Devices 2008 (ICFMD 2008), Malaysia. (ISI-Cited Publication)

**N.A Rashid**, A.H. Jahidin, W.N.L Mahadi, (Sept 2007) Evaluation of Magnetic Properties in Grain-Oriented Silicon Iron Steels Using Single Sheet Tester, Malaysian Science and Technology Congress 2007, Malaysia.

## APPENDICES

---